

Modeling of Precipitation Sequence and Ageing Kinetics in Al-Mg-Si Alloys

PhD thesis

Abbas Bahrami

This research was performed in the department of Materials Science and Engineering of Technical University of Delft.



This research was carried out under Project No. MC4.05213 in the framework of the Strategic Research Program of the Materials Innovation Institute M2i (www.m2i.nl).



Modeling of Precipitation Sequence and Ageing Kinetics in Al-Mg-Si Alloys

Proefschrift
ter verkrijging van de graad van doctor
aan de Technische Universiteit Delft,
op gezag van de Rector Magnificus prof.ir. K.C.A.M. Luyben,
voorzitter van het College voor Promoties,
in het openbaar te verdedigen op woensdag 10 november om 10 uur

door

Abbas Bahrami

Master of Science in Materials Engineering
Sharif University of Technology, Tehran, Iran
geboren te Teharn, Iran

Dit proefschrift is goedgekeurd door de promotor:
Prof.dr.ir. J. Sietsma

Samenstelling promotiecommissie:

Rector Magnificus, voorzitter
Prof. dr.ir. J. Sietsma, Technische Universiteit Delft, Promotor
Dr. A. Miroux, Materials Innovation Institute (M2i)
Prof. dr.ir. R. Benedictus, Technische Universiteit Delft
Prof. ir. L. Katgerman, Technische Universiteit Delft
Prof. dr.ir. L. Kestens, Gent University
Prof. dr.C. Pappas, Technische Universiteit Delft
Prof. J. D. Robson, Manchester University

Keywords: Al-Mg-Si alloys, precipitation sequence, ageing treatment, work-hardening, interrupted ageing, ageing kinetics, modeling, mixed-mode growth

ISBN 978-90-77172-61-2

Copyright © 2010 by A. Bahrami
naderbahrami@yahoo.com

All rights reserved. No part of the material protected by this copy right notice may be reproduced or utilized in any form or by any means, electronically or mechanically, including photocopying, recording, or by the information storage and retrieval system, without written permission from the author.

Printed in the Netherlands

To

Maryam

Contents

List of Symbols.....	i
Chapter 1	
Introduction	1
Chapter 2	
An Age-Hardening Model for Al-Mg-Si Alloys Assuming the Needle-Shaped Morphology for Precipitates	
2.1. Introduction	6
2.2. Microstructure model	7
2.3. Strength model.....	12
2.4. Model implementation.....	16
2.5. Modeling results	18
2.6. Discussion.....	24
2.7. Summary	26
References	27
Chapter 3	
Modelling of the Age-Hardening Behavior of Al-Mg-Si Alloys Considering Simultaneous Nucleation, Growth and Coarsening during Precipitation	
3.1. Introduction	30
3.2. Kampmann-Wagner-Numerical (KWN) model	30
3.3. Strengthening model.....	34
3.4. Results	36
3.5. Discussion	42
3.6. Summary	44
References	45
Chapter 4	
A Mixed-Mode Precipitation Model for Al-Mg-Si Alloys	

4.1. Introduction	48
4.2. Mixed-mode model.....	49
4.3. Modelling results	56
4.3.1. Effects of interfacial energy.....	57
4.3.2. Effects of mobility (accommodation factor).....	59
4.3.3. Effects of diffusivity.....	64
4.3.4. Effects of precipitate size distribution	71
4.3.5. Application of the model	74
4.4. Discussion.....	77
4.5. Conclusions	80
References	81

Chapter 5

Multi-Component Multi-Precipitate Modelling of Ageing Kinetics in Al-Mg-Si Alloys

5.1. Introduction	84
5.2. Multi-component multi-precipitate model.....	87
5.3. Strengthening model.....	91
5.4. Model implementation.....	95
5.5. results.....	101
5.6. Discussion.....	117
5.7. Summary	120
References	122

Chapter 6

Interrupted Ageing in Al-Mg-Si alloys

6.1. Introduction	126
6.2. Materials and methods.....	128
6.3. Results	129
6.4. Discussion.....	133
6.5. Conclusions	135
References	136

Chapter 7

Strain Hardening of Al-Mg-Si alloys

7.1. Introduction	140
-------------------------	-----

7.2. Kocks-Mecking-Estrin (KME) model	141
7.3. Experimental and modeling results.....	144
7.4. Discussion.....	153
7.5. Summary	156
References	157
Summary	159
Samenvatting.....	163
Acknowledgements	167
Curriculum Vitae.....	169

List of Symbols

A_{eq}	Equilibrium aspect ratio
A	Aspect ratio of cylindrical precipitates
A_0	Constant in the nucleation equation
b	Burgers vector (m)
C_0	The initial concentration of Mg in the matrix (wt%)
C_m	The mean concentration of Mg in the matrix (wt%)
C_e	The equilibrium interface concentration (wt%)
C_r	The equilibrium interface concentration, taking into account the Gibbs-Thomson effect (wt%)
$C_{<r>}$	The equilibrium interfacial concentration around the precipitate of mean radius (wt%)
C_β	Concentration of Mg inside the precipitate (wt%)
D	Bulk diffusion coefficient
E_i	Total interface energy of cylindrical precipitate (J)
f	Volume fraction of precipitates
f_{PA}	Precipitate volume fraction at peak-age
f_s	A parameter used to capture the influence of shearing precipitates on the dynamic recovery rate
F	Mean precipitates strength
F_{PA}	Mean precipitates strength at peak-age
F_{trans}	Mean precipitate strength at shearable/non-shearable transition
G	Shear Modulus (MPa)
h	Half-length of cylindrical precipitate (nm)
J_0	Pre-exponential term in nucleation equation
J	Nucleation rate (#/m ³ s)
K_j	Constant at solid solution hardening equations
k_D	additional dislocation storage term due to dislocation-precipitate interaction
k_1	Fitting parameter in work-hardening equations (m ⁻¹)
k_2	Fitting parameter in work-hardening equations
L	Mean precipitate spacing (m)
l	Effective mean precipitates distance (m)
M	Taylor factor
N_{PA}	Number density of precipitates at peak-age
Q_d	Activation energy for bulk diffusion (J/mol)
Q_s	Apparent solvus boundary enthalpy (J/mol)
Q_1	Gibbs energy dissipation by the precipitate-matrix interface movement
Q_2	Gibbs energy dissipation by diffusion of alloying elements inside the precipitate
Q_3	Gibbs energy dissipation by diffusion of alloying elements inside the matrix

$\langle r \rangle$	Mean Radius (nm)
r_{PA}	Mean precipitate radius at peak-age (nm)
r_{trans}	Transition radius from shearable precipitates to non-shearable precipitates (nm)
r_{trans}^*	Modified transition radius used in the work-hardening model (nm)
r_{cl}	Transition radius between unstable Orowan loop regime to the stable Orowan loop regime (nm)
r_{cr}	Critical precipitate radius (nm)
T	Ageing temperature
t_{PA}	Time to peak-age (sec)
V_m	Molar volume of precipitate (m ³)
σ_0	Pure aluminium yield strength (MPa)
σ_{ss}	Solid solution hardening (MPa)
σ_{ppt}	Precipitation hardening (MPa)
σ_y	Yield strength (MPa)
σ_h	Yield strength increase due to dislocation hardening (MPa)
σ	Total flow strength during deformation (MPa)
σ_{PA}	Yield strength at peak-age (MPa)
ρ	Dislocation density (m ⁻²)
ε	Plastic Strain
α	Constant in Taylor equation
α_D	Constant used to calculate k_D
φ	Efficiency of dislocation storage
θ	Work-hardening rate (MPa)
θ_{max}	Dislocation storage parameter (MPa)
β	Dynamic recovery rate
γ	Interfacial energy for spherical precipitate (J/ m ²)
γ_c	Interfacial energy for of the tip of cylindrical precipitate (J/ m ²)
γ_i	Interfacial energy along cylindrical precipitate (J/ m ²)
Γ	Dislocation line tension
μ	Chemical potential of alloying element
β	Atomic attachment rate for precipitate of critical radius
Z	Zeldovich factor
Ω	Partial molar volume of alloying elements
ψ	Dislocation bowing angle
ΔH_0	Standard enthalpy of formation of Mg ₂ Si precipitate
ΔS_0	Standard entropy of formation of Mg ₂ Si precipitate

CHAPTER 1

Introduction

There have been many attempts to improve mechanical properties of aluminum alloys in recent years, mainly due to the increasing governmental demand to reduce the automotive weights and, consequently, fuel consumption. Aluminum alloys are also being widely used for structural components in aerospace industry because they offer an advantageous combination of light weight, strength, and formability. Pure aluminum is too soft to be used in structural components. However, alloying it with other elements increases its strength. The increase in strength is either through solid solution or precipitation hardening. Precipitation hardening occurs during ageing treatment after solutionizing treatment during which the alloying elements in supersaturated solution form precipitates. Adding Mg, Si, and Cu to aluminum constitutes the heat-treatable 6xxx series aluminum alloys. The heat-treatable 6xxx series aluminum alloys are currently being used for various applications including automobile body sheet, extrusion profiles, pipes, welded structures, and aircraft sheets. They are widely used as medium-strength structural alloys with the advantages of relatively low density, good weldability and corrosion resistance. Commercial 6xxx alloys are either balanced in Mg- and Si-content to form quasi-binary Al-Mg₂Si alloys, or they have excess Si or Mg above the concentration needed to form Mg₂Si. Figure 1.1 shows the compositional limits of some common 6xxx alloys, together with contours representing common peak-aged (T6) values of yield strength. Balanced alloys are normally press-quenched, thereby eliminating the need to solutionize them before ageing. However, alloys with excess Si or Mg are more sensitive to the quenching conditions and therefore it is usually necessary to solutionize them before ageing. Si in aluminum alloys may also reduce the ductility of the alloys, mainly due to the partitioning of Si to grain boundaries. 6xxx series aluminum alloys are normally aged at about 150-220 °C during which they undergo a complex precipitation sequence, consisting of a series of metastable precipitates with different stoichiometry and different morphologies. During precipitation three main microstructural processes are taking place simultaneously; nucleation, growth, and coarsening. Further improvement and optimization of the mechanical properties of 6xxx alloys necessitate a better understanding of processing-

1. Introduction

structure-property relationships, which can be achieved by physical modeling. The objective of developing a model for the precipitation process is making a link between processing parameters including ageing time and temperatures, alloy chemistry, and microstructure characteristics like precipitates size and number density. A strengthening model can be used to correlate the precipitate characteristics to the yield strength of the alloy. The first version of precipitation models for aluminum alloys was introduced by Shercliff and Ashby [1]. As the knowledge on the processing-structure-property relationships in aluminum alloys has increased, more and more realistic and optimized precipitation models have been developed. Nevertheless, one of the main traditional assumptions of precipitation models is the assumption of spherical morphology for precipitates. The most important precipitate in terms of strengthening of 6xxx alloys, β'' , is, however, a needle-like precipitate. In chapter 2 an age-hardening model for Al-Mg-Si alloys has been developed considering cylindrical morphology for precipitates, with a constant aspect ratio. Results will be compared with the spherical precipitate simulation to evaluate the influence of aspect ratio on precipitation and strength evolution during ageing. Currently, the Kampmann-Wagner numerical (KWN) model [2] is one of the most realistic precipitation models, which has been applied to 6xxx alloys in this thesis. This model has the advantage of treating nucleation, growth, and coarsening as three concurrent processes, taking place simultaneously. This model is based on a finite difference method in which the flux of precipitates in and out of each size class is calculated at each time step during ageing. A comprehensive introduction of the KWN model is presented in chapter 3. An important assumption of precipitation models, including the KWN model, is the diffusion-controlled growth of precipitates. In reality, however, precipitates, under certain circumstances, grow under mixed-mode or even interface-control condition. The mixed-mode KWN model, introduced in chapter 4, has the possibility to take the character of precipitate growth into consideration. Another important issue, which will be addressed in this thesis, is the precipitation sequence. An ageing model based on the assumption of maximum Gibbs free energy dissipation is applied to model the ageing kinetics for different precipitates forming in 6xxx alloys. The proposed model is a multi-component multi-precipitate model [3], which has already been applied to Fe-based alloying systems. In this modelling framework it is possible to consider simultaneous formation of GP-zones, β'' , β' , β , and free-Si. The outputs of the ageing model are used as inputs of strengthening model to check the effects of each precipitate species on the strengthening of Al-Mg-Si alloys. The details of this model are presented in chapter 5. In chapter 6, the effects of interrupted ageing on the age hardening of 6xxx alloys have been studied. The so-called interrupted ageing is a newly proposed heat treatment cycle [4], which can potentially improve both formability

1. Introduction

and strength of Al-Mg-Si alloys. A series of experiments have been performed to explore and explain the effects of the interruption temperature on the evolution of the microstructure and mechanical properties of Al-Mg-Si alloys. In the last chapter (chapter 7) the effects of ageing on the deformation behavior of 6xxx alloys will be discussed. In this chapter, the evolution of work-hardening and dynamic recovery rates *vs.* the flow stress increase in Al-Mg-Si alloys is presented. The experimental data have been extracted from stress-strain curves and these are related to a model, employed to simulate the work-hardening behavior of Al-Mg-Si alloys. The model is based on a modified version of Kocks-Mecking-Estrin (KME) model [5], in which there are three main components; i) hardening due to forest dislocations, grain boundaries, and sub-grains, ii) hardening due to the precipitates, and iii) dynamic recovery. The modeling results are discussed and compared with the experimental data.

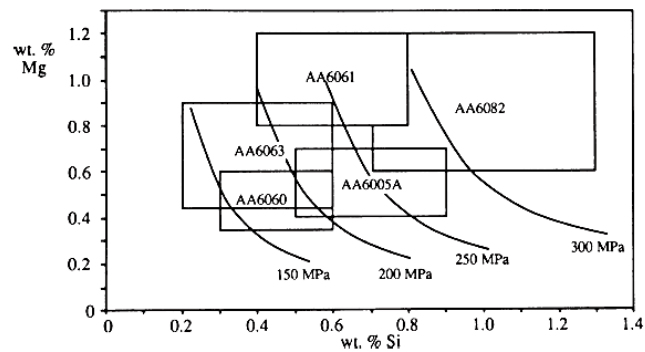


Figure 1.1: Compositional limits of some common 6xxx alloys, together with contours representing common peak aged (T6) values of yield strength [6]

References:

- [1] Shercliff HR, Ashby MF, Acta Metall Mater 38 (1990) 1789.
- [2] Myhr OR, Grong Ø, Andersen SJ, Acta Mater 49 (2001) 65.
- [3] Kozeschnik E, Svoboda J, Fratzl P, Fischer FD. Mater Science Eng A. 2004;385;157–165.
- [4] R.N. Lumley, I.J. Polmear, and A.J. Morton, Mater Sci Forum 426-432 (2003) 303-308.

1. Introduction

[5] Kocks UF, J. Eng Mater Tech, 98 (1976) 76.

[6] Polmear I, Light alloys from traditional alloys to nanocrystals, 4th edition, Elsevier 2006, p 138-142.

CHAPTER 2

An Age-Hardening Model for Al-Mg-Si Alloys Assuming the Needle-Shaped Morphology for Precipitates

In the present study an age-hardening model for Al-Mg-Si alloys has been developed considering cylindrical morphology with constant aspect ratio for precipitates. It is assumed that the precipitate distribution during underageing is controlled by simultaneous nucleation and growth and then after peak-age, it becomes coarsening-controlled. The transition from nucleation/growth regime to the coarsening regime happens when the concentration of the alloying element in the matrix becomes equal to the equilibrium concentration. The developed microstructural model is then combined with a precipitation-strengthening model to predict the evolution of yield strength of Al-Mg-Si alloys during ageing. The predictions of the model from the evolution of yield strength and length, radius, and volume fraction of precipitates are presented and compared with experimental data.

2. An Age-Hardening Model for Al-Mg-Si Alloys Assuming the Needle-Shaped Morphology for Precipitates

2.1. Introduction

Simulations of precipitation and strengthening during ageing of heat treatable aluminum alloys have gained considerable interest during the past decades [1-13]. Numerous attempts have been made to develop age-hardening models for different applications; i.e. isothermal ageing of naturally aged [2], pre-aged [1], and pre-deformed alloys [14], non-isothermal ageing [3], precipitation reactions during ageing [15], and multi-stage ageing [16,17]. The various previously developed age-hardening models use the simple assumption of spherical particles in a metal matrix. Nevertheless, the presence of the elongated needle-like β'' and rods of β' precipitates phase both oriented in $\langle 001 \rangle_{Al}$ directions is thought to be the main source of hardening [18-20]. Kelly [21] showed that the hardening due to non-shearable rod-shaped particles is greater than that produced by the equivalent number of spherical particles with the same volume. Models solving the diffusion-controlled growth of second phase with a paraboloid shape have been proposed [8]. Exact solution has been obtained for large supersaturation [9] and later extended to the case of low supersaturation [10] more suitable for solid state precipitation. Very few applications of these models exist for precipitation in aluminum alloys. Most studies deal with the precipitation of plate like precipitates [22] and only one attempt has been made to model precipitation of elongated precipitates in Al-Mg-Si alloys to predict the strength evolution during ageing [23]. The latter model, however, relies on a series of assumptions including constant supersaturation and non-shearable precipitates, and was fitted on the peak-age strength. A process model for ageing considering elongated precipitates with a more accurate strength model has also been proposed [24] but uses the semi-phenomenological JMAK equation to simulate the precipitation kinetics. The objective of the present chapter is to develop a coupled precipitation and strength model applicable to isothermal ageing of Al-Mg-Si alloys. The model is able to predict the evolution of radius and length of precipitates as well as their number density and volume fraction. The precipitates are assumed to be cylindrical with constant aspect ratio. The microstructural reactions are divided into two parts: (i) Simultaneous nucleation and growth during underageing and (ii) coarsening during overageing. In section 2 the model principles and relations are described. The model is then applied to simulate precipitation in AA6061. The results are compared with experimental data and finally conclusions regarding the relevance of considering the precipitate shape for ageing simulation are discussed.

2. An Age-Hardening Model for Al-Mg-Si Alloys Assuming the Needle-Shaped Morphology for Precipitates

2.2. Microstructure model

Precipitation is a phenomenon where the initial supersaturated alloy is decomposed into matrix and a new phase which is an agglomeration of solute atoms. The precipitation is traditionally categorized into three stages: Nucleation, growth, and coarsening. In this model, simultaneous nucleation and growth is assumed to happen first as long as the matrix concentration is higher than the equilibrium value. As soon as the mean concentration of alloying element in the matrix reaches the equilibrium value, coarsening starts. In the microstructure model, it is also assumed that there is only a single type of precipitate. These assumptions have been already successfully applied to modeling the precipitation hardening in Al-Mg-Si alloys [3-5]. In order to simplify the problem, there are some more assumptions which are given as follows:

- All the precipitates have cylindrical morphology from the beginning, meaning that there is no transition from spherical morphology to cylindrical morphology.
- The aspect ratio of precipitates is constant during ageing. This is an important approximation, whose implications will be discussed in section 4.
- The stoichiometry of precipitates is Mg_2Si from the beginning. So, there is no transition from one type of precipitate to the other one.
- The interfacial energies at the tip and at the rim of precipitates are assumed to be identical. The interfacial energy is constant during ageing and it is not dependent on ageing time, ageing temperature, and alloy composition.
- Mg diffusion in the matrix controls the kinetics of ageing.

Figure 2.1 shows the schematic representation of the assumed cylindrical morphology.

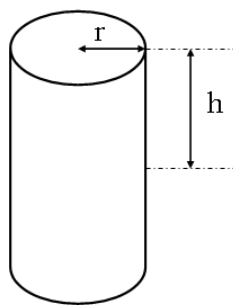


Figure 2.1: Schematic representation of the assumed cylindrical morphology for precipitates, where the aspect ratio (A) of the precipitate is defined as $A=h/r$

2. An Age-Hardening Model for Al-Mg-Si Alloys Assuming the Needle-Shaped Morphology for Precipitates

Assuming that the interfacial energies along the precipitate and at the tip of precipitate are γ_c and γ_i respectively, the total interface energy of precipitate, E_i , is

$$E_i = 2\pi r^2 \gamma_c + 4\pi r^2 A_{eq} \gamma_i, \quad (2.1)$$

with A_{eq} being the equilibrium aspect ratio, assuming that there is no strain effect. Knowing that the system tries to minimize the total interface energy, the equilibrium aspect ratio is calculated as

$$A_{eq} = \frac{\gamma_c}{2\gamma_i}, \quad (2.2)$$

In this study γ_c and γ_i are assumed to be equal, resulting in $A_{eq} = 0.5$. The reason for this assumption is the lack of information about γ_c and γ_i . The real aspect ratio of precipitates is not only a function of γ_c and γ_i but it is also dependent on the strain energy at the interfaces.

Assuming that precipitates nucleate with the cylindrical morphology, the change in the Gibbs free energy of the system due to nucleation can be written as

$$\Delta G_{nuc} = -2\pi r^2 h \Delta G_v + 4\pi r h \gamma + 2\pi r^2 \gamma, \quad (2.3)$$

where ΔG_v is the driving force per mole of solute atom to transform to precipitate from supersaturated solid solution and γ is the interfacial energy between precipitate and the matrix. Using the definition of aspect ratio ($A = h/r$), the critical radius of precipitates corresponding to the maximum of ΔG_{nuc} can be calculated as follows

$$r_{cr} = \frac{2}{3} \left(\frac{2A+1}{A} \right) \frac{\gamma}{\Delta G_v}. \quad (2.4)$$

Putting the expression of ΔG_v [23] into Eq. (2.4) yields

$$r_{cr} = \frac{2}{3} \frac{V_m \gamma}{RT} \left(\frac{2A+1}{A} \right) \left(\ln \left(\frac{C_m}{C_e} \right) \right)^{-1}, \quad (2.5)$$

where C_m is the mean concentration of Mg in the matrix, C_e is the equilibrium interfacial concentration, and V_m is the molar volume of precipitate. Putting the aspect ratio equal to 1.0 yields the classical equation for the critical radius of spherical precipitates used by Grong et al. [7]. Provided that the incubation time and elastic coherency strains around

2. An Age-Hardening Model for Al-Mg-Si Alloys Assuming the Needle-Shaped Morphology for Precipitates

the nucleated particles can be neglected the nucleation rate J is conveniently expressed as [7]

$$J = J_0 \exp\left(-\frac{\Delta G^*}{RT} - \frac{Q_d}{RT}\right), \quad (2.6)$$

where J_0 is a pre-exponential term, and Q_d the activation energy for bulk diffusion of Mg. Based on the classic theory of nucleation, Myhr et al. [16] proposed an approximate expression to calculate the energy barrier ΔG^* . This equation is given below

$$\Delta G_{het}^* = \frac{(A_0)^3}{(RT)^2 [\ln(C_m / C_e)]^2}, \quad (2.7)$$

where A_0 is a constant. Peripheral and longitudinal growth rates of a needle-like precipitate of radius r and half-length h are determined by the composition gradient outside the precipitate, the bulk diffusivity of Mg, D , and the aspect ratio of precipitates. Extending the approach of Ferrante [22] and Liu [23], the diffusion-controlled thickening and lengthening of precipitates approximately obey the following rules

$$r = \frac{2}{3} \left(\frac{C_m - C_r}{C_\beta - C_r} \right)^{1/2} \left(\frac{D}{\pi A} t \right)^{1/2}, \quad (2.8)$$

$$h = Ar, \quad (2.9)$$

where C_β is the concentration of Mg inside the precipitate, and C_r is the equilibrium interface concentration around the precipitates, taking into account the Gibbs-Thomson effect [22], given as

$$C_r = C_e \left\{ 1 + \left(1 + \frac{1}{A} \right) \frac{\gamma V_m}{RT r} \frac{1 - C_e}{C_\beta} \right\}. \quad (2.10)$$

As both C_m and C_r are a function of the degree of precipitation, the ageing time during underageing is divided into a series of smaller time intervals (Δt) in such a way that the ageing time in the i^{th} step (t_i) is given by

$$t_i = t_{i-1} + \Delta t. \quad (2.11)$$

At each time step a new population of $J\Delta t$ precipitates nucleates, having the radius equal to r_{cr} . In the meantime, other previously-formed precipitates keep growing, resulting in a size distribution. If Δt is chosen to be very small, one can assume that the change in

2. An Age-Hardening Model for Al-Mg-Si Alloys Assuming the Needle-Shaped Morphology for Precipitates

supersaturation during the time period Δt is negligible. Therefore, the increment in the radius of precipitates group j , having the radius r_j is calculated as

$$\Delta r = \frac{1}{3} \left(\frac{C_m - C_{r_j}}{C_\beta - C_{r_j}} \right)^{1/2} \left(\frac{D}{\pi A} \right)^{1/2} t^{-1/2} \Delta t, \quad (2.12)$$

being the time derivative of Eq. (2.8) and consequently the radius of precipitates in the group j in the j^{th} time step is written as

$$r_j|_i = r_j|_{i-1} + \frac{1}{3} \left(\frac{C_m - C_{r_j}}{C_\beta - C_{r_j}} \right)^{1/2} \left(\frac{D}{\pi A} \right)^{1/2} t_i^{-1/2} \Delta t. \quad (2.13)$$

Keeping track of growth of each group of precipitates formed during ageing, one can calculate the mean radius of precipitates, $\langle r \rangle$. At the end of each time step, the mean concentration of alloying element in the matrix is updated using.

$$C_m = C_0 - C_\beta \sum_j 2\pi r_j^2 h_j N_j, \quad (2.14)$$

where N_j is the number density of precipitates in the j^{th} group with radius r_j and half-length h_j . The ageing time would increase step-by-step until the calculated mean concentration of Mg in the matrix becomes equal to the equilibrium interface concentration of precipitates of smallest size. This is a numerically imposed criterion. Smallest precipitates have the highest interfacial concentration (due to Gibbs-Thomson effect). This group of precipitates is, therefore, the first group reaching the criterion $C_m < C_r$, where the growth stops (see Eq. (2.13)). From the moment that $C_m < C_r$, nucleation/growth stages is terminated and coarsening starts. According to Gibbs-Thomson equation, during coarsening, the stability of precipitates increases by increasing their size meaning that fine precipitates dissolve and bigger precipitates grow to reduce the free energy of the system. Therefore, the driving force for coarsening is provided by the difference between the size-dependent interfacial concentrations of alloying element and the concentration of alloying element in the matrix. Assuming that precipitates of the average size are in equilibrium with the matrix, the supersaturation during coarsening for a precipitate of size r can be written as [22]

$$\Omega = \frac{C_{\langle r \rangle} - C_r}{C_\beta - C_e} \approx \frac{C_{\langle r \rangle} - C_r}{C_\beta}, \quad (2.15)$$

2. An Age-Hardening Model for Al-Mg-Si Alloys Assuming the Needle-Shaped Morphology for Precipitates

where $C_{\langle r \rangle}$ is the equilibrium interfacial concentration around the precipitate of mean radius $\langle r \rangle$. The value of $C_{\langle r \rangle}$ can be obtained from Eq. (2.10) as follows

$$C_{\langle r \rangle} = C_e \left\{ 1 + \left(1 + \frac{1}{A} \right) \frac{\gamma V_m}{RT \langle r \rangle} \frac{1 - C_e}{C_\beta} \right\}. \quad (2.16)$$

Inserting the values of C_r (Eq. (2.10)) and $C_{\langle r \rangle}$ (Eq. (2.16)) into Eq. (2.15) yields

$$\Omega = \frac{\gamma V_m}{RT} \left(1 + \frac{1}{A} \right) \frac{C_e (1 - C_e)}{C_\beta^2} \left(\frac{1}{\langle r \rangle} - \frac{1}{r} \right). \quad (2.17)$$

This equation clearly shows that for precipitates bigger than $\langle r \rangle$, the supersaturation is positive meaning that during coarsening, when r is bigger than $\langle r \rangle$, precipitates keep growing. From Eq. (8), the coarsening rate can be written as

$$\frac{dr}{dt} = \frac{2}{9} \frac{D}{\pi A} \frac{\Omega}{r}. \quad (2.18)$$

Inserting the value of supersaturation from Eq. (2.17) into the coarsening rate equation yields

$$\frac{dr}{dt} = \frac{2}{9} \frac{D}{\pi} \frac{\gamma V_m}{RT} \left(\frac{1+A}{A^2} \right) \frac{C_e (1 - C_e)}{C_\beta^2} \left(\frac{r - \langle r \rangle}{r^2 \langle r \rangle} \right). \quad (2.19)$$

Figure 2.2 shows the calculated evolution of thickening rate as a function of radius of precipitate, assuming $\langle r \rangle = 2.0$ nm. As it is seen, when the radius is $2 \cdot \langle r \rangle$, the thickening rate is maximum. Using the approximation that the mean radius changes at the same rate that the maximum thickening rate [22], the coarsening rate can be written as

$$\frac{d \langle r \rangle}{dt} = \frac{1}{18} \frac{D}{\pi} \frac{\gamma V_m}{RT} \left(\frac{1+A}{A^2} \right) \frac{C_e (1 - C_e)}{C_\beta^2} \frac{1}{\langle r \rangle^2}. \quad (2.20)$$

And then, integrating this equation gives an analytical equation for precipitates radius during coarsening as follows

$$\int_{r_{PA}}^{\langle r \rangle} \langle r \rangle^2 d \langle r \rangle = \frac{1}{18} \frac{D}{\pi} \frac{\gamma V_m}{RT} \frac{1}{A} \left(1 + \frac{1}{A} \right) \frac{C_e (1 - C_e)}{C_\beta^2} \int_{t_{PA}}^t dt. \quad (2.21)$$

$$\langle r \rangle^3 = r_{PA}^3 + \frac{1}{6} \frac{D}{\pi} \frac{\gamma V_m}{RT} \frac{1}{A} \left(1 + \frac{1}{A} \right) \frac{C_e (1 - C_e)}{C_\beta^2} (t - t_{PA}). \quad (2.22)$$

2. An Age-Hardening Model for Al-Mg-Si Alloys Assuming the Needle-Shaped Morphology for Precipitates

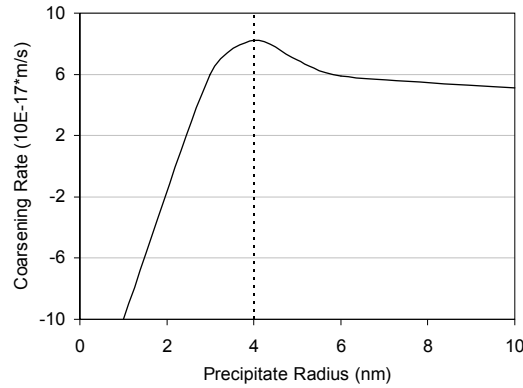


Figure 2.2: Calculated variation of thickening rate during coarsening assuming $\langle r \rangle = 2.0$ nm

2.3. Strength model

Strengthening model is a framework in which the overall strength of the artificially aged alloy can be obtained by the addition of the intrinsic strength of aluminum, the solid solution, and precipitates strength [4]. Precipitation-strengthening model is a framework which correlates the size and volume fraction of precipitates with mechanical properties. Two main mechanisms exist for precipitation hardening. When a dislocation meets a precipitate it will either cut through it, a mechanism known as shearing, or bypass the precipitate by looping around it. Shearing is more common when precipitates are relatively small, whereas bypassing is mostly seen when precipitates are large. Initial precipitation hardening involves strengthening of the alloy due to the formation of a high density of small coherent precipitates. These precipitates are sheared during deformation by moving dislocations. By increasing the ageing time, the precipitates become larger and stronger. Precipitates larger than a transition radius cannot be sheared any more and dislocation can only bypass by looping around them. This leaves an Orowan loop around the precipitates that enhances the mechanical properties of the alloy. Let F and l denote mean precipitates (obstacle) strength and effective mean precipitates distance along the dislocation line respectively. Then, precipitate-strengthening is given by [3]

$$\sigma_{ppt} = \frac{MF}{bl}, \quad (2.23)$$

2. An Age-Hardening Model for Al-Mg-Si Alloys Assuming the Needle-Shaped Morphology for Precipitates

where M is the Taylor factor and b is the Burgers vector. There are two influencing parameters in precipitation-strengthening; (i) mean precipitates strength, and (ii) effective precipitates spacing. The mean obstacle strength, F , is defined as the interaction force between the obstacle and the dislocation. Experimental observation of dislocation-precipitates interaction in Al-Mg-Si alloys reveals that precipitates are still shearable at the peak-age condition [2] and a part of them remain shearable even after a long-time overaging [24]. Based on this observation, Esmaeili et al. [2] divided the ageing process to three parts: (i) underageing up to peak-age when precipitates are shearable, (ii) peak-age point to the transition point where precipitates are still shearable, and (iii) from transition point on where precipitates behave like non-shearable particles. The transition radius, r_{trans} , is defined as the radius where the strengthening mechanism is changing from shearing mechanism to bypassing mechanism. The mean obstacle strengths at these three stages are given as, assuming m close to 0.6 [2],

$$\left\{ \begin{array}{ll} F = 2\beta Gb^2 \frac{r_{pA}^{m-1}}{r_{trans}^m} \langle r \rangle & (\langle r \rangle) < r_{pA} \quad (a) \\ F = 2\beta Gb^2 \left(\frac{\langle r \rangle}{r_{trans}}\right)^m & r_{pA} < (\langle r \rangle) < r_{trans} \quad (b) \\ F = 2\beta Gb^2 & r_{trans} < (\langle r \rangle) \quad (c) \end{array} \right. \quad (2.24)$$

where β is a constant close to 0.5. The effective obstacle spacing, l , is dependent on the obstacle strength [24]. Obstacle spacing can be estimated based on the planar center-to-center distance between precipitates. Since the most important precipitate species, β'' , is elongated in $\langle 100 \rangle_{Al}$ direction, it is very important to consider the effect of its needle-like morphology and its orientation on the effective obstacle spacing. Considering the orientation relationship between the needle-shape precipitates along $\langle 100 \rangle_{Al}$ and the $\{111\}_{Al}$ slip planes in Aluminium (see Fig. 2.3a), the intersection of the precipitates with the slip plane can be approximated by a triangular array of obstacles on the slip plane. The center-to-center obstacle spacing on the slip plane, L , can be obtained using the reference triangle ABC on the triangular array of precipitates on the slip plane (see Fig. 2.3b). Knowing that

$$H = L \cos(30^\circ). \quad (2.25)$$

The area of the triangle ABC is calculated as

2. An Age-Hardening Model for Al-Mg-Si Alloys Assuming the Needle-Shaped Morphology for Precipitates

$$A_{ABC} = \frac{\sqrt{3}}{4} L^2. \quad (2.26)$$

The number of precipitates per unit area of slip plane, N_A , is given by

$$N_A = \frac{n_a}{A_{ABC}}, \quad (2.27)$$

where n_a is the number of precipitates in the reference triangle ABC ($=0.5$). Putting the value of A_{ABC} from Eq. (2.26) into Eq. (2.27) yields

$$L = \sqrt{\frac{2}{\sqrt{3}N_A}}, \quad (2.28)$$

where N_A is obtained by [24]

$$N_A = P.N, \quad (2.29)$$

where P is the probability that a needle shape precipitate oriented along $\langle 100 \rangle_{Al}$ intersects a $\{111\}_{Al}$ plane and N is the number density of precipitates per unit volume. P can be estimated as follows [24]:

$$P = \frac{2H}{\sqrt{3}}. \quad (2.30)$$

Knowing that the volume of one precipitate is $2\pi \langle r \rangle^2 H$, the number of precipitates per unit volume is given by

$$N = \frac{f}{2\pi \langle r \rangle^2 H}, \quad (2.31)$$

Inserting Eqs. (2.29), (2.30), and (2.31) into Eq. (2.28) yields L which is the shortest center-to-center precipitate spacing

$$L = \left(\frac{2\pi}{f} \right)^{1/2} \langle r \rangle. \quad (2.32)$$

For non-shearable precipitates, the effective obstacle spacing is the center-to-center distance between precipitates ($l=L$). For shearable precipitates, the effective mean obstacle spacing is larger than the physical center-to-center distance between the precipitates. The effective obstacle spacing for these obstacles is derived based on the

2. An Age-Hardening Model for Al-Mg-Si Alloys Assuming the Needle-Shaped Morphology for Precipitates

so-called Friedel statistics [26]. The Friedel spacing (effective spacing) for shearable precipitates is given by [25]

$$l = L \left(\frac{\sqrt{3}\Gamma}{F} \right)^{1/2} = \left(\frac{2\sqrt{3}\pi\Gamma}{Ff} \right)^{1/2} \langle r \rangle, \quad (2.33)$$

where Γ is the dislocation line tension.

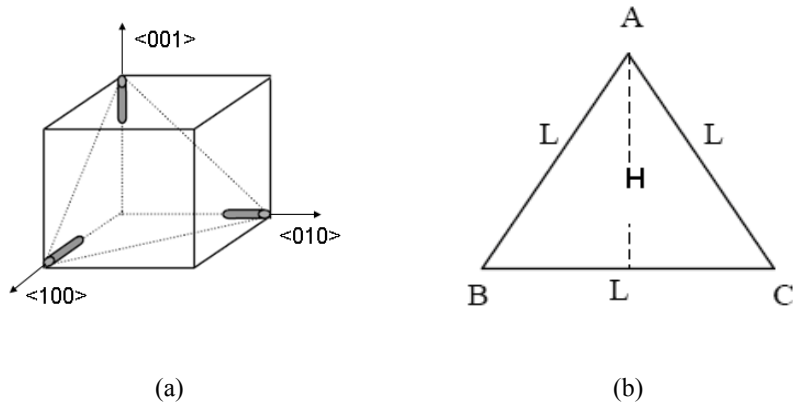


Figure 2.3: Schematic representation of a) Orientation relationship between needle-shape precipitates and a $\{111\}_{Al}$ plane of the matrix and b) Triangular array of precipitates on a $\{111\}_{Al}$ plane on the reference triangle ABC [24]

Now, the values of effective precipitate spacing for shearable and non-shearable precipitates as well as the values of mean obstacle strength are known. Inserting l and F into Eq. (2.24) gives the contribution of precipitates to the strength through the ageing as

$$\left\{ \begin{array}{l} \sigma_{ppt} = 2\beta GbM \left(\frac{f}{\sqrt{3}\pi} \right)^{1/2} \frac{r_{pA}^{\frac{3(m-1)}{2}}}{r_{trans}^{\frac{3m}{2}}} \langle r \rangle^{1/2} \quad (\langle r \rangle) < r_{pA} \quad (a) \\ \sigma_{ppt} = 2\beta GbM \left(\frac{f_{pA}}{\sqrt{3}\pi} \right)^{1/2} \frac{\langle r \rangle^{\frac{3m-1}{2}}}{r_{trans}^{\frac{3m}{2}}} \quad r_{pA} < (\langle r \rangle) < r_{trans} \quad (b) \\ \sigma_{ppt} = 2\beta GbM \left(\frac{f_{pA}}{2\pi} \right)^{1/2} \frac{1}{\langle r \rangle} \quad r_{trans} < (\langle r \rangle) \quad (c) \end{array} \right. , \quad (2.34)$$

2. An Age-Hardening Model for Al-Mg-Si Alloys Assuming the Needle-Shaped Morphology for Precipitates

where f_{PA} is the volume fraction of precipitates at peak-age. Assuming that different strengthening contributions to the overall strength can be added linearly, the yield strength of Al-Mg-Si alloys can be obtained as

$$\sigma_y = \sigma_i + \sigma_{ss} + \sigma_{ppt}, \quad (2.35)$$

where σ_i is the yield strength of pure aluminium chosen as 10 MPa [3], σ_{ss} is the solid solution strengthening term, given by [3]

$$\sigma_{ss} = \sum_{j=Mg, Si, Cu} k_j C_j^{2/3}, \quad (2.36)$$

where k_j is a constant with a specific value for element j .

2.4. Model implementation

In this model, it is assumed that all precipitates are cylindrical with a constant aspect ratio which is a chosen parameter. The alloy used to check the validity of the model is AA6061 (1.12 wt% Mg, 0.57 wt% Si, 0.25 wt% Cu). Assuming that all Si atoms take part in precipitation, the chemical composition of the alloy is balanced. The equilibrium interfacial concentration of Mg for a flat interface, C_e , is given by

$$C_e = (970 \text{ wt}\%) \exp\left(\frac{-Q_s}{RT}\right). \quad (2.37)$$

In the strength model there are two important radii: r_{PA} and r_{trans} . The value r_{PA} is dependent on the ageing temperature and chosen aspect ratio. The microstructure model is developed in such a way that at peak-age the precipitation reaction is changing from nucleation-growth regime to coarsening regime, assuming that at peak-age the mean concentration of alloying elements in the matrix is equal to the equilibrium concentration, C_r^{peak} . Rewriting Eq. (2.14) at peak-age yields

$$C_r^{peak} = C_0 - 2C_\beta \pi r_{PA}^3 AN_{PA}, \quad (2.38)$$

where N_{PA} is the number density of precipitates at peak-age. r_{PA} is obtained by rearranging Eq. (2.38), assuming that C_r^{peak} is very small compared to C_0 , as

$$r_{PA} = \left(\frac{C_0}{2\pi AN_{PA} C_\beta} \right)^{1/3}. \quad (2.39)$$

2. An Age-Hardening Model for Al-Mg-Si Alloys Assuming the Needle-Shaped Morphology for Precipitates

As it is seen, r_{PA} is a function of aspect ratio, the maximum number density of precipitates, which is obtained from the simulation, the initial concentration of alloying elements, and the concentration in the precipitate. Another important parameter in the strength model is the transition radius, r_{trans} , at which the strengthening mechanism changes from shearing to bypassing. Cheng et al. [27] proposed that for the alloy AA6111 the shearable to non-shearable transition occurs when yield strength is equal to $0.8\sigma_{PA}$ (σ_{PA} is the yield strength at peak-age). Assuming that this is also the case in alloy AA6061 and knowing that the peak-strength of the alloy AA6061 is in the range of 250-270 MPa, σ_{ppt} at the transition point, σ_{ppt}^{trans} , is given by

$$\sigma_{ppt}^{trans} = 0.8\sigma_{PA} - \sigma_i - \sigma_{ss} . \quad (2.40)$$

σ_{ppt}^{trans} can also be obtained from Eq. (2.34c). Equating σ_{ppt}^{trans} from Eq. (2.34c) with σ_{ppt}^{trans} from Eq. (2.34) give the value of r_{trans} as follows

$$r_{trans} = \frac{2\beta GbM}{\sigma_{ppt}^{trans}} \left(\frac{f_{PA}}{2\pi} \right)^{1/2} . \quad (2.41)$$

Assuming that the volume per atom is constant, by the lever rule of phase equilibria, the final volume fraction of precipitates at the peak-age can be approximated as:

$$f_{peak} = \frac{C_0 - C_e}{C_\beta - C_e} . \quad (2.42)$$

Also, the modelling results show that σ_{ss} at the transition point is around 20-50 MPa. Depending on the chosen values, r_{trans} is varied between 3.0 nm to 4.0 nm. In the developed model the approximate value of 3.5 nm is used for all conditions. Table 2.1 shows the input data used in the microstructure and strength model.

2. An Age-Hardening Model for Al-Mg-Si Alloys Assuming the Needle-Shaped Morphology for Precipitates

Table 2.1: Summary of input data used for the KWN and strengthening model [3]

Input parameter	Value	Input parameter	Value
C_β (wt%)	63.0	γ (J/m ²)	0.26
D_0 (m ² /s)	2.2×10^{-4}	r_{trans} (nm)	3.5
Q_d (kJ/mol)	130	M	2.6-3.1
Q_s (kJ/mol)	45.35	β	0.3-0.5
j_0 (#/m ³ s)	3.07×10^{36}	b (m)	2.84×10^{-10}
V_m (m ³ /mol)	7.62×10^{-5}	G (N/m ²)	2.7×10^{10}
k_{Si} (MPa/wt% ^{2/3})	66.3	k_{Mg} (MPa/wt% ^{2/3})	29.0
k_{Cu} (MPa/wt% ^{2/3})	46.4	A_0 (kJ/mol)	16

2.5. Modeling results

Figure 2.4 shows the simulation of the length of precipitates in the alloy AA6061 during ageing at 190 °C together with experimental data. The aspect ratio is adjusted to get the right value for the length of precipitate at peak-age (≈ 10 ks). The aspect ratio which gives the correct prediction of peak-length is 10. In the underage regime the model slightly overestimates the length of precipitates, showing the highest overestimation in the beginning of ageing. By increasing the ageing time, the difference between the modelling results and experimental data becomes smaller. In the overage regime, the modelling results are in good agreement with experimental data.

2. An Age-Hardening Model for Al-Mg-Si Alloys Assuming the Needle-Shaped Morphology for Precipitates

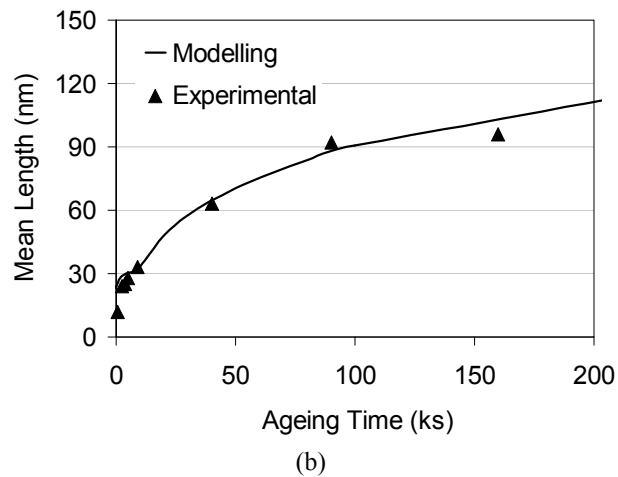
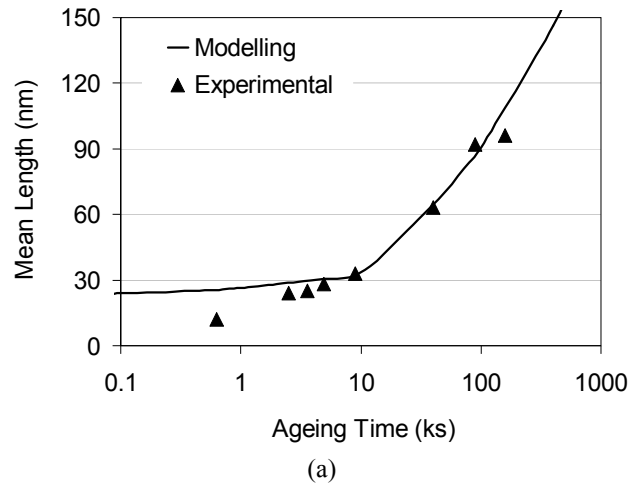


Figure 2.4: Prediction of the length of precipitates in the alloy AA6061 aged at 190 °C in the a) Log-scale and b) linear scale (Experimental data is from Ref [23], the error bar is approximately the size of symbols)

Figure 2.5 shows the prediction of the volume fraction of precipitates in the alloy AA6061 aged at 190 °C together with experimental data. As it is seen the model shows a faster ageing kinetics during underageing compared to the real ageing kinetics. This is possibly due to the assumption of the incubation time being zero. Besides, the maximum precipitate volume fraction, predicted by the model is slightly higher than the

2. An Age-Hardening Model for Al-Mg-Si Alloys Assuming the Needle-Shaped Morphology for Precipitates

experimental maximum value. This is due to the fact that it is assumed that all Si atoms are all consumed during precipitation. In reality, a part of Si-content of the alloy is used by Fe- and Mn-containing particles. Figure 2.6 shows the effects of aspect ratio on the evolution of number density, mean radius, volume fraction, and precipitate spacing during ageing at 190 °C. The model shows that precipitates with $A=1$ have maximum values of both number density and mean radius compared to precipitates of $A=10$ and $A=50$. The fact that precipitates of $A=1$ are thicker is in accordance with Eq. (2.6), where the lower aspect ratio results in a higher thickening rate. Figure 2.6c shows that even though both the number density and thickness of precipitates in case $A=1$ are higher compared to those of precipitates with $A=10$ and $A=50$, the volume fraction of precipitate in the underage regime (when $A=1$) shows the lowest magnitude. This is due to the fact that longer precipitates have larger volumes (and therefore lower number density). This also has an effect on the precipitate spacing, as is seen in Fig. 2.6d, where initially, the mean precipitate distance is largest for precipitates of $A=1$. The difference between the mean precipitate distance for precipitates of different aspect ratio decreases until the peak-age. At peak-age the mean precipitate distance values for different aspect ratios are very similar.

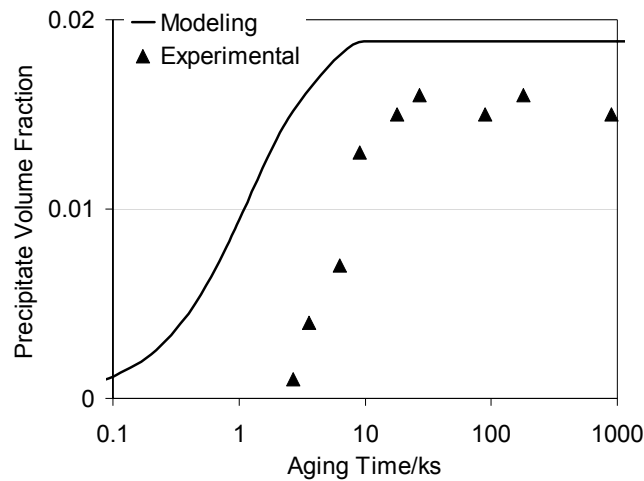


Figure 2.5: Prediction of the precipitate volume fraction in the alloy AA6061 aged at 190 °C (Experimental data is from Ref [23]; the error bar is in the range of the size of symbols)

2. An Age-Hardening Model for Al-Mg-Si Alloys Assuming the Needle-Shaped Morphology for Precipitates

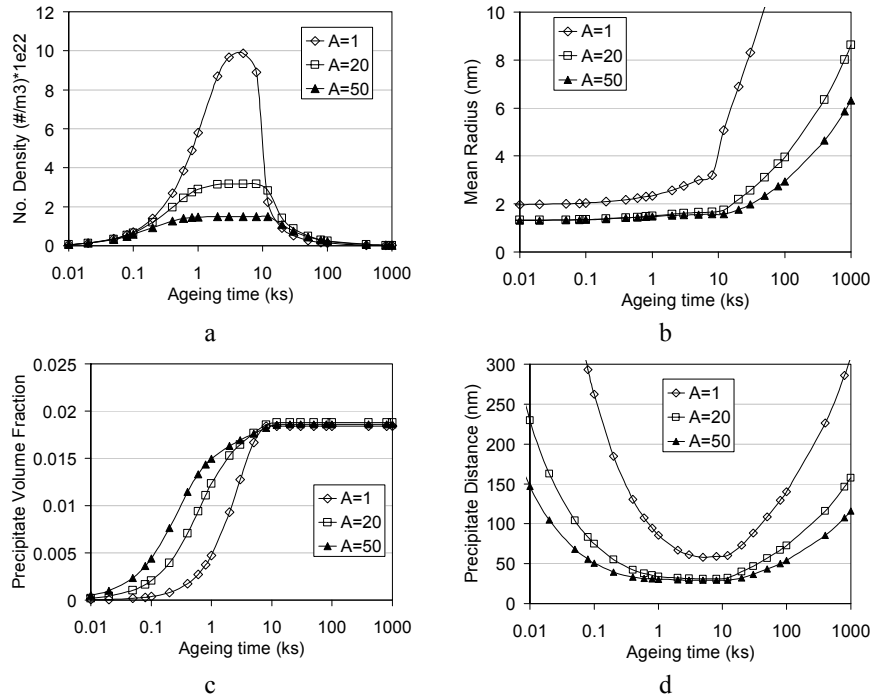


Figure 2.6: Prediction of the a) precipitate number density, b) mean radius, c) volume fraction, and d) precipitate mean distance for the AA6061 aged at 190 °C, assuming different values for aspect ratio

Figure 2.7 shows the effects of aspect ratio on the predicted yield strength of the alloy AA6061. Clearly, the higher the aspect ratio, the faster the hardening kinetics. Also, the yield strength on the whole increases by increasing aspect ratio. This is more pronounced in the underage regime. Figure 2.8 shows the prediction of the yield strength of the alloy AA6061 at different temperatures, using $A=10$, compared with experimental data. Except for ageing temperature 170°C in which there is a reasonably good agreement between model and experiment, the model overestimates the yield strength of the alloy AA6061 in both underage and overage regimes. The overestimation is however more pronounced in the underage regime.

2. An Age-Hardening Model for Al-Mg-Si Alloys Assuming the Needle-Shaped Morphology for Precipitates

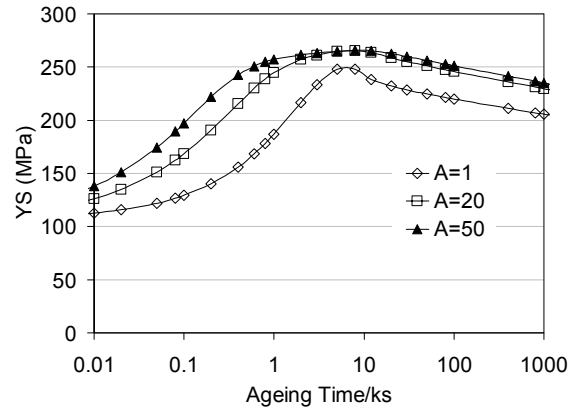


Figure 2.7: Effects of A on the predicted YS of the alloy AA6061 aged at 190 °C

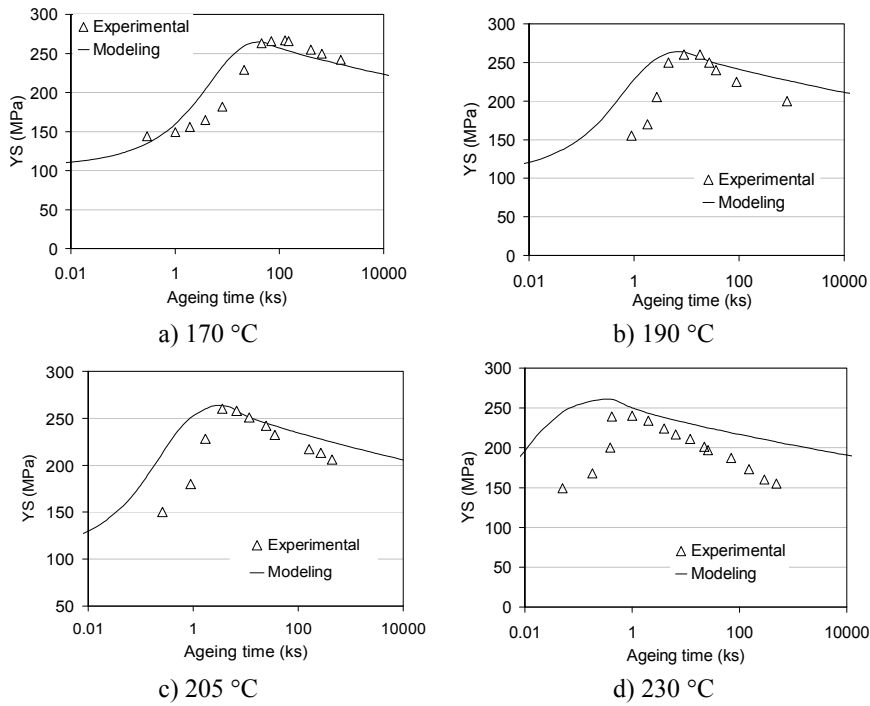


Figure 2.8: Prediction of YS of the alloy AA6061 aged at different temperatures assuming $A=10$ (Experimental data is from Ref [23]; the error bar is in the range of the size of symbols)

2. An Age-Hardening Model for Al-Mg-Si Alloys Assuming the Needle-Shaped Morphology for Precipitates

Figure 2.9 shows the comparison between the modelling results for $A=1$ with the case when $A=10$. Obviously, for $A=1$, the model yields a better fit for the yield strength of the alloy in the underage regime. However, the peak-strength is predicted more accurately when $A=10$. Also it is interesting to note that the yield strength at the early stage of coarsening is predicted very well when $A=10$, while when $A=1$, the model underestimates the yield strength in the beginning of coarsening. This is changed by increasing the overageing time in such a way that the model with $A=1$ becomes more accurate, while the model with $A=10$ gradually loses its accuracy.

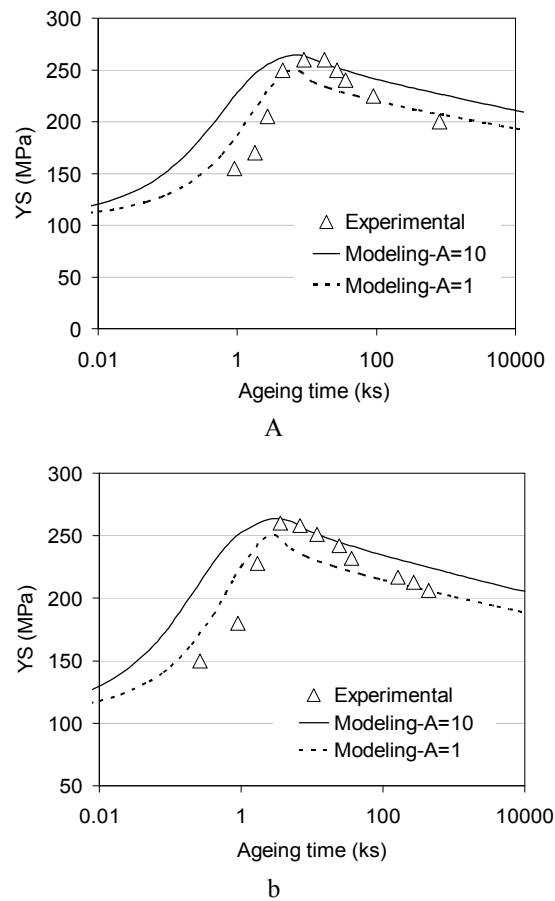


Figure 2.9: Prediction of YS of the alloy AA6061 aged at a) 190 °C and b) 205 °C using $A=1$ and $A=10$ (Experimental data is taken from Ref [23])

2. An Age-Hardening Model for Al-Mg-Si Alloys Assuming the Needle-Shaped Morphology for Precipitates

2.6. Discussion

The precipitation sequence in Al-Mg-Si alloys is very complex with a series of precipitates having different morphologies. β'' phase, the most important precipitate in terms of strengthening, is a needle-like precipitate. Apart from that, other precipitates including pre- β'' , β' , and Q' have elongated cylindrical morphologies. Therefore, having a model which is able to predict the evolution of precipitates radius and length would be more realistic than having an ageing model based on the assumption of spherical morphology for precipitates. An age-hardening model has been developed considering a cylindrical morphology for precipitates. The model is fitted in such a way that it gives a right prediction of the precipitates mean-length in the alloy AA6061 aged at 190 °C. With the fitted value of aspect ratio equal to 10 the model yields a reasonably good prediction of precipitates mean-length in the overage regime (see Fig. 2.4). However, it overestimates the mean length in the underage regime. The reason for this overestimation is that not all precipitates formed in the beginning of ageing have a needle-like morphology. Especially a large portion of GP-zones have spherical morphology. Figure 2.10 shows the morphological evolution of precipitates in a Al-Mg-Si taken from literature. It is clearly seen that even in the alloy aged for four hour at 190 °C (see Fig. 2.10c), a large fraction of precipitates still are not very well elongated. In addition, the aspect ratio of β'' phase is changing during the ageing process in such a way that it initially increases up to a maximum value and thereafter decreases [23], meaning that in the beginning of ageing and in the very end of overage regime, the value 10 is too high for the aspect ratio of precipitates. For this reason, the yield strength in the beginning of ageing and in the very end of overageing is predicted more accurately when $A=1$ (see Fig. 2.9). The aspect ratio of precipitates is influenced not only by ageing time but also by ageing temperature. At higher ageing temperatures, the aspect ratio becomes lower due to a smaller lengthening driving force and the readily occurred loss of coherency or semi-coherency of peripheral plane [23]. This would results in a stronger deviation of predicted yield strength from the experimental values in case $A=10$, when ageing temperature increase.

2. An Age-Hardening Model for Al-Mg-Si Alloys Assuming the Needle-Shaped Morphology for Precipitates

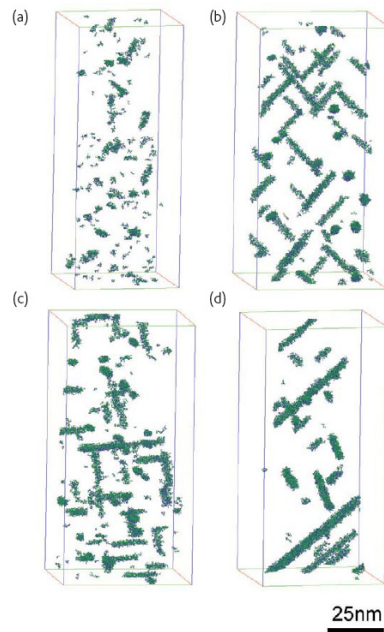


Figure 2.10: Atom maps showing the 3D elemental distribution in an Al-0.5 wt. % Mg-1.0 wt. % Si alloy aged at 180°C for a) 0.6 ks, b) 1.8 ks, c) 14.4 ks, and d) 64.8 ks [28]

Precipitation strengthening has two main contributions from the strength of each individual precipitates through the precipitate strength, F , and from the kinetics of ageing through the effective precipitate distance l . In order to separate these two effects suppose that the number density and volume fraction of precipitates are not dependent on the chosen value of aspect ratio, i.e. the volume fraction and number density of precipitates for the case $A=1$ are supposed to be the same for the case $A=20$ and $A=50$. The only difference in this case is the difference between radius and length of precipitates, i.e. shape difference. Figure 2.11 shows the evolution of σ_{ppt} in the alloy AA6061 with different aspect ratio and similar number density and volume fraction. As it is seen if there is no kinetics effect, the evolution of strength up to peak-age is the same. This implies that in the underage regime the effects of precipitates thickness and number of precipitate/slip-plane intersections are cancelling. For example, when precipitates become thinner, they become weaker (due to lower F). However, they also become longer having more intersections with slip planes and consequently having lower l . So, in the underage regime the morphology by itself does not have a significant

2. An Age-Hardening Model for Al-Mg-Si Alloys Assuming the Needle-Shaped Morphology for Precipitates

effect on the yield strength. The difference in the yield strength of the alloy at underage regime, as is seen in Fig. 2.7, is just a kinetics effect (see Fig. 2.6). Longer precipitates, due to the faster kinetics in the underage regime (see Fig. 2.6c), have more intersections with slip planes (less precipitates distances as is shown in Fig. 2.6d), making their contributions to yield strength higher. By entering the overageing regime, the strength becomes independent of F . It is also obvious that the ageing kinetics does not have any influence on the yield strength, since both number density and volume fraction are the same, independent of aspect ratio (see Fig. 2.6a, c). This implies that the only influencing parameter in the overage regime is the shape of the precipitates. The longer precipitate, the higher the density of precipitate/slip-plane intersections, leading to higher strength. Looking at Figure 2.11 one can conclude that this effect, however, is not particularly strong.

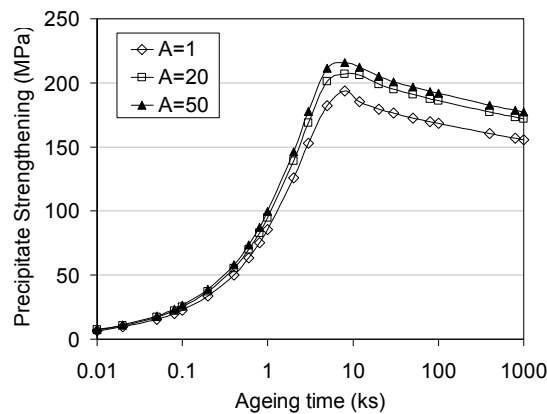


Figure 2.11: Precipitate strengthening in alloy AA6061 at 190 C for different values of aspect ratio, assuming similar number density and volume fraction

2.7. Summary

A precipitation strengthening model is developed for Al-Mg-Si alloys, assuming cylindrical morphology with a constant aspect ratio for precipitates. The model is applied to the alloy AA6061 and the obtained results are compared with experimental data. Out of the results of this study, the following conclusions can be drawn:

- Choosing a constant value for the aspect ratio results in an overestimation of precipitates mean-length in the underage regime. This is due to the fact that the

2. An Age-Hardening Model for Al-Mg-Si Alloys Assuming the Needle-Shaped Morphology for Precipitates

aspect ratio of precipitates in the underage regime varies from values close to one to its maximum value.

- Needle-like precipitates with higher aspect ratio have more positive contributions to yield strength compared to precipitates of lower aspect ratio.
- When $A=1$, the model yields a better fit for the yield strength of the alloy in the underage regime. However, the peak-strength is predicted more accurately when $A=10$.
- The yield strength at the early stage of coarsening is predicted very well when $A=10$, while when $A=1$, the model underestimates the yield strength in the beginning of coarsening.
- By increasing the overageing time the model with $A=1$ becomes more accurate, while the model with $A=10$ gradually loses its accuracy.
- Ageing models assuming elongated precipitates of constant aspect ratio do not give an overall better prediction of precipitation and strength evolution during ageing and the assumption of spherical precipitates remains, as a first approximation, an acceptable assumption.
- Improving ageing prediction would require the development of models capable of simulating non-constant aspect ratio and, therefore, a better knowledge of interfacial energy and interface reaction kinetics as a function of the precipitate-matrix interface character. Such information is, however, currently not available with enough details to be incorporated in numerical models.

References:

- [1] Esmaeili S and Lloyd DJ, *Acta Mater* 53 (2005) 5257.
- [2] Esmaeili S, Lloyd DJ, and Poole WJ, *Acta Mater* 51 (2003) 2243.
- [3] Myhr OR, Grong Ø, and Andersen SJ, *Acta Mater* 49 (2001) 65.
- [4] Myhr OR and Grong Ø, *Acta Metall Mater* 39 (1991) 2693.
- [5] Myhr OR and Grong Ø, *Acta Metall Mater* 39 (1991) 2703.
- [6] Schercliff HR and Ashby MF, *Mater Sci Tech* 7 (1991) 85.
- [7] Myhr OR and Grong Ø, *Acta Mater* 48 (2000) 1605.
- [8] Horvay G and Cahn WJ, *Acta Metall* 9 (1961) 695.
- [9] Trivedi R, *Acta Metall* 18 (1970) 287.
- [10] Rivera-Diaz-del-Castillo PEJ and Bhadeshia HKDH, *Mater Sci Tech* 17 (2001) 25.

2. An Age-Hardening Model for Al-Mg-Si Alloys Assuming the Needle-Shaped Morphology for Precipitates

- [11] Aaronson HI, Kinsman KR, and Russell KC, *Scripta Mater* 4 (1970) 101.
- [12] Shercliff HR and Ashby MF, *Acta Metall Mater* 38, No. 10 (1990) 1789.
- [13] Shercliff HR and Ashby MF, *Acta Metall Mater* 38, No. 10 (1990) 1803.
- [14] Deschamps A and Brechet Y, *Acta Mater* 47 (1999) 293.
- [15] Bratland DH, Grong Ø, Shercliff HR, Myhr OR, and Tjøtta ST, *Acta Mater* 45 (1997) 1.
- [16] Myhr OR, Grong Ø, Faejr HG, and Marioara CD, *Acta Mater* 52 (2004) 4997.
- [17] Grong Ø and Schercliff HR, *Progress in Mater Sci* 47(2002) 163.
- [18] Miao WF and Laughlin DE, *Scripta Mater*, Vol. 40, No. 7 (1999) 873.
- [19] Nie JF, Muddle BC, and Polmear IJ, *Mater Sci Forum Vols. 217-222* (1996) 1257.
- [20] Russell KG, and Ashby F, *Acta Meter* 18 (1970) 891.
- [21] Kelly PM, *Scripta Metall* 6 (1972) 647.
- [22] Ferrante M and Doherty RD, *Acta Metall* 27 (1979) 1603.
- [23] Liu G, Zhang GJ, Ding XD, Sun J, and Chen KH, *Mater Sci Eng A344* (2003) 113.
- [24] Esmaeili S, *Precipitation hardening behavior of AA6111*, PhD thesis, Feb. 2002, p. 132.
- [25] Ardell AJ, *Metall Trans A1985* 16 (12) 2131.
- [26] Friedel J., (1962), in *Electron Microscopy and Strength of Crystals*, eds., Thomas G. & Washburn J., Interscience Publishers, New York, NY, 605.
- [27] Cheng LM, Poole WJ, Embury JD and Lloyd DJ (2001), *Metall Mater Trans* 34A, Nov. 2003, p. 2473.
- [28] Cerezo A, Clifton PH, Galtrey MJ, Humphreys CJ, Kelly TF, Larson DJ, Lozano-Perez S, Marquis EA, Oliver RA, Sha G, Thompson K, Zandbergen M, and Alvis RL, *Atom Probe Tomography Today, Materials today* 10 (2007) 36.

CHAPTER 3

Modelling the Age-Hardening Behavior of Al-Mg-Si Alloys Considering Simultaneous Nucleation, Growth and Coarsening during Precipitation

The Kampmann-Wagner numerical (KWN) framework has been applied to model precipitation behavior of Al-Mg-Si alloys. The KWN model is a finite difference method for modelling coupled nucleation, growth, and coarsening. In this method, the precipitate distribution is divided into a series of discrete size classes. The flux of precipitates in and out of each size class is calculated at each time step during ageing. A strength model is then applied to predict the yield strength, taking into account the contributions of precipitation and solid solution hardening. The model is validated using microstructure and yield strength data for some Al-Mg-Si alloys.

3. Modelling the Age-Hardening Behavior of Al-Mg-Si Alloys Considering Simultaneous Nucleation, Growth and Coarsening during Precipitation

3.1. Introduction

The majority of phase transformations, including precipitation of a second phase from a supersaturated matrix, involve three major reactions, i.e. nucleation, growth and coarsening. Nucleation, the initial stage in precipitation, is a stochastic process started by microscopic compositional fluctuations in the matrix. Growth is the controlled attachment of atoms to the precipitate, driven by thermodynamic driving forces. The growth process involves the long-range diffusion of atoms from the matrix towards precipitates. In case precipitate and matrix have different crystal structures, there is also a short-range atomic rearrangement at the precipitate/matrix interface. In most cases diffusion is often the slower process and, therefore, the rate-controlling reaction [1]. The last process, coarsening, is defined as the dissolution of small precipitates in favor of larger ones, driven by the Gibbs–Thomson effect. Modelling of precipitation, involving nucleation, growth, and coarsening has recently gained a lot of attention [1-6]. Among different available models, the Kampmann-Wagner-Numerical (KWN) framework is the best option for modelling coupled nucleation, growth and coarsening. The KWN model is essentially a finite difference method, where the relevant range of precipitate size is divided into a series of size classes. At each time step the flux of particles in and out of each size class is calculated, resulting in the prediction of the precipitate size distribution. The effect of supersaturation, interfacial energy, and solute diffusivity on the overlap between nucleation, growth and coarsening during precipitation has already been studied using the KWN method [7]. It has been shown that the interfacial energy strongly affects the extent of overlap. However, the solute diffusivity more strongly influences the kinetics of transformation than the overlap between precipitation reactions [7]. In this chapter, first the KWN model is introduced and then applied to some cases. Spherical precipitates are assumed, which was shown to be an acceptable approximation in chapter 2. The predictions of the model are compared with the experimental data to check the predictive power of the model. In the next chapter a modified version of the KWN model will be introduced in which the mixed-mode character of precipitation has been taken into account.

3.2. Kampmann-Wagner-Numerical (KWN) model

The Kampmann-Wagner numerical (KWN) precipitation model developed by Myhr et al. [3] is used. The model consists of the following three parts:

3. Modelling the Age-Hardening Behavior of Al-Mg-Si Alloys Considering Simultaneous Nucleation, Growth and Coarsening during Precipitation

a) A model for the nucleation of precipitates. If the incubation time is neglected, the steady state nucleation rate is expressed as:

$$j = j_0 \exp\left(-\frac{\Delta G^*}{RT} - \frac{Q_d}{RT}\right), \quad (3.1)$$

where j is the nucleation rate, j_0 is a pre-exponential term, ΔG^* is the energy barrier for nucleation, Q_d is the activation energy for the diffusion of the controlling alloying element (here Mg), R is the universal gas constant and T the temperature. Considering heterogeneous nucleation, Myhr et al. proposed the following equation for energy barrier for nucleation [3]

$$\Delta G^* = \frac{(A_0)^3}{(RT \ln(C_m / C_e))^2}, \quad (3.2)$$

where C_m is the mean concentration of alloying element (in this model Mg) in the matrix, C_e is the equilibrium solute concentration at the matrix/precipitate interface (without the Gibbs-Thomson effect), and A_0 is a constant related to the heterogeneous nucleation sites [3]. The solubility limits for Mg and Si can be used to calculate the value of C_e . The solubility limit for Mg and Si in the aluminum matrix, assuming the stoichiometry Mg_2Si for precipitates, can be expressed as

$$[C_e^{Mg}]^2 [C_e^{Si}] = \exp\left(\frac{-\Delta H_0}{RT}\right) \exp\left(\frac{\Delta S_0}{R}\right), \quad (3.3)$$

where ΔH_0 and ΔS_0 are the standard enthalpy and entropy of formation of Mg_2Si precipitate. When the alloy is balanced or it has some Si in excess the following empirical equation is proposed to calculate C_e for Mg element

$$C_e = C_s \exp\left(-\frac{Q_s}{RT}\right), \quad (3.4)$$

where C_s is a pre-exponential factor and Q_s is the apparent solvus boundary enthalpy.

b) A rate law, which calculates either the growth or dissolution of precipitates in each size class. If the precipitates are assumed spherical and the growth is controlled by the diffusion of alloying elements, the rate at which the precipitates grow or dissolve is given by:

3. Modelling the Age-Hardening Behavior of Al-Mg-Si Alloys Considering Simultaneous Nucleation, Growth and Coarsening during Precipitation

$$v = \frac{dr}{dt} = \frac{C_m - C_r}{C_\beta - C_r} \frac{D}{r}, \quad (3.5)$$

where D is the diffusion coefficient of alloying element (in this model Mg), r is the radius of precipitates, C_β is the concentration of alloying element in the precipitate, and C_r is the equilibrium concentration of alloying element at the precipitate/matrix interface considering Gibbs-Thomson effect. C_r is given by

$$C_r = C_e \exp\left(\frac{2\gamma V_m}{rRT}\right), \quad (3.6)$$

where γ is the interfacial energy and V_m is the molar volume of precipitate.

c) A continuity equation, which keeps a record of the flux of precipitates. The continuity equation is expressed as:

$$\frac{\partial N(r,t)}{\partial t} = -\frac{\partial(N(r,t)v(r,t))}{\partial r} + \delta(r - r_{cr}(t))j(t), \quad (3.7)$$

where N is the number density of precipitates of size r , δ is the Kronecker delta, and r_{cr} is the critical radius of precipitates taken as the radius of the nuclei and given by

$$r_{cr} = \frac{2\gamma V_m}{RT} \left(\ln\left(\frac{C_m}{C_e}\right) \right)^{-1}, \quad (3.8)$$

In this model precipitates smaller than r_{cr} dissolve and precipitates bigger than r_{cr} grow. Applying a partitioning of the precipitate size distribution in a finite number of size classes, the number of precipitates in each size interval, N_i , is given by

$$N_i = \int_{r_i}^{r_{i+1}} N(r,t) dr. \quad (3.9)$$

Applying this equation to equation (3.7) yields

$$\frac{\partial N_i}{\partial t} = -\int_{r_i}^{r_{i+1}} \frac{\partial(Nv)}{\partial r} dr + \int_{r_i}^{r_{i+1}} \delta(r - r_{cr})j dr \quad (3.10)$$

Depending on the sign of growth function, equation (3.10) may be written [8]

$$\frac{\partial N_i}{\partial t} = -\frac{N_i}{\Delta r} v(r_{i+1},t) + \frac{N_{i-1}}{\Delta r} v(r_i,t) + \delta_{ij} j(t) \quad (v(r_{i+1},t) > 0 \text{ and } v(r_i,t) > 0). \quad (3.11)$$

3. Modelling the Age-Hardening Behavior of Al-Mg-Si Alloys Considering Simultaneous Nucleation, Growth and Coarsening during Precipitation

$$\frac{\partial N_i}{\partial t} = -\frac{N_i}{\Delta r} v(r_{i+1}, t) + \frac{N_i}{\Delta r} v(r_i, t) + \delta_{ij} j(t) \quad (v(r_{i+1}, t) > 0 \text{ and } v(r_i, t) < 0). \quad (3.12)$$

$$\frac{\partial N_i}{\partial t} = -\frac{N_{i+1}}{\Delta r} v(r_{i+1}, t) + \frac{N_{i-1}}{\Delta r} v(r_i, t) + \delta_{ij} j(t) \quad (v(r_{i+1}, t) < 0 \text{ and } v(r_i, t) > 0). \quad (3.13)$$

$$\frac{\partial N_i}{\partial t} = -\frac{N_{i+1}}{\Delta r} v(r_{i+1}, t) + \frac{N_i}{\Delta r} v(r_i, t) + \delta_{ij} j(t) \quad (v(r_{i+1}, t) < 0 \text{ and } v(r_i, t) < 0). \quad (3.14)$$

Δr is the width of a size class, and r_{cr} falls in class j . Figure 3.1 shows schematic of the KWN algorithm used to model precipitation in Al-Mg-Si alloys.

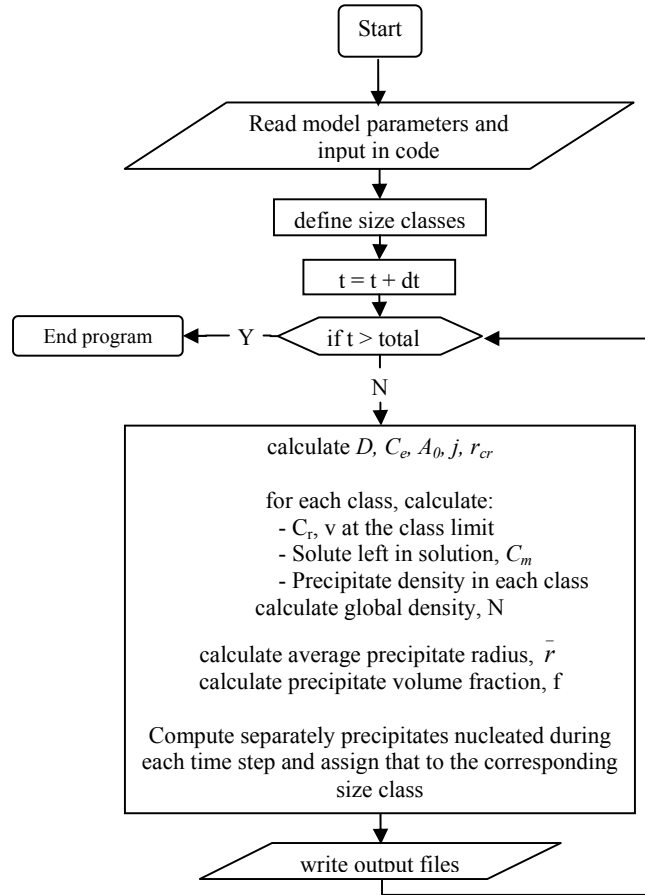


Figure 3.1: Algorithm of KWN method

3. Modelling the Age-Hardening Behavior of Al-Mg-Si Alloys Considering Simultaneous Nucleation, Growth and Coarsening during Precipitation

3.3. Strengthening model

Al-Mg-Si alloys are precipitation-hardened alloys, meaning that precipitates play the main role in the strengthening. In the beginning of ageing precipitates are more likely to be coherent and dislocations can cut through them, as illustrated in Figure 3.2 (TEM image of the alloy AA6111 after 2 months ageing at 180 °C and 5% deformation). It can be observed in Fig. 3.2a that the precipitate has been bent due to the passage of many dislocations on parallel planes. Figure 3.2b is an example of a high resolution TEM image of one precipitate in the sample. The steps on the precipitate–matrix interface clearly indicate that the precipitate has been sheared by the glide dislocations. In contrast, in a very over-aged sample, there is no evidence that the precipitates are sheared [9]. As the size of precipitates increases during ageing, it becomes increasingly difficult for dislocations to cut through larger precipitates. In this case dislocations start bowing around precipitates and at sufficiently large stresses, the two dislocation sides meet and thus recombine with each other, leaving Orowan loops around precipitates. Every time a dislocation bows around a precipitate, it leaves an Orowan loop around the precipitate and therefore dislocation density increases with increasing plastic strain. For the case of alloy AA6111 aged for 7 days at 250 °C and then deformed up to 1, 2 and 5%, dislocation lines are tangled between the precipitates, as illustrated in Figure 3.3. It is notable that by increasing the plastic strain, the density of accumulated Orowan loops increases. Assuming that different strengthening contributions to the overall strength can be added linearly, the yield strength of Al-Mg-Si alloys can be expressed as

$$\sigma_y = \sigma_i + \sigma_{ss} + \sigma_{ppt} , \quad (3.15)$$

where σ_i is the yield strength of pure aluminum, chosen as 10 MPa [3], σ_{ss} is the solid solution strengthening term, and σ_{ppt} is the precipitation strengthening term. σ_{ss} is given by [3]

$$\sigma_{ss} = \sum_{j=Mg, Si, Cu} k_j C_j^{2/3} , \quad (3.16)$$

where k_j is a constant with a specific value for element j [3]. For spherical precipitates, σ_{ppt} equals [3]

$$\sigma_{ppt} = \frac{M}{(2\beta G)^{1/2} b^2 \langle r \rangle} \left(\frac{3f}{2\pi} \right)^{1/2} \left(\frac{\sum_i N_i F_i}{\sum_i N_i} \right)^{3/2} , \quad (3.17)$$

3. Modelling the Age-Hardening Behavior of Al-Mg-Si Alloys Considering Simultaneous Nucleation, Growth and Coarsening during Precipitation

where $\langle r \rangle$ is the mean precipitate radius, M is the Taylor factor, f is the volume fraction of precipitates, β a dislocation-line tension related parameter, G is the shear modulus of precipitates, and F_i is the strength of precipitates in i^{th} size class given by

$$\begin{cases} F_i = 2\beta Gb^2 \left(\frac{r_i}{r_{trans}}\right) & \text{for } r_i < r_{trans} \\ F_i = 2\beta Gb^2 & \text{for } r_i \geq r_{trans} \end{cases}, \quad (3.18)$$

where r_{trans} is the transition radius above which the precipitate is non-shearable.

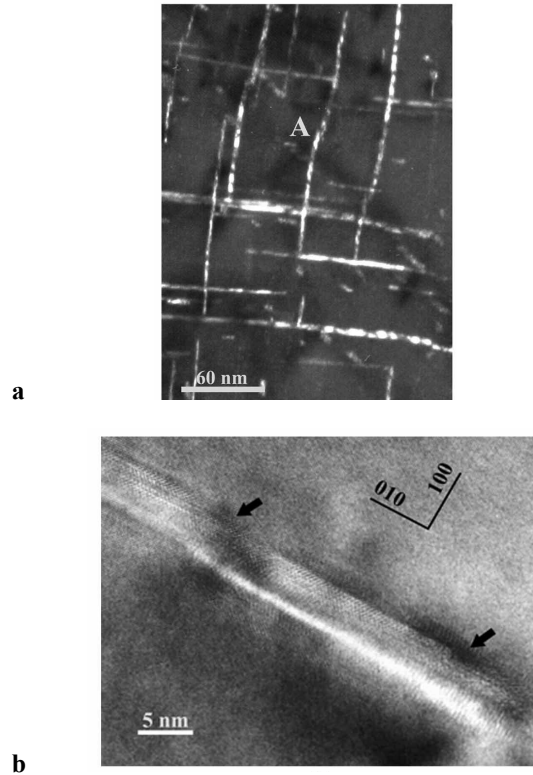


Figure 3.2: Precipitate shearing in the alloy AA6111 aged at 180 °C for two months and then deformed up to 5% [9]

3. Modelling the Age-Hardening Behavior of Al-Mg-Si Alloys Considering Simultaneous Nucleation, Growth and Coarsening during Precipitation

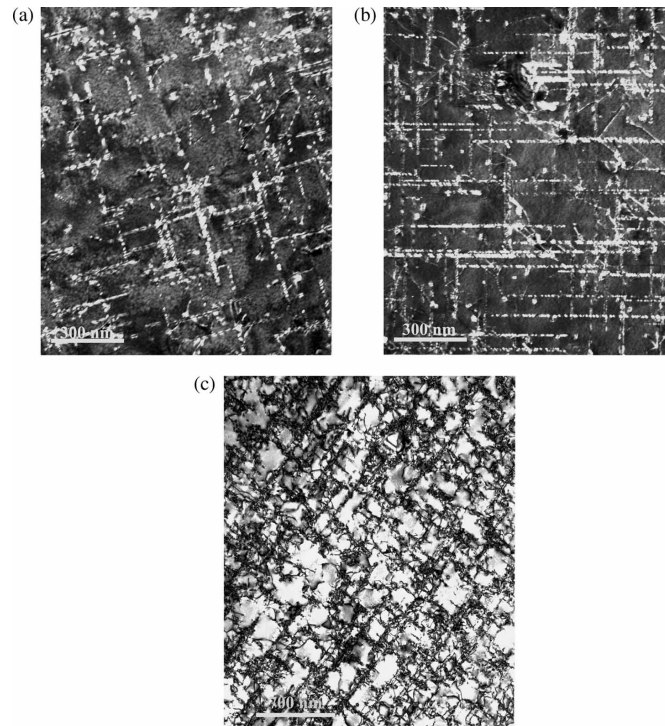


Figure 3.3: Formation of Orowan loops around precipitates in the alloy AA6111 aged for 7 days at 250 °C and then deformed up to a) 1, b) 2 and c) 5% [9]

3.4. Results

The KWN-based ageing model has been applied to the precipitation behavior of Al-Mg-Si alloys during ageing. The calculated values for size, volume fraction, and number density of precipitates are then used as input for the strengthening model, which yields the yield strength of the alloy. Table 3.1 shows the input data used in the precipitation and strength models. It is important to mention again that Mg is taken as the controlling alloying element. Since Si and Mg have similar diffusivity, it is also possible to choose Si as the controlling alloying element and the results would not be very different. The model has been developed based on the assumption of single stoichiometry Mg_2Si throughout the ageing. The precipitation sequence issue will be addressed in chapters 4 and 5. The alloys chosen for the application of the model are named alloy I and II with the compositions given in table 3.2. Alloy I is used to fit the

3. Modelling the Age-Hardening Behavior of Al-Mg-Si Alloys Considering Simultaneous Nucleation, Growth and Coarsening during Precipitation

values of j_0 , A_0 and β . Other parameter values are either well known (D_0 , Q_d , V_m , b , G), or assumed within their expected range (γ , r_{trans} , M) or have been fitted on independent experimental data (Q_s , k_{Si} , k_{Mg} , k_{Cu}) [3]. The model is then validated by comparing the predictions with experimental data of alloy II. The effective silicon content in solid, calculated in Eq. (19), is used instead of nominal composition. This is because of the formation of α -Al₁₅(FeMn)₃Si₃ particles.

$$C_{eff}^{Si} = C_0^{Si} - 0.33(C_0^{Fe} + C_0^{Mn}), \quad (3.19)$$

Table 3.1: Summary of input data used for the KWN and strengthening model [3]

Input parameter	Value	Input parameter	Value
C_β (wt%)	63.0	γ (J/m ²)	0.26
D_0 (m ² /s)	2.2×10^{-4}	r_{trans} (nm)	5.0
Q_d (kJ/mol)	130	M	2.6-3.1
Q_s (kJ/mol)	45.35	β	0.3-0.5
j_0 (#/m ³ s)	3.07×10^{36}	b (m)	2.84×10^{-10}
V_m (m ³ /mol)	7.62×10^{-5}	G (N/m ²)	2.7×10^{10}
k_{Si} (MPa/wt% ^{2/3})	66.3	k_{Mg} (MPa/wt% ^{2/3})	29.0
k_{Cu} (MPa/wt% ^{2/3})	46.4	A_0 (kJ/mol)	16

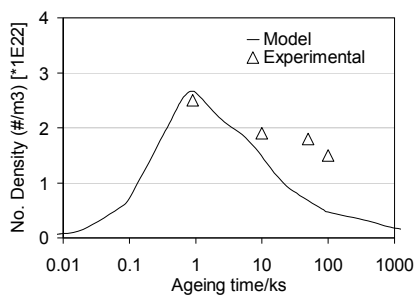
Table 3.2: Chemical composition of alloys used to validate the model (wt%) [3]

Alloy	Si	Mg	Cu	Mn	Fe
I	0.82	0.55	0.016	0.5	0.2
II	1.2	0.8	0.1	0.4	0.5

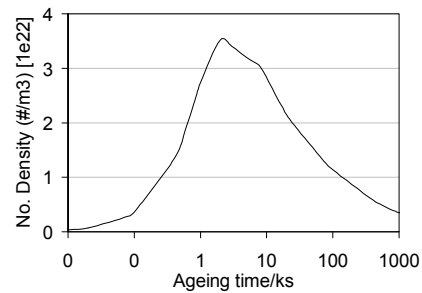
Figure 3.4 shows how the precipitate number density and mean radius as a function of ageing time at ageing temperature 185 °C in alloys I and II. It is seen that the mean radius for the alloy I fits reasonably well the experimental data. However, there is an underestimation of number density of precipitates in the overaged regime. It is also

3. Modelling the Age-Hardening Behavior of Al-Mg-Si Alloys Considering Simultaneous Nucleation, Growth and Coarsening during Precipitation

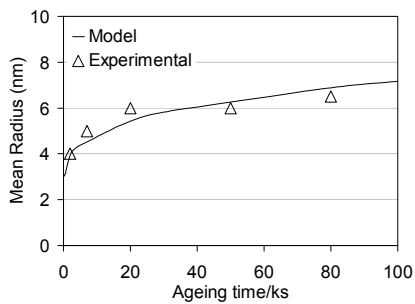
worth noting that the coarsening becomes dominant in alloy I after one hour ageing and in alloy II after 5 hour ageing, where the precipitate number density starts decreasing. The reason that the number density of precipitates in alloy II is more than that in alloy I is the higher content of Mg in alloy II, resulting in higher nucleation driving force.



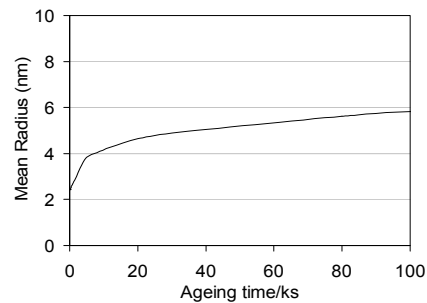
a) alloy I



b) alloy II



c) alloy I



d) alloy II

Figure 3.4: Comparison between experimental and predicted values of a,b) precipitate number density and c,d) precipitate mean radius in the alloy I and II aged at 185 °C (Experimental data are from Ref. [3])

Figure 3.5 shows the nucleation rate and precipitate volume fraction in the alloy I and II, aged at 185 °C. From this figure, one can roughly categorize the ageing process into three stages; (i) nucleation, (ii) nucleation/growth, (iii) coarsening. In the first step (up to 100 sec), where the nucleation rate is maximum, there is only a very little increase in the

3. Modelling the Age-Hardening Behavior of Al-Mg-Si Alloys Considering Simultaneous Nucleation, Growth and Coarsening during Precipitation

volume fraction of precipitates. The second stage (ageing time between 100 to 4000 s) is accompanied with a decrease of the nucleation rate and a rapid increase of the volume fraction. The decrease in the nucleation rate is obviously due the consumption of alloying elements by growing precipitates so C_m decreases. In the last stage, when coarsening is dominant, the volume fraction is almost constant.

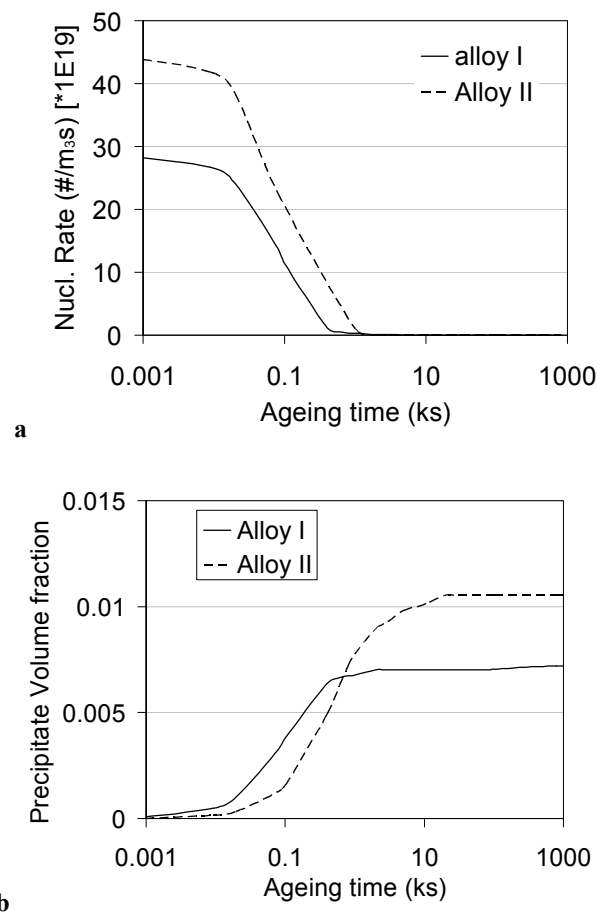


Figure 3.5: Simulated values of a) nucleation rate and b) precipitate volume fraction in alloys I and II aged at 185 °C

3. Modelling the Age-Hardening Behavior of Al-Mg-Si Alloys Considering Simultaneous Nucleation, Growth and Coarsening during Precipitation

Figure 3.6 shows the evolution of the size distribution of precipitates in the alloy I aged at 185 °C. It shows that after 3 min of ageing the mean radius is around 2 nm, before it starts increasing. It is also obvious that by increasing the ageing time, the size distribution curve becomes broader; indicating that smaller precipitates have dissolved and bigger ones have grown. Figure 3.7 shows the comparison between the experimental [3] and predicted size distributions of alloy II aged at 185 °C for 5 h. Although the predicted radius corresponding to the maximum of the size distribution is close to the experimental one, there is not a very good complete quantitative fit between experimental data and model result. However, the model qualitatively predicts the observed log-normal distribution of precipitates.

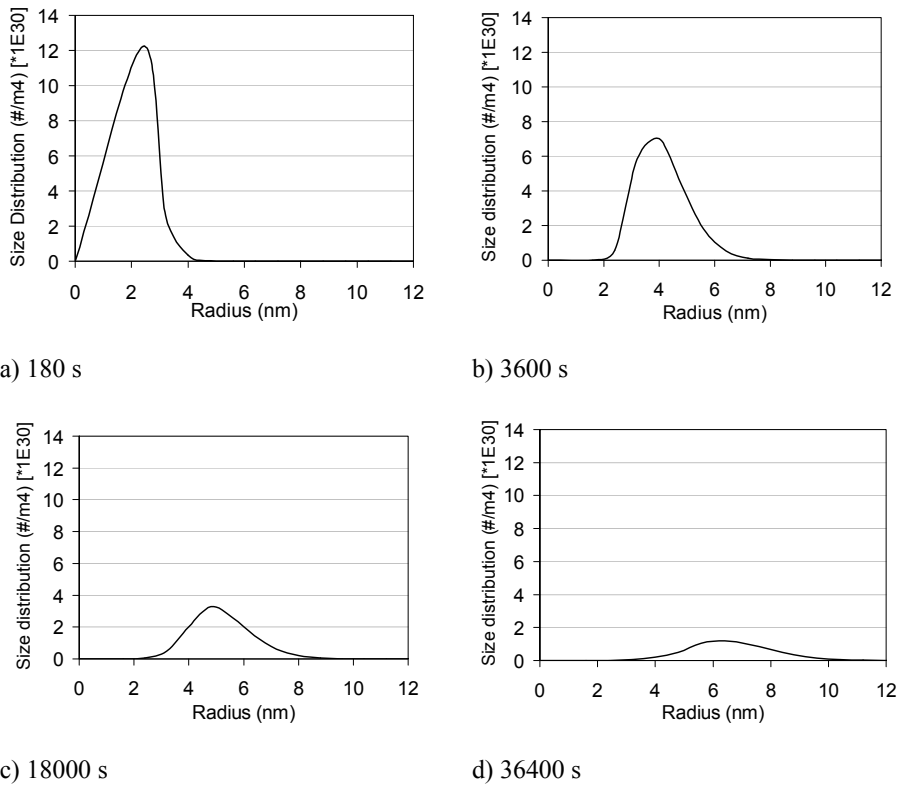


Figure 3.6: Predicted size distribution of precipitate at different times in the alloy I aged at 185 °C

3. Modelling the Age-Hardening Behavior of Al-Mg-Si Alloys Considering Simultaneous Nucleation, Growth and Coarsening during Precipitation

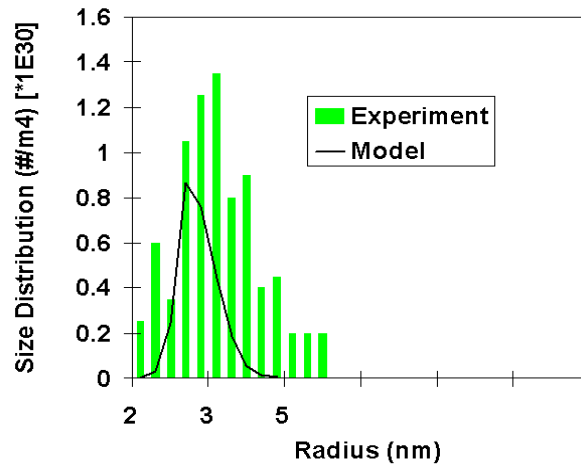


Figure 3.7: Simulated size distribution of precipitates at for the alloy II aged at 185 °C for 5 h (Experimental data is from Ref. [3])

Figure 3.8 shows the prediction of yield strength of the alloys I and II aged at different temperatures. The comparison with the experimental data shows that the model is capable of predicting the yield strength with a good accuracy. However, looking at Fig. 3.4, one might expect the strengthening model to underestimate the yield strength of the alloy I in the overage regime due to the underestimation of number density (Fig. 3.4a). It is important to remind that the yield strength, to some extent, can be fitted to the experimental data by choosing a right value for dislocation line tension constant, β , in the given range in table 3.1.

3. Modelling the Age-Hardening Behavior of Al-Mg-Si Alloys Considering Simultaneous Nucleation, Growth and Coarsening during Precipitation

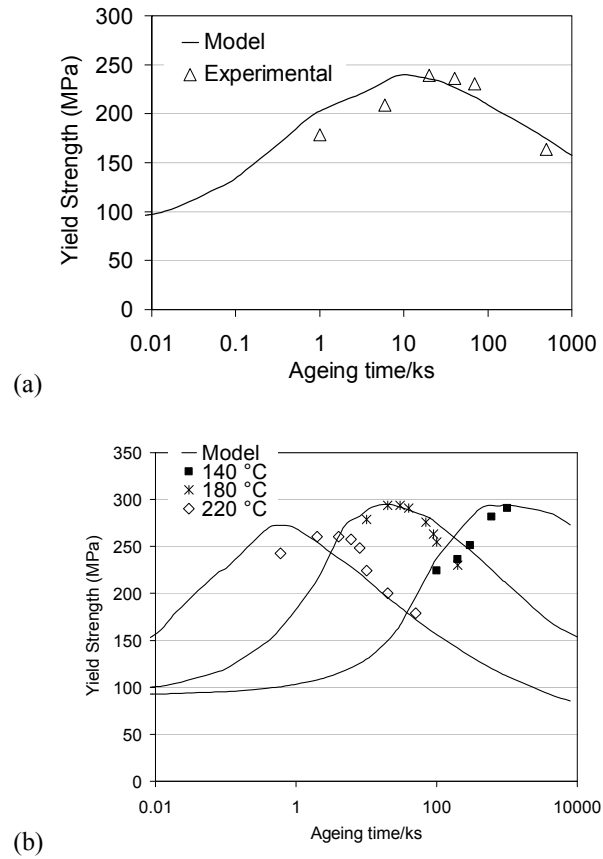


Figure 3.8: Simulated yield strength of a) alloy I aged at 185°C and b) alloy II aged at different temperatures

3.5. Discussion

A finite difference-based model is used to simulate the precipitation behavior of Al-Mg-Si alloys. The precipitation process involves the long-range transport of atoms by diffusion. In many cases, precipitate and matrix have also different crystal structures, necessitating a short-range lattice rearrangement at the interface of matrix/precipitate. The possible influence of this interface reaction is investigated in chapter 4. The current precipitation model applies the classical assumption of diffusion-controlled kinetics usually used when the diffusing alloying element is substitutional. The precipitation

3. Modelling the Age-Hardening Behavior of Al-Mg-Si Alloys Considering Simultaneous Nucleation, Growth and Coarsening during Precipitation

includes the nucleation, growth and coarsening, which can occur simultaneously. The nucleation of the second phase takes place in order to decrease the total Gibbs free energy. Formed nuclei continue to grow involving the diffusion of alloying elements in the matrix phase, as long as there is supersaturation in the matrix. As the growth process proceeds up to peak-age with a subsequent matrix depletion of alloying elements, coarsening appears as the dominant mechanism in the last stages of the precipitation. During coarsening, the system reduces the total Gibbs free energy by decreasing the interface area between matrix and precipitates. The solute content C_r of the matrix at the interface of a small precipitate with a large ratio of surface to volume is larger than that at a large precipitate referred as Gibbs Thomson effect. Due to this difference of interfacial concentrations a solute flux occurs from small to large precipitates. Coarsening, therefore, results in the broadening of precipitate size distribution (see Fig. 3.6). The applied model assumes spherical precipitates of constant stoichiometry and properties during the whole ageing process. With the current assumptions simulation results show that the effects of ageing temperature and alloy composition on ageing kinetics and yield strength evolution are qualitatively well predicted. Quantitative differences, however, still remain. For instance the model predicts faster kinetics for coarsening as compared to experimental data (see Fig. 3.4a). This could be attributed to the multi-precipitate nature of the system. Suppose that smaller β'' precipitates are dissolving in favor of the bigger β' precipitates. In the current version of the model, the difference between interfacial concentration of these precipitates is only coming from the difference in their size (all precipitates have similar interfacial energy). Nevertheless, in reality β' has higher interfacial energy compared to β'' phase. This, consequently, results in higher interfacial concentration in the vicinity of β' precipitate and, therefore, lower coarsening driving force [3]. The material's final mechanical properties depend on the volume fraction and radius of the particles and consequently on the precipitate size distribution. The contribution of shearable and non-shearable precipitates to the precipitation hardening is given by

$$\begin{cases} \sigma_{ppt} = c_1 f_v^{1/2} \langle r \rangle^{1/2} & \text{for } \langle r \rangle < r_{trans} \\ \sigma_{ppt} = c_2 f_v^{1/2} \langle r \rangle^{-1} & \text{for } \langle r \rangle \geq r_{trans} \end{cases}, \quad (3.21)$$

where c_1 and c_2 constants, which are dependent on parameters such as Taylor factor, Burgers vector, precipitate shear modulus and interfacial energy. During growth precipitate volume fraction increases and then remains constant during coarsening. The strength evolution during ageing is schematically shown in Fig. 3.9 for both the case

3. Modelling the Age-Hardening Behavior of Al-Mg-Si Alloys Considering Simultaneous Nucleation, Growth and Coarsening during Precipitation

where coarsening starts when most precipitates are shearable (Fig. 3.9a) and for the case where coarsening starts when most precipitates are by-passed (Fig. 3.9b). Comparison of figure 3.4, 3.5 and 3.8 show that for alloy I and II the model predicts coarsening starts before peak age is reached. Peak age then corresponds to the moment when the average radius is closed to the transition radius as in figure 3.9a. At this time, a large proportion of the precipitates are still shearable, which is in accordance with experimental data [10]. This precipitation sequence is also in accordance with experimental observations that show coarsening starts in underaged regime when precipitates are still shearable [3] and indicates the model predicts properly the sequence of precipitation stages.

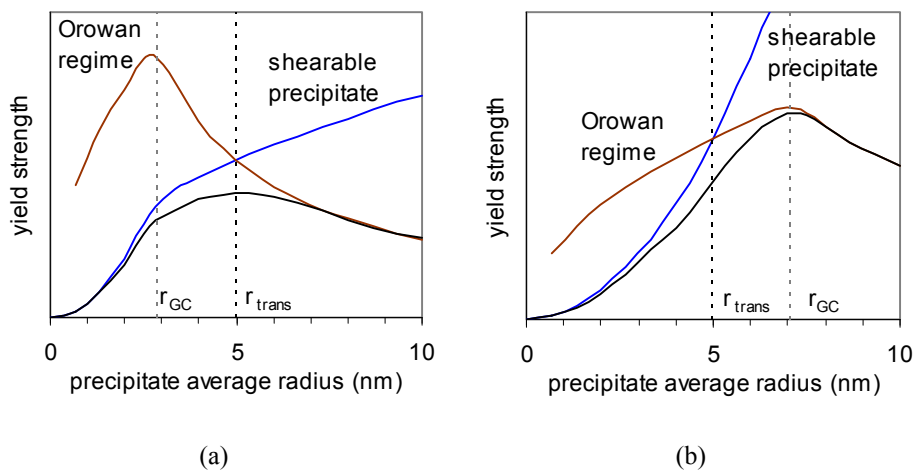


Figure 3.9: Schematic of the contribution of shearable and non-shearable precipitates to the yield strength of the alloy (r_{GC} is the radius when coarsening becomes dominant)

3.6. Summary

The Kampann-Wagner numerical (KWN) model is applied to simulate the precipitation behavior of Al-Mg-Si alloys. The model is developed assuming constant stoichiometry Mg_2Si and spherical morphology throughout the ageing. It is also assumed that diffusion of Mg controls the kinetics of ageing. The results of the precipitate model are then used as input parameters for the age-hardening model, which is based on the interaction of shearable and non-shearable precipitates with moving dislocations. In this model, precipitates smaller than 5 nm are assumed to be sheared by dislocation, while

3. Modelling the Age-Hardening Behavior of Al-Mg-Si Alloys Considering Simultaneous Nucleation, Growth and Coarsening during Precipitation

those bigger than 5 nm not. The results show that the precipitation transformation can be divided into three stages; (i) nucleation, (ii) nucleation/growth, and (iii) coarsening. In the first stage, when nucleation is the governing reaction, the volume fraction of precipitates shows very slow increase. However, in the second stage, it increases significantly before it reaches a plateau. The plateau in the volume fraction of precipitate is due to the activation of coarsening regime. The coarsening kinetics, predicted by the model, is not in a good agreement with the experimental data. It could be attributed to the multi-component nature of the system, where there are different precipitate species with different interfacial energies.

References:

- [1] Janssens K, Raabe D, Kozeschnik E, Computational Mater Eng an Introduction to Microstructure Evolution, Elsevier Inc., 2007;194:196.
- [2] Esmaeili S, Lloyd DJ, and Poole WJ, Acta Mater 51 (2003) 2243.
- [3] Myhr OR, Grong Ø, Andersen SJ, Acta Mater 49 (2001) 65.
- [4] Myhr OR and Grong Ø, Acta Met Mater 39 (1991) 2693.
- [5] Myhr OR and Grong Ø, Acta Met Mater 39 (1991) 2703.
- [6] Schercliff HR and Ashby MF, Mater Sci. Tech. 7 (1991) 85.
- [7] Robson JD, Acta Mater 52 (2004) 4669.
- [8] Samaras SN, Model. Sim. Mater Sci Eng 14 (2006) 1271.
- [9] Poole WJ, Wang X, Lloyd DJ, Embury DJ, Philosophical Magazine, Vol. 85, Nos. 26–27, 11–21 September 2005, 3113–3135.
- [10] Vivas M, Lours P, Levaillant C, Couret C, Casanove MJ, Coujou A, Materials Science and Engineering A234L236 (1997) 664-667.

3. Modelling the Age-Hardening Behavior of Al-Mg-Si Alloys Considering Simultaneous Nucleation, Growth and Coarsening during Precipitation

CHAPTER 4

A Mixed-Mode Precipitation Model for Al-Mg-Si Alloys

In the present study a mixed-mode growth model has been implemented in the Kampmann-Wagner numerical (KWN) model to systematically study the effects of interfacial energy, diffusivity, and interface mobility on the kinetics and character of precipitation in Al-Mg-Si-Cu alloys. A parameter η is introduced, which is proportional to the diffusivity of the rate-determining alloying element and inversely proportional to the mobility of the interface and to the radius of precipitates. The definition of this parameter is such that for $\eta \rightarrow 0$ the transformation is diffusion-controlled while for $\eta \rightarrow \infty$ it is interface-controlled. η -values between 0.1 and 10 form a characteristic of the mixed-mode precipitation where both bulk diffusion of alloying elements and interface processes are both determining the precipitation rate. It is seen that by increasing the ageing time, the character of precipitation has a tendency towards diffusion control. The bigger the precipitates, the larger the amount of solute needed to increase the precipitates' mean radius, meaning that solutes need to diffuse from further away, making the growth reaction more diffusion-controlled. The results also show that changes in the interfacial energy have almost no effect on the precipitation character. However, changes in diffusivity and interface mobility have significant influence on the character of precipitation.

4.1. Introduction

The modelling of precipitation in Al-Mg-Si alloys has always been of great interest since precipitates have a significant contribution to the mechanical properties of these alloys. Recently, Kampmann and Wagner have developed a numerical model that is capable of predicting the evolution of number density, size, and volume fraction of precipitates considering simultaneous nucleation, growth, and coarsening [1]. The Kampmann-Wagner numerical (KWN) model has been successfully applied to Cu-Co, Ni-Al, Al-Sc, Fe-Ni, Al-Mg-Si, and Al-Cu-Mg [2-5]. In all previously developed KWN models, the growth kinetics is based on the local-equilibrium hypothesis, meaning that thermodynamic equilibrium is established when the two phases are in contact, i.e. the chemical potentials of alloying elements at the two sides of the interface are equal. This implies the assumption of an infinite mobility, which means very fast transformation of matrix to precipitate as soon as the local equilibrium is disturbed by diffusion. The opposite extreme, named interface-controlled growth, takes place when the solute diffusion is infinitely rapid and atom transport across the interface is relatively slow, indicated by a finite value for the interface mobility. In this case the solute-depleted region around the precipitate is effectively eliminated by rapid diffusion. These two approaches are two extreme possibilities for the actual kinetics during precipitation. In general, neither the diffusion rate nor the interface mobility will be infinite, and therefore an intermediate (mixed-mode) case can usually more accurately describe the character of precipitation. Figure 4.1a shows a schematic binary phase diagram according to which, when the temperature is decreased from the single phase region α to the two phase region $\alpha+\beta$, the initial phase with the concentration of C_0 will experience a driving force for decomposition towards the matrix with concentration C_α and precipitate with concentration C_β (see Fig. 4.1a). However, if the reaction character is mixed-mode, the precipitate-matrix interfacial concentration is equal to C_i (see Fig. 4.1b). In their attempt to take into consideration the mixed-mode character of the phase transformation in Fe-C alloys, Van Leeuwen et al. [6] introduced a mode parameter varying between pure diffusion control and pure interface control. It is found that this parameter, and therefore the transformation character, gradually changes during the phase transformation. Following this study, Sietsma et al. [7] introduced a straightforward approach, in which a single parameter Z , comprising the relevant thermodynamic, geometrical, and kinetic parameters, determines the character of phase transformation. The introduced Z -parameter is proportional to the diffusivity of the partitioning element and the area to volume ratio of the growing grain, and inversely proportional to the interface mobility and to the driving pressure per unit of

4. A Mixed-Mode Precipitation Model for Al-Mg-Si Alloys

concentration difference. In the literature neither traditional ageing models dealing with precipitation as a reaction divided into three distinct stages nucleation, growth, and coarsening, nor more advanced KWN models taking into account simultaneous nucleation, growth, and coarsening, have considered mixed-mode character for precipitate growth in Al-Mg-Si alloys. In the only available study, Wu and Ferguson [9] have used the interface concentration C_i , obtained on the basis of the mixed-mode assumption of ref. [7], to modify the KWN model and applied their model to the Al-Mg-Si system. In the present paper, a straightforward approach is used to implement the mixed-mode character into KWN model within the steady-state diffusion field approximation. Using this modified KWN model a systematic study is done for precipitation in Al-Mg-Si alloys on the effects of kinetically and thermodynamically important parameters such as diffusivity, interfacial energy, and interface mobility on the character of precipitation, on the kinetics of ageing, and eventually on the yield strength of these alloys.

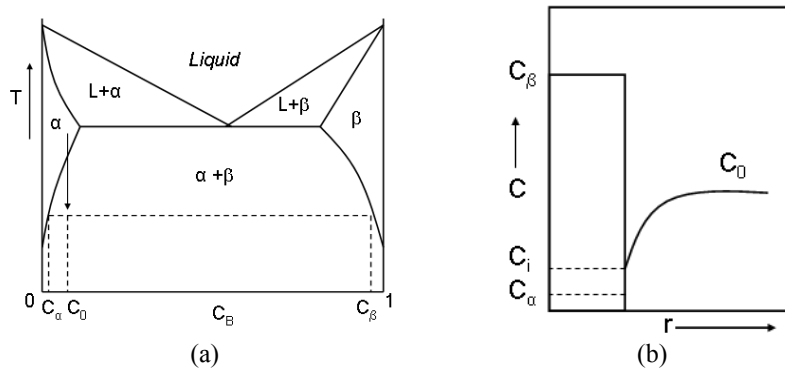


Figure 4.1: Schematics of a) simple binary phase diagram and b) concentration profile around spherical precipitate with radius r

4.2. Mixed-mode model

In the mixed-mode condition (see fig. 4.1) the interface concentration at the matrix-precipitate interface, C_i , is between the equilibrium value, C_α , and the average matrix composition, C_m , which becomes different from C_0 when precipitation proceeds. If the matrix phase is a dilute solid solution, the deviation from the interfacial equilibrium concentration produces a driving force for growth $\Delta G_{\alpha\beta}$ acting at the interface, given by [10]

4. A Mixed-Mode Precipitation Model for Al-Mg-Si Alloys

$$\Delta G_{\alpha\beta} = RT \ln\left(\frac{C_i}{C_\alpha}\right), \quad (4.1)$$

with R the gas constant and T the temperature. The growth rate can be given by the following relationship

$$\frac{dr}{dt} = M_{\alpha\beta} \Delta G_{\alpha\beta}, \quad (4.22)$$

where r is the precipitate radius, t is time, and $M_{\alpha\beta}$ is the mobility of the interface. Putting the value of $\Delta G_{\alpha\beta}$ from Eq. (4.1) into Eq. (4.2) yields

$$\frac{dr}{dt} = M_{\alpha\beta} RT \ln\left(\frac{C_i}{C_\alpha}\right). \quad (4.3)$$

Using the steady-state approximation, the growth rate, which also applies for dissolution, for spherical precipitates of constant stoichiometry can also be related to solute diffusion by [4,8,11,12,13]

$$\frac{dr}{dt} = \frac{D}{r} \frac{C_m - C_i}{C_\beta - C_i}, \quad (4.4)$$

where D is the diffusion coefficient of alloying element in the matrix and C_β is the concentration of alloying element in the precipitate. This equation is valid where [8],

$$\frac{C_m - C_i}{C_\beta - C_i} \ll 1, \quad (4.5)$$

which is the case for precipitation in Al-Mg-Si alloys (due to the large value of C_β compared to C_0). The combined influence of interface mobility and diffusivity will lead to a composition of the matrix phase at the interface, C_i that fulfills both Eqs. (4.3) and (4.4) simultaneously. This means that C_i can be obtained by equating Eqs. (4.3) and (4.4) and solving the obtained equation either numerically (i.e. using bisection method) or analytically. Analytical methods to calculate C_i will be explained later. Numerical solution gives the exact values for both C_i and driving force. In case the precipitation character is close to either diffusion or interface control, one can use a linear function instead of Eq. (4.3) to get an analytical solution for the growth rate, given by

$$\frac{dr}{dt} = M_{\alpha\beta} RT \left[\kappa \left(\frac{C_i - C_\alpha}{C_\alpha} \right) \right], \quad (4.6)$$

4. A Mixed-Mode Precipitation Model for Al-Mg-Si Alloys

where κ is a constant, which is dependent on the character of precipitation. If the precipitation character is close to diffusion control, it is fair to assume that κ is equal to one. This solution, hereafter, is named diffusion control analytical (DCA) solution. On the other hand when the precipitation character is close to interface control, κ can be taken equal to

$$\kappa = \left(\frac{C_\alpha}{C_0 - C_\alpha} \right) \ln \left(\frac{C_0}{C_\alpha} \right). \quad (4.7)$$

This is named the interface control analytical (ICA) solution. Figure 4.2 shows the variation of driving force versus C_i in numerical, DCA, and ICA solutions, assuming $C_0 = 0.6$ wt% and $C_\alpha = 0.0074$ wt%.

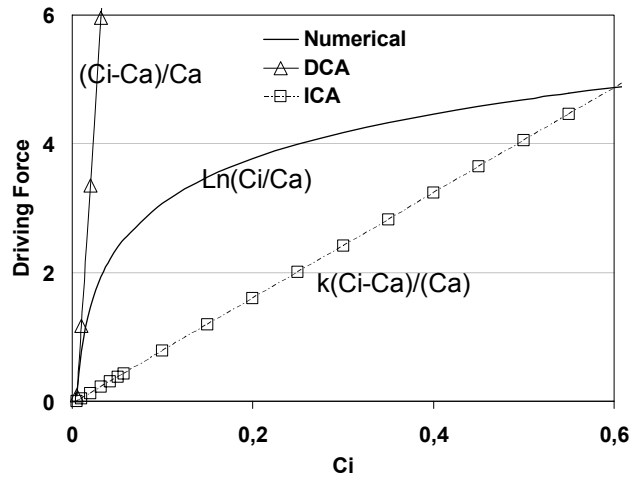


Figure 4.2: The driving force as a function of C_i in numerical, DCA, and ICA solutions, assuming $C_0 = 0.6$ wt% and $C_\alpha = 0.0074$ wt%

A modified analytical solution can be developed choosing κ as a time-dependent parameter. Starting from an interface-controlled precipitation character just after nucleation [7] and assuming that after peak-age (at time t_{peak}) the character of precipitation becomes almost diffusion controlled, κ is given by

$$\kappa = \left(1 - \left(\frac{C_\alpha}{C_m - C_\alpha} \right) \ln \left(\frac{C_m}{C_\alpha} \right) \right) \left(\frac{t}{t_{peak}} \right) + \left(\frac{C_\alpha}{C_m - C_\alpha} \right) \ln \left(\frac{C_m}{C_\alpha} \right). \quad (4.8)$$

4. A Mixed-Mode Precipitation Model for Al-Mg-Si Alloys

At times longer than t_{peak} , κ is taken equal to one. This modified analytical solution is named mixed-mode analytical (MMA) solution.

The growth character of precipitates can be identified by the dimensionless parameter η , which is introduced as

$$\eta = \frac{C_i - C_\alpha}{C_m - C_i}. \quad (4.9)$$

When $C_i \rightarrow C_m$, then $\eta \rightarrow \infty$, meaning that the solute diffusion is so rapid that the solute-depleted region around the precipitate is effectively eliminated. It is also seen that Eq. (4.9) yields $\eta=0$ for $C_i=C_\alpha$, giving the condition of local equilibrium and diffusion-controlled growth. This means that in this case the interface reaction is so fast that any further increase of mobility does not significantly accelerate the overall reaction. The interface concentration of the alloying element in the mixed-mode precipitation reaction can be expressed as a function of η according to

$$C_i = \frac{C_\alpha + \eta C_m}{1 + \eta}. \quad (4.10)$$

Figure 4.3 shows the evolution of C_i as a function of η plotted from Eq. (4.10) for the alloy AA6082 with $C_m = 0.6$ wt% and $C_\alpha = 0.0074$ wt%. It is seen that when $\eta=1$, the interface concentration, C_i , is exactly between the equilibrium concentration, C_α , and the mean concentration, C_m . For $\eta>1$, the precipitation character moves towards the interface-controlled regime, while for $\eta<1$, the precipitation becomes more diffusion-controlled. Looking at Fig. 4.3, it is fair to assume that for $\eta>10$ the precipitation reaction is predominantly interface-controlled (i.e. $C_i \approx C_m$), while for $\eta<0.1$ it becomes almost diffusion-controlled (i.e. $C_i \approx C_\alpha$).

Equating the growth rate equations (Eqs. (4.4) and (4.6)) and neglecting the value of C_i relative to C_β , which is normally fulfilled for precipitate formation in aluminium alloys, an analytical equation for the η -parameter can be derived as

$$\eta = \frac{C_i - C_\alpha}{C_m - C_i} = \frac{D}{\kappa r M_{\alpha\beta} RT} \left(\frac{C_\alpha}{C_\beta - C_i} \right) \approx \frac{D}{\kappa r M_{\alpha\beta} RT} \frac{C_\alpha}{C_\beta}. \quad (4.11)$$

As is seen in this equation, the η -parameter is directly proportional to the diffusivity and inversely proportional to the mobility and the radius of precipitates. It also has an indirect functionality from the interfacial energy through C_β , which is introduced by the

4. A Mixed-Mode Precipitation Model for Al-Mg-Si Alloys

Gibbs-Thomson effect. Equation (4.11) allows determining the mixed-mode character of precipitation for given values of kinetic, geometrical, and thermodynamic parameters.

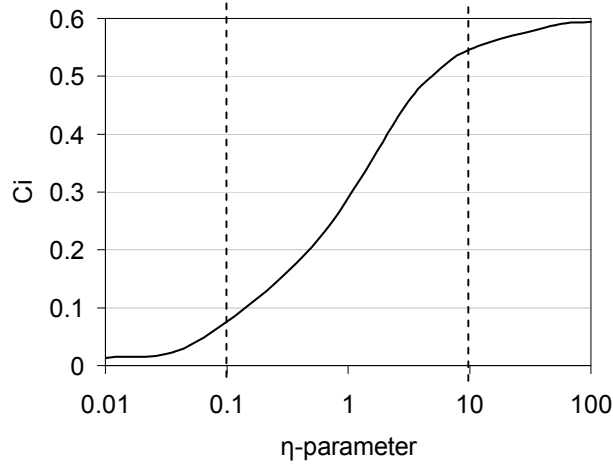


Figure 4.3: The evolution of C_i as a function of η plotted for $C_m=0.6$ wt% and $C_a=0.0074$ wt%. For $0.1 < \eta < 10$, the transformation character is mixed-mode

A fairly simple approach is used to estimate the mobility of the precipitate-matrix interface. The fluxes of atoms from precipitate to the matrix, $J_{\beta\alpha}$, and the reverse flux, $J_{\alpha\beta}$, are given by

$$\begin{cases} J_{\beta\alpha} = \nu A_{ac} \exp\left\{-\frac{(\Delta G_a + \Delta G_{a\beta})}{RT}\right\}, \\ J_{\alpha\beta} = \nu A_{ac} \exp\left(\frac{-\Delta G_a}{RT}\right) \end{cases}, \quad (4.12)$$

where ν is the vibration frequency of atoms at the interface, typically about 10^{13} s^{-1} , ΔG_a is the activation energy barrier for atomic jumping across the interface, and A_{ac} is the accommodation factor, the probability that an atom, having left one of the matrix atomic sites, finds a site in the precipitate across the interface. A_{ac} for an incoherent interface is usually assumed to be a constant close to unity [10]. However, when the interface is coherent or semi-coherent, this quantity is most delicate and it can only be obtained by indirect methods, i.e. by comparison of suitable experiments with the corresponding

4. A Mixed-Mode Precipitation Model for Al-Mg-Si Alloys

theoretical treatment that includes A_{ac} as a parameter. A problematic aspect of determining A_{ac} for coherent and semi-coherent interfaces with indirect methods is the fact that A_{ac} , apart from coherency of the interface, is dependent on a number of parameters, such as crystallographic misorientation, elastic misfit strains, and solute segregation. All this means that it is extremely difficult to have an accurate estimate of the evolution of A_{ac} during ageing. However, the general trend is from values close to zero for initially coherent precipitates, which preferentially form at the nucleation stage, to unity for incoherent equilibrium precipitates. The net flux of atoms, J_{net} , is given by the difference of the two fluxes, $J_{\beta\alpha}$ and $J_{\alpha\beta}$, given by

$$J_{net} = J_{\alpha\beta} - J_{\beta\alpha} = \nu A_{ac} \exp\left(\frac{-\Delta G_a}{RT}\right) \left\{ 1 - \exp\left(-\frac{\Delta G_{a\beta}}{RT}\right) \right\}. \quad (4.13)$$

The velocity of the interface is given as the product of the net flux per mole atom sites and the displacement per atom, which is the atomic spacing, b , into the growing precipitate

$$\frac{dr}{dt} = b J_{(net)} = M_{\alpha\beta} \Delta G_{a\beta}, \quad (4.14)$$

assuming $\Delta G_{a\beta} \ll RT$. The mobility is determined from Eqs. (4.13) and (4.14) as [8]

$$M_{\alpha\beta} = \frac{b\nu A_{ac}}{RT} \exp\left(\frac{-\Delta G_a}{RT}\right). \quad (4.15)$$

Inserting the mobility from Eq. (4.15) and C_i from Eq. (4.10) into the growth equation (Eq. 4.6), gives

$$\frac{dr}{dt} = b\nu\kappa A_{ac} \exp\left(\frac{-\Delta G_a}{RT}\right) \left(\frac{\eta}{1+\eta}\right) \left(\frac{C_m - C_\alpha}{C_\alpha}\right). \quad (4.16)$$

There is no reported value for the activation energy barrier for jumping of atoms across the interface, ΔG_a . As an approximation, this value is taken equal to the activation energy of diffusion of Mg in annealed Al-Mg-Si alloys, i.e. 130 kJ/mol [4]. Taking b as the lattice parameter of Al (0.4 nm) and ν equal to 10^{13} s^{-1} , the growth equation can be written as

$$\frac{dr}{dt} = (4000 \text{ m/s})\kappa A_{ac} \exp\left(\frac{-\Delta G_a}{RT}\right) \left(\frac{\eta}{1+\eta}\right) \left(\frac{C_m - C_\alpha}{C_\alpha}\right). \quad (4.17)$$

4. A Mixed-Mode Precipitation Model for Al-Mg-Si Alloys

The equilibrium concentration of Mg at the interface, including the Gibbs-Thomson effect, is obtained by [4]

$$C_\alpha = (970 \text{ wt}\%) \exp\left(\frac{2\gamma V_m}{rRT} - \frac{Q_s}{RT}\right), \quad (4.18)$$

where Q_s is the free energy of the solution of Mg (47 kJ/mol), γ is the interfacial energy, and V_m is the molar volume of the precipitate ($7.62 \times 10^{-5} \text{ m}^3/\text{mol}$).

The obtained growth/dissolution rate is then implemented in the KWN model. The basic idea behind the KWN model is dividing the precipitate-size distribution into a series of discrete size classes. By applying a standard finite difference method the flux of particles in and out of each size class is calculated during ageing time [4]. The governing continuity equation to calculate the evolution of size distribution is expressed as

$$\frac{\partial N}{\partial t} = -\frac{\partial(N \frac{dr}{dt})}{\partial r} + \delta(r - r_{nuc}) j_0 \exp\left[-\left(\frac{A_0}{RT}\right)^3 \left(\frac{1}{\ln(C_m/C_e)}\right)^2 - \frac{Q_d}{RT}\right], \quad (4.19)$$

where N is the number density of precipitates of a given size, r_{nuc} is the radius of the nuclei, j_0 is a constant (chosen as $9.66 \times 10^{34} \text{ m}^{-3}\text{s}^{-1}$ [12]), Q_d is the activation energy for diffusion of Mg, C_e the equilibrium solute concentration at a flat interface, and A_0 is a constant related to the potency of the heterogeneous nucleation sites. The way to calculate A_0 is explained in the literature [4]. Other parameters in Eq. (4.19) have already been introduced.

Assuming that different strengthening contributions to the overall strength can be added linearly, the yield strength of Al-Mg-Si alloys can be obtained as

$$\sigma_y = \sigma_i + \sigma_{ss} + \sigma_p, \quad (4.20)$$

where σ_i is the yield strength of pure aluminium chosen as 10 MPa [10], σ_{ss} is the solid solution strengthening term, and σ_p is the precipitation strengthening term. σ_i and σ_p are given by [10]

$$\sigma_{ss} = \sum_{j=\text{Mg, Si, Cu}} k_j C_j^{2/3}, \quad (4.21)$$

$$\sigma_p = \frac{M}{G^{1/2} b^2 r} \left(\frac{3f}{2\pi}\right)^{1/2} \left(\frac{\sum_i N_i F_i}{\sum_i N_i}\right)^{3/2}, \quad (4.22)$$

4. A Mixed-Mode Precipitation Model for Al-Mg-Si Alloys

where k_j is a constant with a specific value for element j [10], M is the Taylor factor (taken as 2.7), f is the volume fraction of precipitates, G is the shear modulus of precipitates (2.7×10^{10} N/m²), and F_i is the strength of precipitates in i^{th} size class given by

$$\begin{cases} F_i = Gb^2 \left(\frac{r_i}{r_{trans}} \right) & \text{for } r_i < r_{trans} \\ F_i = Gb^2 & \text{for } r_i \geq r_{trans} \end{cases}, \quad (23)$$

where r_{trans} is the transition radius above which precipitate become non-shearable. r_{trans} is taken as 5 nm [10].

4.3. Modelling results

The modified KWN model taking into account the mixed-mode character of transformation is used as a tool to investigate the effects that interfacial energy, mobility, and diffusivity have on the precipitate evolution during ageing. The effects of changing each of these variables will be explained in turn. Before doing that, it is useful to introduce a standard case corresponding to the growth of incoherent precipitates in an undeformed matrix. So, the parameter A_{ac} in the standard case is taken equal to one. The diffusion coefficient of Mg was used as the input for the model as it is given by

$$D = (2.2 \times 10^{-4} \text{ m}^2 / \text{s}) \exp\left(\frac{-Q_d}{RT}\right), \quad (4.24)$$

where Q_d is taken equal to 130 kJ/mol. Since in the standard case the interface is incoherent it is fair to assume that the activation energy barrier for atomic jumping across the interface, ΔG_a , is equal to the activation energy for diffusion of Mg. The interfacial energy is taken equal to 0.26 Jm⁻². The simulation, as well as the ones in the following sections, was performed for the alloy AA6082 (Al-0.6wt%Mg-0.9wt%Si-0.2wt%Fe-0.35wt%Mn), assuming the precipitates to be Mg₂Si with spherical morphology. Figure 4.4 shows the evolution of the η -parameter for precipitates having the average size during ageing at 190 °C obtained from the modified KWN model. It is seen that after an initial plateau, the η -parameter decreases continuously. Obviously, the standard case, apart from the very beginning of ageing, has a diffusion-controlled transformation character. Figure 4.5 shows the comparison of the mean precipitate radius and precipitate number density obtained from the mixed-mode KWN model (for the standard case) and the purely diffusion-control-based KWN model.

4.3.1. Effects of interfacial energy

The effect of changing the interfacial energy over the range $0.16\text{-}0.36 \text{ Jm}^{-2}$ on precipitates evolution was predicted using the mixed-mode KWN model. This range is chosen since the average value of interfacial energy used in the classical KWN model for Al-Mg-Si alloys is taken as 0.26 Jm^{-2} [4]. Other parameters are identical to the ones for the standard case. Figure 4.6 shows the evolution of the η -parameter during ageing for precipitates having the average size at different values of interfacial energy calculated by numerical, DCA, ICA, and MMA solutions. As it is seen, the precipitation starts with a mixed-mode character by a plateau in the value of the η -parameter and then a decrease of the η -parameter towards diffusion control. The difference between the η -parameter for the highest interfacial energy ($\gamma=0.36 \text{ Jm}^{-2}$) and the lowest one ($\gamma=0.16 \text{ Jm}^{-2}$) in all solutions is very small. Therefore, one can conclude that the change in the interfacial energy within the chosen range does not have a significant influence on the character of precipitation. The effects of interfacial energy on the kinetics of precipitation are not discussed here, since the interfacial energy does not have any significant influence on the precipitation character. It is also seen that the ICA solution gives slower decrease of η -parameter compared to other solutions, showing that in the standard case the ICA assumption is not a good approximation of driving force.

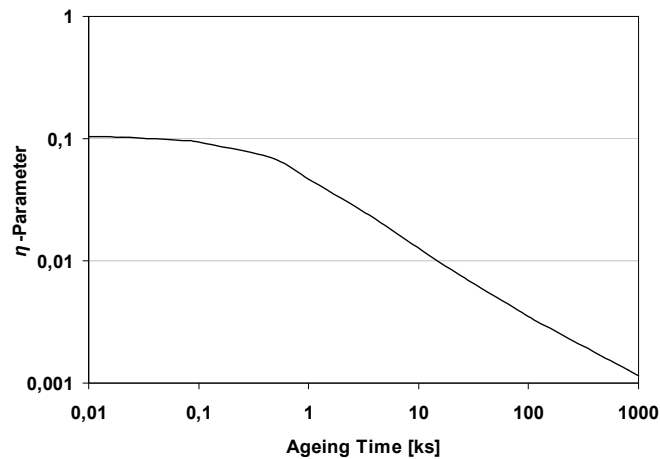


Figure 4.4: Evolution of the η -parameter for the standard case during ageing at $190 \text{ }^\circ\text{C}$

4. A Mixed-Mode Precipitation Model for Al-Mg-Si Alloys

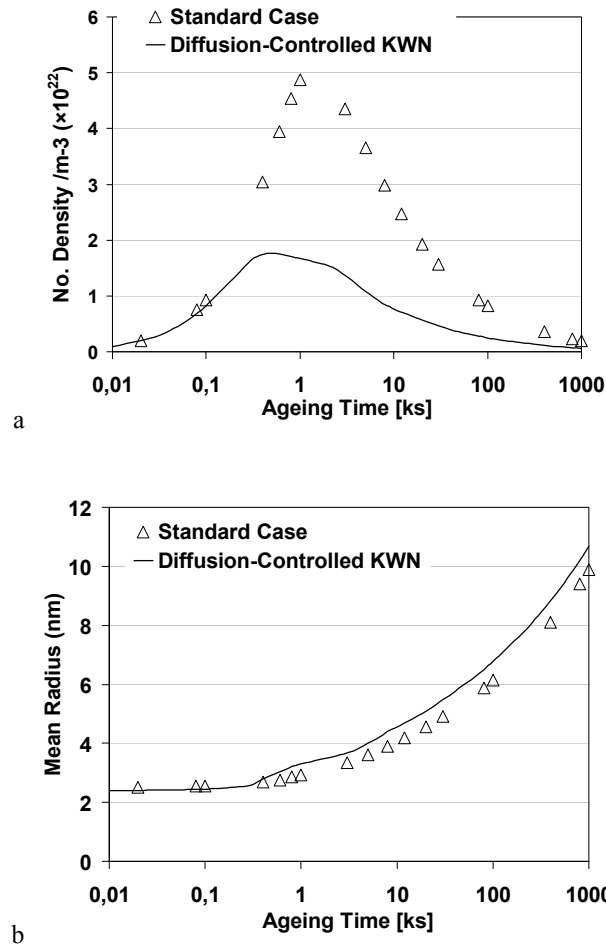


Figure 4.5: The comparison of a) precipitate number density and b) the mean precipitate radius obtained from the modified KWN model (for the standard case) and the purely diffusion-controlled-based KWN model for the alloy AA6082 during ageing at 190 °C

4. A Mixed-Mode Precipitation Model for Al-Mg-Si Alloys

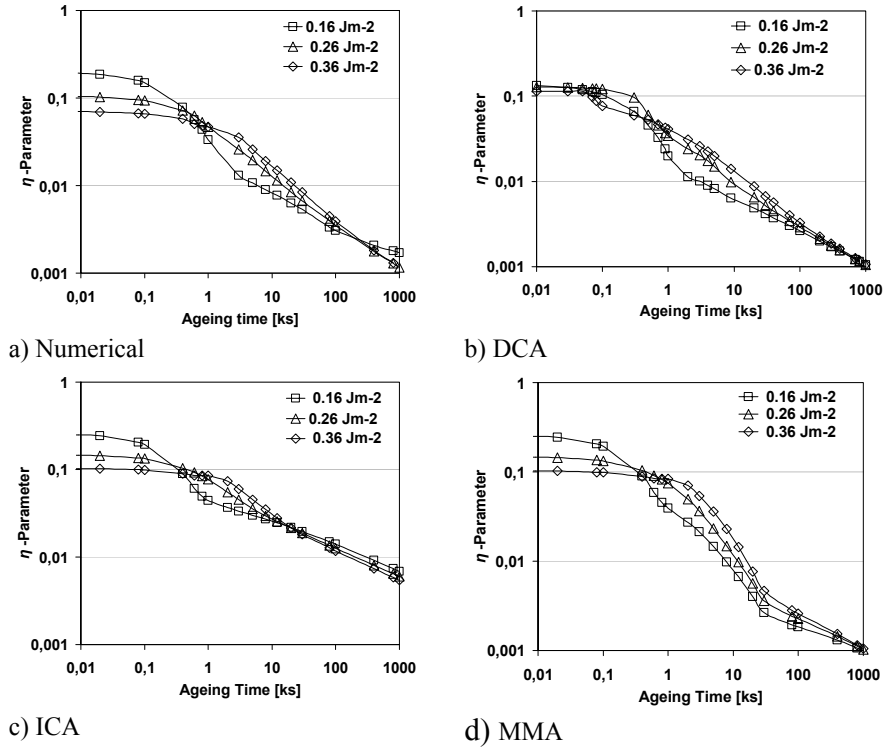
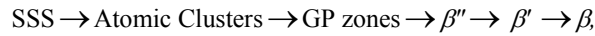


Figure 4.6: Effects of interfacial energy on the η -parameter, calculated by a) numerical, b) DCA, c) ICA, and d) MMA methods

4.3.2. Effects of mobility (accommodation factor)

During ageing, the Al-Mg-Si alloys undergo a complex precipitation, which is conventionally believed [14] to be:



where SSS is the supersaturated solid solution followed by the formation of atomic clusters and GP-zones in the form of Si and/or Mg colonies, β'' is a precipitate with the stoichiometry of Mg_5Si_6 , β' is $\text{Mg}_{1.7}\text{Si}$, and β is the stable Mg_2Si precipitate [14]. Due to this complex precipitation sequence, the parameter A_{ac} is changing during ageing in such a way that in the beginning of ageing the parameter A_{ac} is very small, while this term at the end of ageing becomes close to unity related to the incoherency of the interface. So, it is useful to check the effect of changing the mobility, obtained by changing the

4. A Mixed-Mode Precipitation Model for Al-Mg-Si Alloys

parameter A_{ac} , on precipitates evolution. To do this, A_{ac} is varied from 0.01 to 1.0 and the obtained mobility values are used in the mixed-mode KWN model (Eq. (4.17)). Other parameters are the same as for the standard case. Figure 4.7 shows the effects of the parameter A_{ac} on the mixed-mode character of precipitation for numerical, DCA, ICA, and MMA solutions. As it is seen ICA approach shows slower kinetics of decrease in the η -parameter compared to other methods. In all cases there is a plateau in the beginning followed by a decrease towards diffusion-controlled character. Precipitates with lower values of A_{ac} show a longer plateau in the beginning of ageing. Initial values of the η -parameter for A_{ac} equal to 0.01, 0.1, and 1.0 are approximately 13, 1.2, and 0.12 respectively, meaning that at $A_{ac}=0.01$ precipitation begins with the interface-controlled character, at $A_{ac}=0.1$ it starts with the mixed-mode character, and at $A_{ac}=1.0$ it has a diffusion-controlled character from the beginning. Figures 4.8 and 4.9 show the predicted evolutions of precipitates mean radius and number density of precipitates for different values of A_{ac} . It is seen that when the parameter A_{ac} is increased, the mean radius of precipitates on the whole increases and the number density of precipitates, at the same time, decreases. Obviously, the higher A_{ac} , the higher the interface velocity is (Eq. (4.17)), resulting in the formation of a lower number density of precipitates with larger size. It is also noticeable that there is an initial plateau in the values of mean radius similar to the one in the values of η -parameter. Since the character of precipitation is a geometry-dependent parameter (Eq. (4.11)), having a plateau in the mean precipitate radius is related to a plateau in the values of η -parameter. The plateau in the value of mean radius ends when coarsening starts, associated with the beginning of the decrease in the number density of precipitates (see Figs. 4.8 and 4.9). Figure 4.10 shows the prediction of yield strength for the alloy AA6082 aged at 190 °C at different values of accommodation factor, calculated by numerical, DCA, ICA, and MMA approaches. As it is seen at $A_{ac}=0.01$, DCA, ICA, and numerical solutions show that there is an initial increase in the yield strength, followed by a decrease and then a secondary increase. However, this is not seen in MMA solution. Besides, one can see that by increasing A_{ac} , accompanied by a decrease in number density (see for example Fig. 4.9a) and an increase in the mean radius (Fig. 4.8a), the peak-strength increases (Fig. 4.10a).

4. A Mixed-Mode Precipitation Model for Al-Mg-Si Alloys

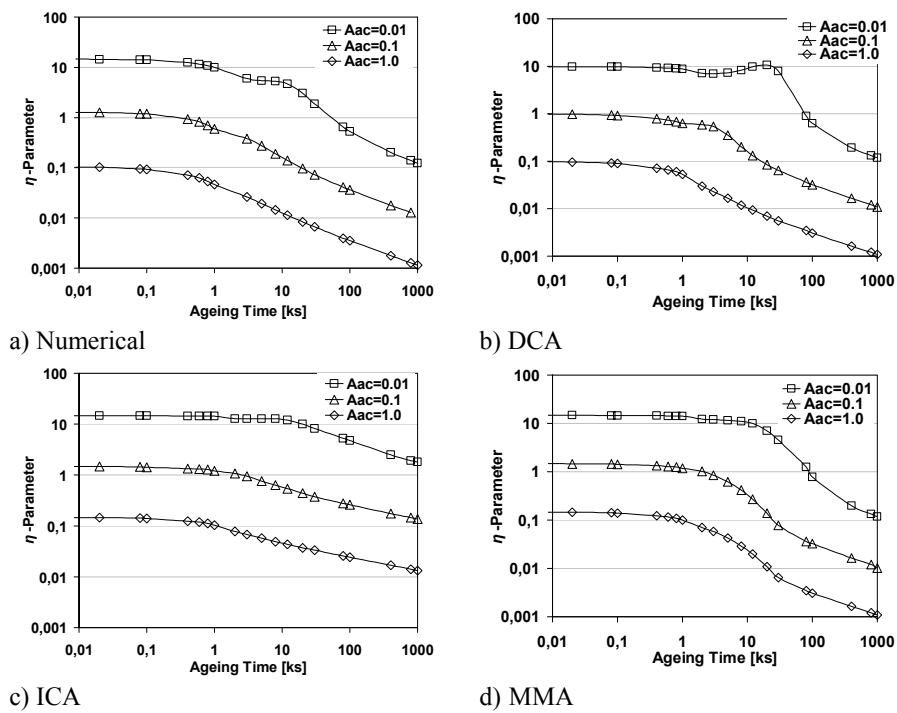


Figure 4.7: Effects of the parameter A_{ac} on the η -parameter during ageing at 190 °C, calculated by different approaches

4. A Mixed-Mode Precipitation Model for Al-Mg-Si Alloys

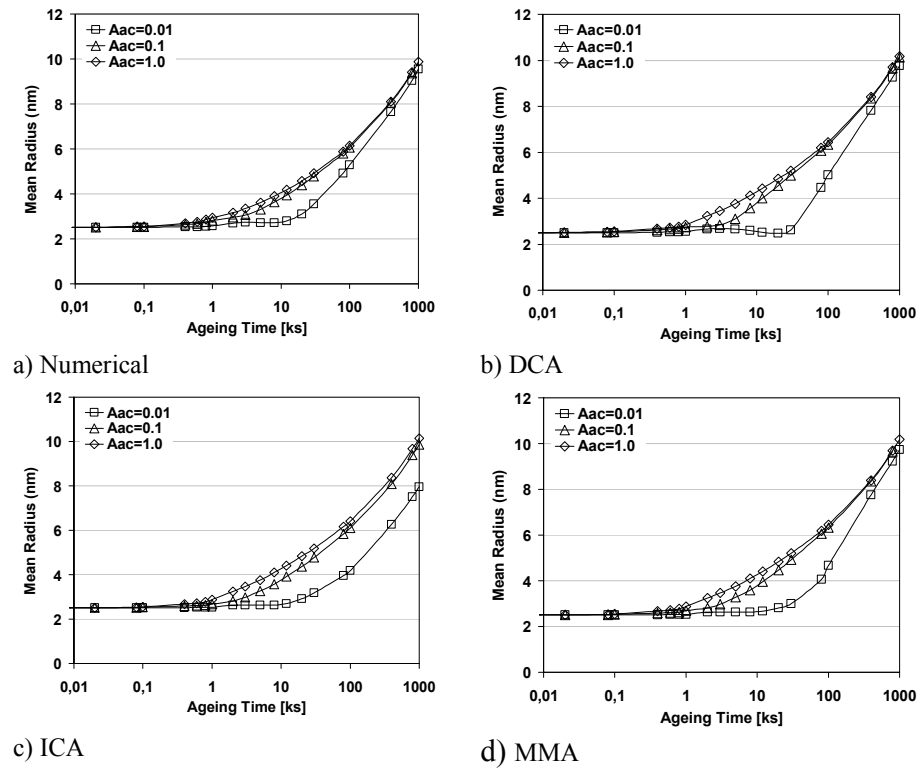
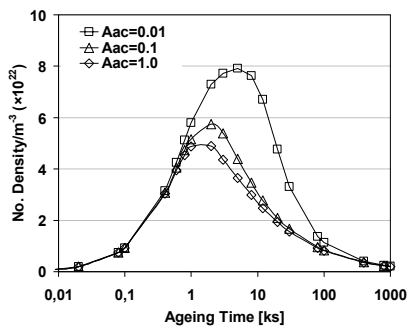
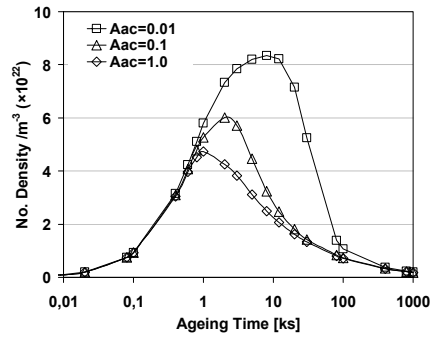


Figure 4.8: Effects of the parameter A_{ac} on the on the evolution of mean precipitate radius during ageing at 190 °C, calculated by different approaches

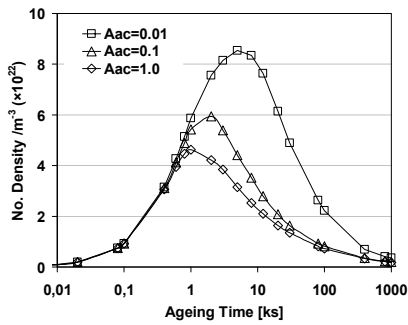
4. A Mixed-Mode Precipitation Model for Al-Mg-Si Alloys



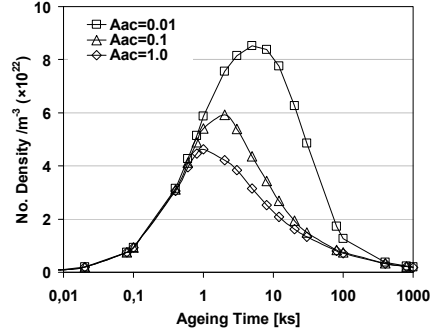
a) Numerical



b) DCA



c) ICA



d) MMA

Figure 4.9: Effects of the parameter A_{ac} on the evolution of number density of precipitates during ageing at 190 °C, calculated by different approaches

4. A Mixed-Mode Precipitation Model for Al-Mg-Si Alloys

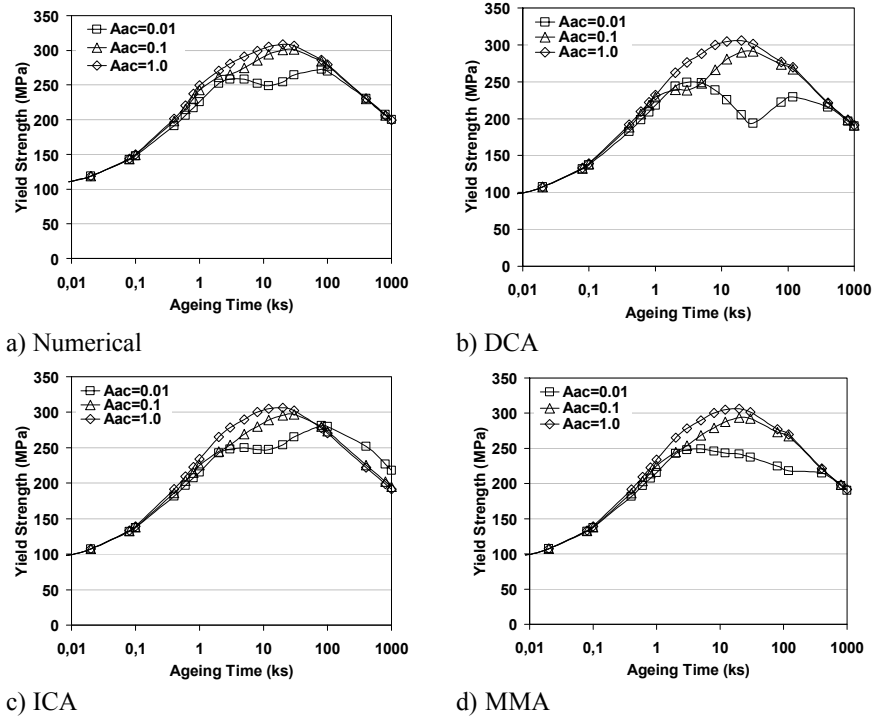


Figure 4.10: Effects of the parameter A_{ac} on the evolution of yield strength of the alloy AA6082 during ageing at 190 °C, calculated by different approaches

4.3.3. Effects of diffusivity

To check the effects of the diffusion rate on the character and kinetics of precipitation, three activation-energy values ($Q_d=90, 110, \text{ and } 130 \text{ kJ/mol}$) were used in Eq. (4.24), keeping the other parameters the same as for the standard case. Q_d was not changed in the nucleation equation (Eq. (4.19)) in order to study only the influence on growth. Figure 4.11 shows the effects of diffusivity on the character and kinetics of precipitation. The previously observed two characteristic stages in the evolution of the η -parameter (initial plateau followed by a decrease towards diffusion-controlled regime) are less distinctly present in Fig. 4.11. Clearly the decrease in the η -parameter starts in the very beginning of ageing. When the activation energy of diffusion is lower, the diffusion takes place at a higher rate, and the precipitation reaction consequently

4. A Mixed-Mode Precipitation Model for Al-Mg-Si Alloys

deviates from diffusion-controlled regime to mixed-mode and interface-controlled regimes. Due to this fact, at $Q_d=90$ and 110 kJ/mol, the transformation starts with the interface-controlled character. However, at $Q_d=130$ kJ/mol, which corresponds to the standard case, the precipitation reaction is almost diffusion-controlled from the beginning. The growth of precipitates is directly dependent on the diffusivity of the alloying element. Therefore, the higher the diffusivity of the alloying element, the faster the velocity of the interface, resulting in the formation of larger precipitates with a smaller number density (see for example Figs. 4.12a and 4.13a). Figure 4.14 shows the effects of diffusivity on the yield strength of the alloy AA6082. Of course, the higher the diffusivity, the faster the kinetics of hardening is, meaning that the alloy reaches the peak-age faster. It is also seen that faster diffusion, accompanied by a decrease in number density of precipitates and an overall increase in the mean radius, results in a lower peak-strength. From Figs. 4.11-4.14, one can see that differences between the outcomes of numerical, DCA, ICA, and MMA approaches in some cases are very large. The mean radius predicted by DCA solution, when $Q_d=90$ kJ/mol, is considerably larger than that predicted by ICA, MMA, and numerical solutions. This is due to the huge overestimation of driving force by DCA, when the growth is far from diffusion control character (i.e. $Q_d=90$ kJ/mol) as is seen in Fig. 4.2. This certainly affects the predicted yield strength, such a way that the predicted yield strength by DCA method in the case of $Q_d=90$ or 110 kJ/mol is much lower than the predictions of other methods. As one can expect, when the growth character is far from diffusion control, DCA solution is not a good approximation of driving force.

4. A Mixed-Mode Precipitation Model for Al-Mg-Si Alloys

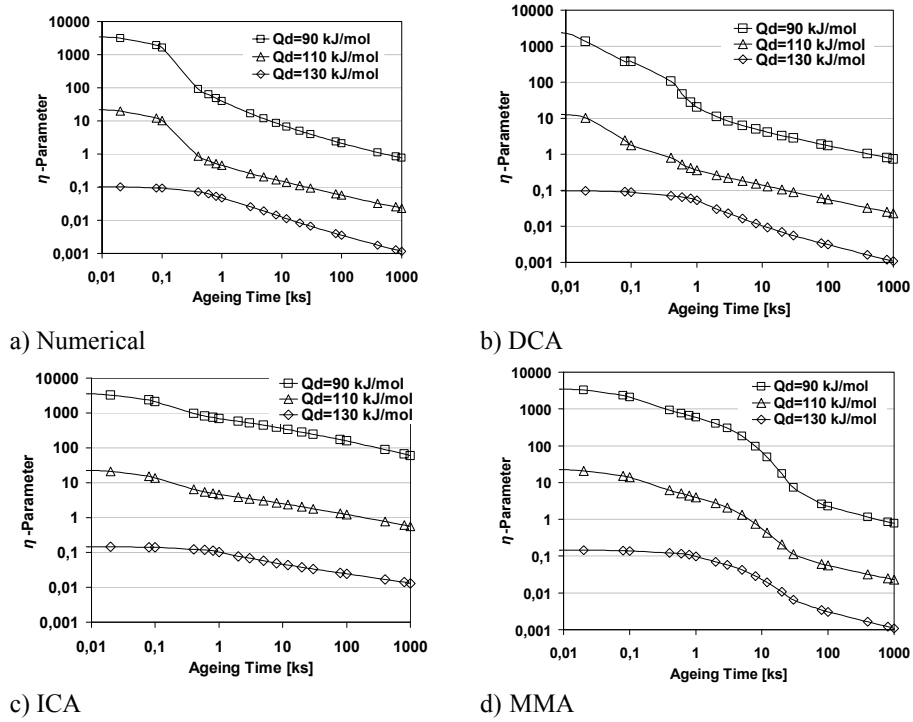
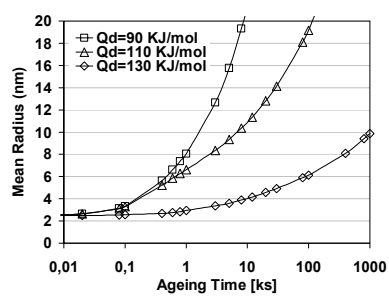
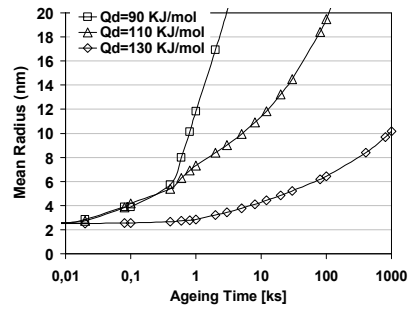


Figure 4.11: Effects of diffusivity on the η -parameter during ageing at 190 °C, calculated by different approaches

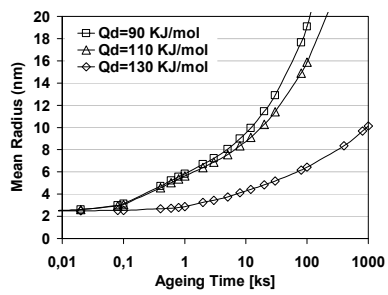
4. A Mixed-Mode Precipitation Model for Al-Mg-Si Alloys



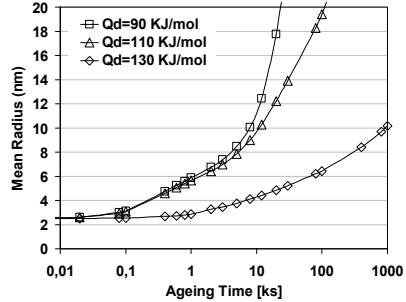
a) Numerical



b) DCA



c) ICA



d) MMA

Figure 4.12: Effects of diffusivity on the evolution of mean precipitate radius during ageing at 190 °C, calculated by different approaches

4. A Mixed-Mode Precipitation Model for Al-Mg-Si Alloys

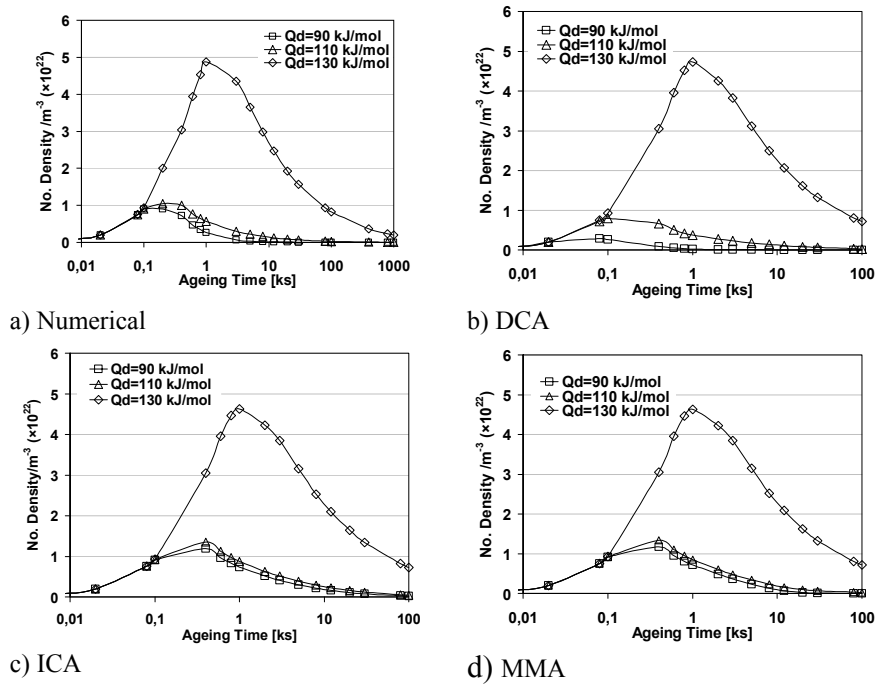


Figure 4.13: Effects of diffusivity on the evolution of a) number density of precipitates and b) mean precipitate radius during ageing at 190 °C

4. A Mixed-Mode Precipitation Model for Al-Mg-Si Alloys

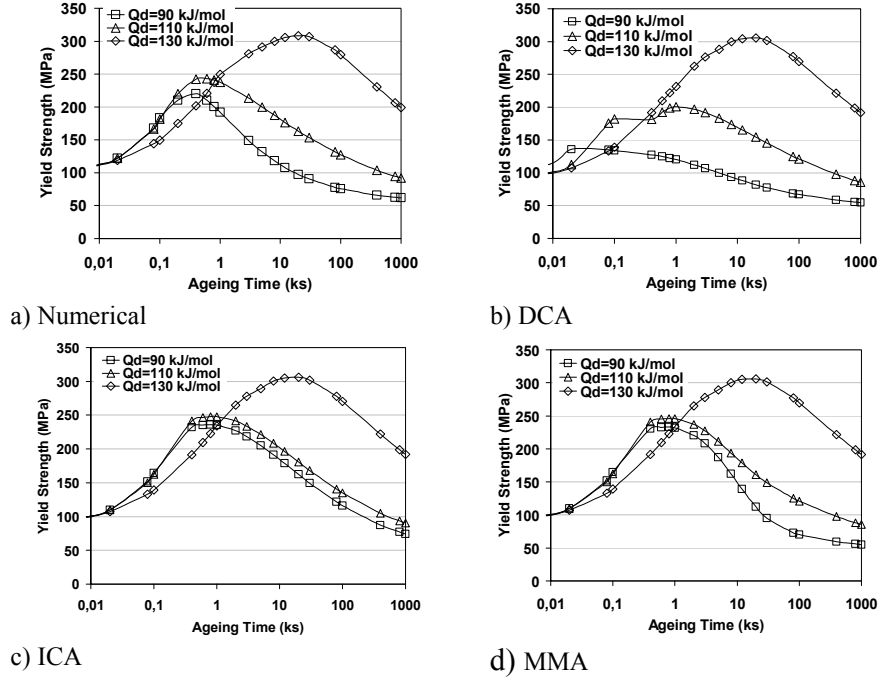


Figure 4.14: Effects of the parameter A_{ac} on the evolution of yield strength of the alloy AA6082 during ageing at 190 °C

To acquire a better understanding of the effects of deviation from diffusion-controlled character on the kinetics of precipitation, it is useful to check the precipitate size distribution during ageing. The size distribution of precipitates, for the case of $Q_d=90$ kJ/mol, which implies a mainly interface-controlled character, and 130 kJ/mol, which implies a diffusion-controlled transformation, at 10 s, 100 s, and 1000 s is shown in Fig. 4.15. Also, the critical radius corresponding to each size distribution is shown by a vertical line. The critical radius, r_{cr} , the size below which precipitates are not stable and they dissolve, is given by [4]

$$r_{cr} = \frac{2\gamma V_m}{RT} \left(\ln \left(\frac{C_m}{C_e} \right) \right)^{-1} \quad (4.25)$$

It is seen that at 10 s for both cases, $Q_d=90$ and 130 kJ/mol, the critical radius is lower than the minimum size in the precipitate-size distribution, indicating that all existing precipitates are stable and they tend to grow. At this point, only nucleation and growth are controlling the ageing kinetics. When the ageing time is increased to 100 s, the critical radius in the case of $Q_d=90$ kJ/mol shifts to higher values than the maximum in

4. A Mixed-Mode Precipitation Model for Al-Mg-Si Alloys

the precipitates size distribution, making the smaller precipitates unstable. For $Q_d=130$ kJ/mol this is not the case. This indicates that in the case of $Q_d=90$ kJ/mol, a large fraction of precipitates is likely to dissolve. However, the sudden increase of critical radius to the right side of the size distribution is not seen when $Q_d=130$ kJ/mol. At ageing time equal to 1000 s, the size distribution in both cases is divided into dissolving precipitates and growing precipitates; the dissolving part is shifting to lower size values, while the growing part is moving to higher values, obviously meaning that coarsening is active.

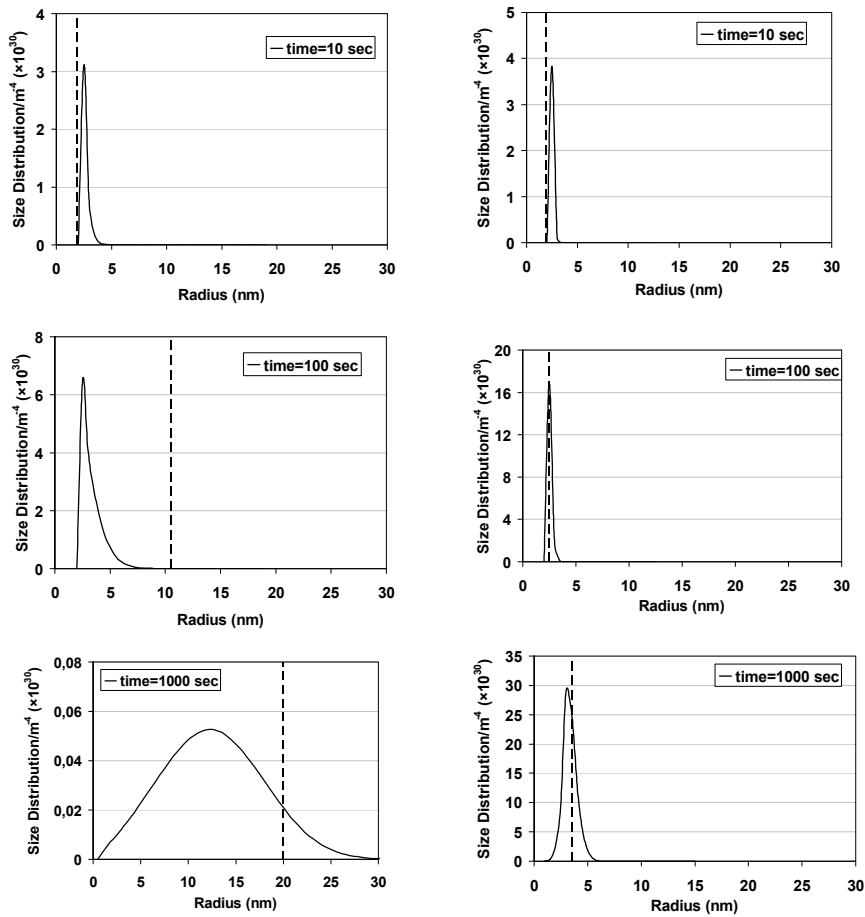


Figure 4.15: Size distribution of precipitates at 10, 100, 1000 sec for $Q_d=90$ kJ/mol (left column) and $Q_d=130$ kJ/mol (right column)

4. A Mixed-Mode Precipitation Model for Al-Mg-Si Alloys

In order to explain the shift of the critical radius to the right side of the precipitate size distribution when $Q_d=90$ kJ/mol, it is useful to plot the evolution of the mean concentration of alloying element in the matrix during ageing (see Fig. 4.16a), considering the fact that there is an inverse relation between the matrix concentration and the critical radius (see Eq. (25)). Figure 4.16 shows that the higher the diffusivity (lower Q_d), the faster depletion of alloying elements one can expect. In the case of $Q_d=90$ kJ/mol, this depletion happens very fast (due to the faster growth kinetics, see Figs. 4.12 and 4.13), in such a way that before 100 s the matrix is depleted to the equilibrium value. However, in the case of $Q_d=130$ kJ/mol this depletion happens gradually with at a lower rate. Figure 4.16b shows that this also happens for critical radius; i.e. the faster the depletion is, the faster the critical radius increases.

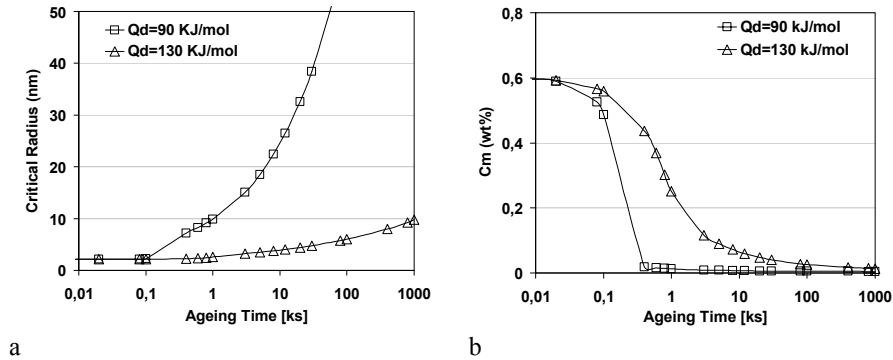


Figure 4.16: Evolution of a) mean concentration of alloying elements and b) critical radius during ageing at 190 °C for $Q_d=90$ and 130 kJ/mol

4.3.4. Effects of precipitate size distribution

It is worth mentioning that during ageing there is always a size distribution of precipitates. The growth character of smaller precipitates, as GP-zones, will tend to be mixed mode or interface controlled because of their small size and higher interface coherency, hence lower mobility. Bigger and more incoherent precipitates as the β phase are more likely to have a diffusion-controlled growth type. As a case in point, the variation of the η -parameter as a function of the precipitate size is shown in Fig. 4.17 for the case $Q_d=130$ kJ/mol and 90 kJ/mol with $A_{ac}=1.0$ after 3000 s ageing. Smaller precipitates in the size distribution have more interface-controlled growth character. This interface-controlled growth character changes towards diffusion-controlled character for bigger precipitates. Figure 4.18 gives a more complete overview of the effects of size of precipitates on the precipitation character. In this map the boundaries between different

4. A Mixed-Mode Precipitation Model for Al-Mg-Si Alloys

precipitation characters are shown for different values of the parameter A_{ac} and precipitate radius at for different values of Q_d . Interestingly, one can see that for the standard case (Fig. 4.18a) precipitates smaller than 2 nm are always growing in the interface-controlled regime whatever the type of their interface is, while those having sizes between 2 and 4 nm are most likely to grow under mixed-mode character. Precipitates bigger than 4 nm, depending on the parameter A_{ac} , can have either mixed-mode or diffusion-controlled character. By decreasing the value of Q_d , the interface-controlled transformation domain ($\eta > 10$) increases, in such a way that at $Q_d = 100$ kJ/mol precipitates smaller than 10 nm have an interface-controlled character through ageing (see Fig. 4.18d).

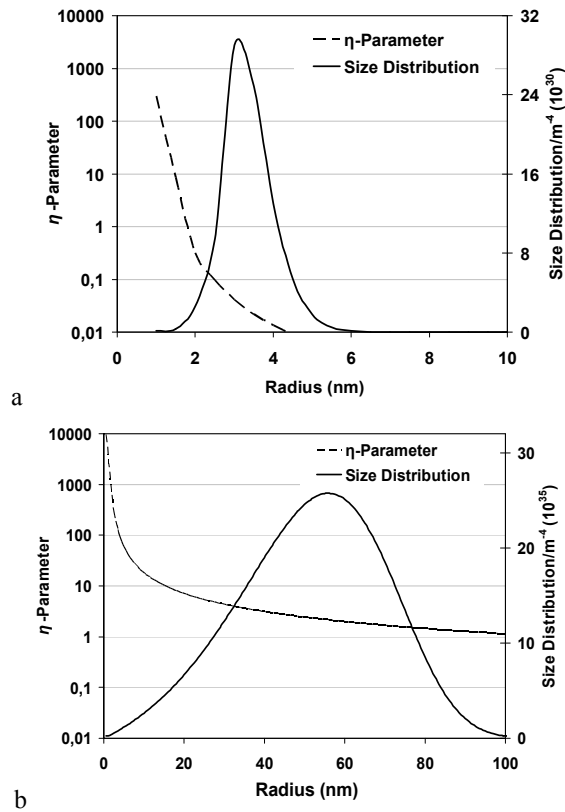


Figure 4.17: η -parameter as a function of the precipitate size after 3000 sec for a) standard case and b) $Q_d = 90$ kJ/mol

4. A Mixed-Mode Precipitation Model for Al-Mg-Si Alloys

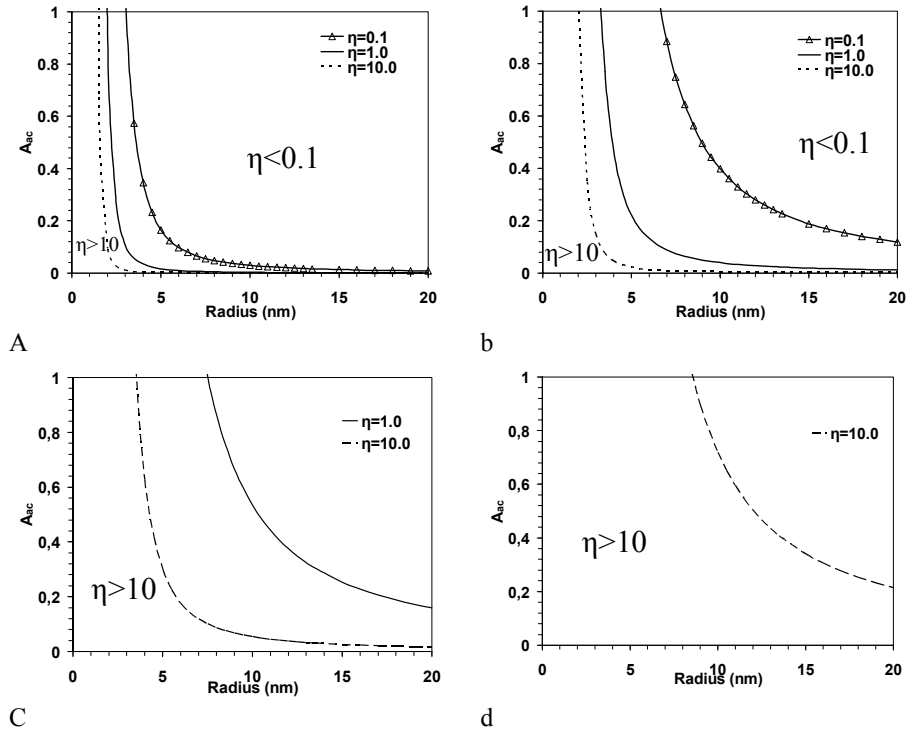


Figure 4.18: Domains corresponding to different precipitation characters for different values of Q_d : a) 130, b) 120, c) 110, and d) 100 kJ/mol. (Note: the area under the dashed line is corresponding to interface-controlled character, and area above the solid line is corresponding to diffusion-controlled character)

Figure 4.19 shows the effects of temperature on the boundaries between different growth characters. In this figure the solid lines and the dashed lines are for 190 °C and 140 °C, respectively. Obviously, the effect of temperature on the transition radius between the interface control regime and the mixed-mode character is very small. However, there is a much more pronounced effect on the transition radius between the mixed-mode regime and the diffusion-control character. This means that the precipitation character becomes diffusion-controlled at smaller radius, when ageing temperature is lower.

4. A Mixed-Mode Precipitation Model for Al-Mg-Si Alloys

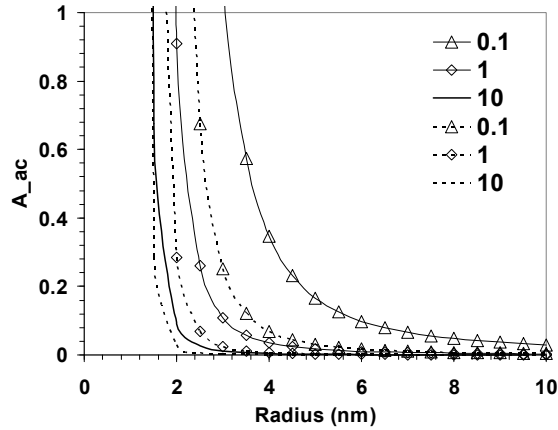


Figure 4.19: Effects of temperature on the domains corresponding to different precipitation characters for $Q_d=130$ kJ/mol (Note: the dashed lines show the boundaries for 140 °C and the solid lines are drawn for 190 °C)

4.3.5. Application of the model

In order to make a more physically realistic mixed-mode model, one should consider the increase of both interfacial energy and A_{ac} during ageing. Precipitation starts with the formation of GP-zone, having lowest values of γ and A_{ac} , followed by the formation of other precipitates and gradual increasing of both γ and A_{ac} . There are considerable uncertainties about the evolution of γ and A_{ac} of different precipitates during ageing. For example, the values of these parameters and their size dependence for each type of precipitate are not known. A relatively simple way of dealing with this complexity would be assigning constant γ and A_{ac} to each precipitate species instead of using constant values for the whole ageing sequence. In this approach, values of γ , A_{ac} , and C_β are changed when the mean radius reaches a certain value. Table 4.1 shows the values of γ , C_β , and A_{ac} chosen for different precipitates. The transition radius for GP $\rightarrow\beta''$ (2 nm) and $\beta''\rightarrow\beta'$ (7 nm) is obtained from the literature [15] (see table 4.2), while that of $\beta'\rightarrow\beta$ (15 nm) is a chosen value. Of course the assumption of complete transition of one precipitate species to the other precipitate at a specific mean radius is an approximation. However, this is much closer to the physical reality of the system than assuming constant values of γ , A_{ac} , and C_β throughout the entire ageing sequence.

4. A Mixed-Mode Precipitation Model for Al-Mg-Si Alloys

Table 4.1: Chosen input values for different precipitates

Precipitate	Stoichiometry	C_β (wt%)	Radius (nm)	γ (J/m ²)	A_{ac}
GP	$Mg_2Si_3Al_6$	17	$R_m < 2$	0.1	0.01
β''	Mg_5Si_6	42	$2 < R_m < 7$	0.26	0.1
β'	$Mg_{1.8}Si$	61	$7 < R_m < 15$	0.37	0.5
β	Mg_2Si	63	$15 < R_m$	0.45	1.0

Table 4.2: Precipitates present in the alloy AA6082 [15]

Precipitate	Stoichiometry	C_β (wt%)	Morphology/typical size
GP	Si/Mg>1	17	Almost spherical/1-2 nm
β''	Mg_5Si_6	42	Needles/up to $40 \times 40 \times 350 \text{ \AA}^3$
β'	$Mg_{1.7}Si$	60	Ribbons/several μm long
β	Mg_2Si	63	Plates or cubes/up to 10-20 μm

Figure 4.20 shows the evolution of mean radius together with η -parameter at three different ageing temperatures; 140, 180, and 220 °C obtained from the modified mixed-mode model. There is an initial plateau in the value of mean radius and accordingly in that of η -parameter, which is due to the formation of GP nuclei, followed by a smooth increase of mean radius and consequently decrease of η -parameter. It is also apparent that the higher the ageing temperature, the sooner the growth of initial nuclei takes place and due to the faster growth kinetics, precipitates formed at higher temperatures are bigger. Also it is noticeable that at higher temperature, precipitation starts with more interface controlled character.

Figure 4.21 shows the evolution of the yield strength of the alloy AA6082 at four different ageing temperatures, which shows a good agreement with the experimental data from ref. [16].

4. A Mixed-Mode Precipitation Model for Al-Mg-Si Alloys

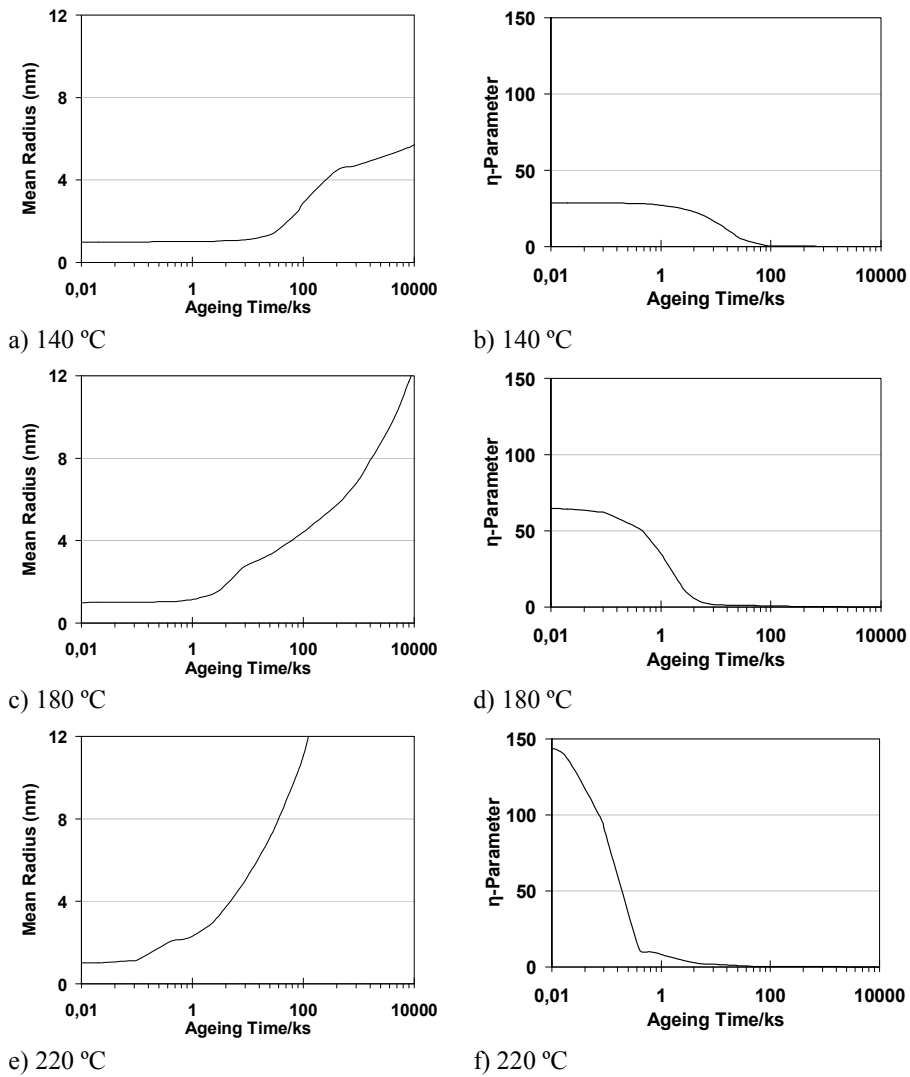


Figure 4.20: Prediction of mean radius (a,c,e) and η -parameter (b,d,f) of the alloy AA6082 obtained from the modified mixed-mode model using the DCA approach at three different temperatures.

4. A Mixed-Mode Precipitation Model for Al-Mg-Si Alloys

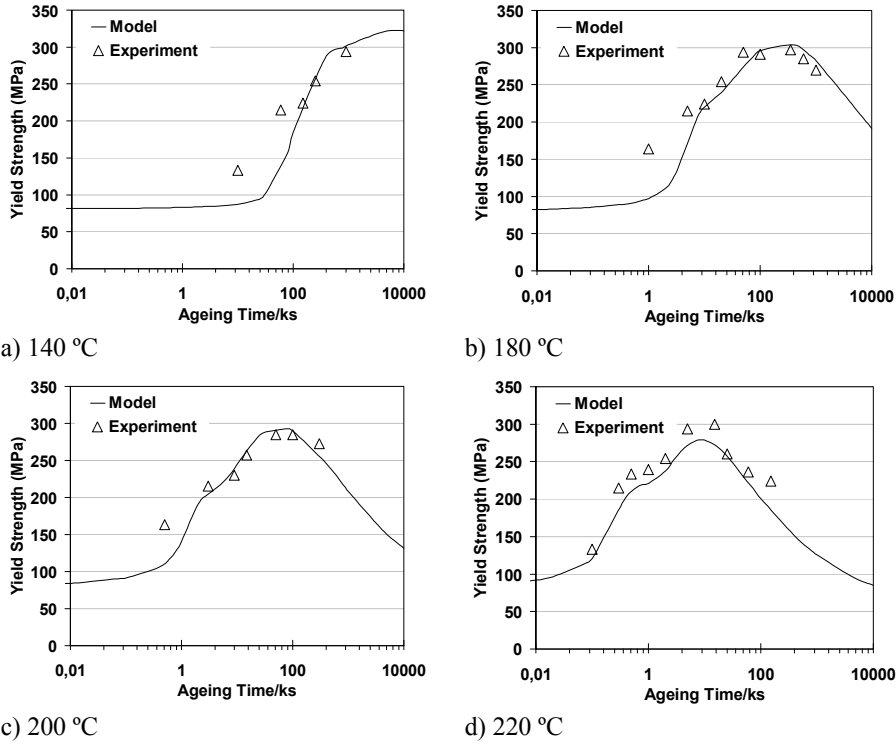


Figure 4.21: Evolution of the yield strength of the alloy AA6082 obtained from the modified mixed-mode model using the DCA approach at four different temperatures (the accuracy of experimental data is ± 10 MPa). Experimental data from ref. [16].

4.4. Discussion

Al-Mg-Si alloys undergo a very complex precipitation sequence during ageing in which the coherency and interfacial energy of precipitates change, resulting in a varying precipitation character. A mixed-mode KWN model has been developed to systematically study the effects of interfacial energy, mobility, and diffusivity on the kinetics and character of precipitation. Three solutions have been proposed to model the growth rate of precipitates; i) numerical solution in which the matrix composition at the interface, C_b , is calculated numerically and then is used in the growth equation (either Eq. (4.3) or Eq. (4.4)), ii) DCA and ICA methods, which are mainly suitable when the growth character is almost diffusion controlled or interface controlled respectively, and

4. A Mixed-Mode Precipitation Model for Al-Mg-Si Alloys

iii) MMA solution where the constant κ is varying during ageing until peak-age (Eq. (4.10)). After peak-age, κ is assumed to be unity. The results show that in the mixed-mode and diffusion-controlled conditions, all three DCA, ICA, and MMA approximations give results, which are relatively close to that of numerical solution (see Figs. 4.7-4.10). On the other hand, when the growth is interface-controlled (see Fig. 4.11), using DCA methods results in the predicted mean radius, which is considerably larger than those predicted by numerical, ICA, and MMA solutions (Fig. 4.12). This is due to the fact that the driving force in the interface-controlled regime (when C_i is close to C_0), predicted by DCA, is much larger than that predicted by either numerical or ICA solutions. This results in much lower predicted yield strength as is seen in Fig. 4.14 compared to other methods. The η -parameter, directly proportional to the diffusivity and inversely proportional to the mobility and the radius of precipitates, is introduced in the analytical solutions to show how the character of precipitation changes during ageing. The evolution of the η -parameter during ageing shows a similar pattern in all cases; an initial stage in the beginning of ageing, where the η -parameter is either constant (see Figs. 4.6 and 4.7) or decreases with a very slow kinetics (see Fig. 4.11), followed by a faster decrease towards diffusion-controlled character. In the beginning of ageing, the precipitation reaction is mainly governed by nucleation. So, the increase in the value of mean precipitate radius is very small, leading to the mentioned plateau in the magnitude of the η -parameter. The increase in the mean precipitate radius due to growth and coarsening results in the decrease of the η -parameter, since this term is inversely proportional to the radius of precipitates (see Eq. (4.11)). This indicates that at constant $M_{\alpha\beta}$ and D , the evolution of the η -parameter during ageing is mainly controlled by geometrical effects. The bigger the precipitates, the larger amount of solute needed to increase the precipitates mean radius, meaning that solutes on average need to diffuse from further away, thus making the growth more diffusion-controlled. The change in the value of interfacial energy, arising from the change in the coherency of interface during ageing, has a very small effect on the character of precipitation (see Fig. 4.4). In all three chosen values of interfacial energy, the precipitation reaction, initially having a small deviation from diffusion-controlled character, rapidly becomes diffusion-controlled. The parameter A_{ac} changes during ageing from very small values for coherent precipitates to values close to one for incoherent ones. By decreasing A_{ac} , related to the degree of coherency of the interface, and consequently decreasing the mobility, the value of the η -parameter increases, making the transformation less diffusion-controlled. The effects of change in the diffusivity on the character of precipitation shows that by increasing the rate of diffusion, the overall value of the η -parameter increases, indicating that the

4. A Mixed-Mode Precipitation Model for Al-Mg-Si Alloys

character of precipitation becomes more affected by the interface reaction. This might occur when the diffusing alloying element is an interstitial atom or the alloy is heavily deformed before ageing. From industrial point of view, there are many cases where the deformed alloy is aged without solutionizing. For example, extruded products are normally aged directly after extrusion. In the case when ageing is done on the heavily deformed alloy, due to the faster dislocation-core diffusion, the assumption of mixed-mode controlled growth would be more accurate than assuming diffusion-controlled kinetics. Figure 4.10 shows the evolution of the yield strength of the alloy AA6082 during ageing for different values of A_{ac} . As it is seen the yield strength of this alloy, when $A_{ac} = 0.01$, is notably lower than that of the alloy with $A_{ac} = 0.1$ or more. Considering that a higher yield strength is usually desired, comparing Fig. 4.8a, 4.9a, and 10a, one can conclude that the mechanical properties at the combination of lower number density of precipitates with larger average size are much better. On the other hand, looking at Figs. 4.12a, 4.13a, and 4.14a, one can see that the diffusivity of the alloying element induces an inverse relation between precipitate radius and density, and yield strength. These two different conclusions are not contradictory. As it is mentioned before, the precipitates, depending on their size, can be either shearable or non-shearable. When their size is less than a critical value (which is 5 nm in case of Al-Mg-Si alloys), precipitates are considered shearable. In this case the strength of precipitates depends on their radius, as is shown in Eq. (4.23). Looking at Fig. 4.8a, it is easily seen that the precipitates radius at three different accommodation factors are less than 5 nm up to well inside the overageing regime meaning that the strength of precipitates and accordingly the alloy is dependent on the radius of precipitates. Therefore, the combination of larger precipitates with smaller number density gives better mechanical properties. On the other hand, when the precipitates radius is bigger than 5 nm, their strength is independent of their size (Eq. (4.23)). In this case, the mechanical properties of the alloy changes with the precipitates mean distance or the precipitates density. The higher the precipitates density (the lower the precipitates distance), the better mechanical properties can be achieved. This is the case in Figs. 4.12a, 4.13a, and 4.14a. It is also worth mentioning that the concurrent presence of different precipitates in the material, having different growth characters, is very much possible. It is seen that small nuclei, no matter how much their accommodation factor is, grow with the interface control character (see Fig. 4.18). At some point, the growth character of these small nuclei changes to mixed-mode and eventually diffusion control. The range of interface-controlled growth is very much dependent on the diffusion rate of alloying element; the higher the diffusion rate, the longer precipitate grow under interface-control character (see Fig. 4.18). Regarding

4. A Mixed-Mode Precipitation Model for Al-Mg-Si Alloys

the effects of temperature on the growth character domains, it is seen that the position of the boundary for $\eta=0.1$ is more sensitive to temperature than the boundary for $\eta=10$. Since it is assumed that the activation energy for the jumping of atoms across the interface is equal to the activation energy of bulk diffusion, one can rewrite the analytical equation for growth character (Eq. (4.11)) as follows, putting the values corresponding to the mobility of interface (from Eq. (4.15)) and diffusion rate (from Eq. (4.24)) into Eq. (4.11)

$$\eta = \frac{2.2 \times 10^{-4} (m^2 / s)}{rbvA_{ac}C_{\beta}} C_{\alpha}. \quad (4.26)$$

Putting the value of C_{α} from Eq. (18) into Eq. (26) yields

$$\eta = \frac{2.2 \times 10^{-4} (m^2 / s) \times 970 (wt\%)}{rbvA_{ac}C_{\beta}} \exp\left(\frac{2\gamma V_m}{rRT} - \frac{Q_s}{RT}\right), \quad (4.27)$$

in which the exponential term, representing the Gibbs-Thomson effect, is the only temperature-dependent term. Mathematical examination of eq. (4.27) shows that the lower the η , the more sensitive is the corresponding radius (boundary) with temperature. This is more a mathematical effect than a physical reason

4.5. Conclusions

The effects of interfacial energy, mobility, and diffusivity on the growth character, precipitation kinetics, and yield strength of the alloy AA6082 during isothermal ageing has been studied using a mixed-mode KWN model. The classical KWN is modified in such a way that the effects of the character of precipitation on the growth kinetics have been taken into consideration using the mixed-mode parameter η . This parameter is directly proportional to the diffusion rate and is inversely related to the radius of precipitate and the mobility. Three analytical approaches; i.e. DCA, ICA, and MMA as well as a numerical method have been used to calculate the growth rate during ageing. The following conclusions are the main outcomes of the model.

- Modelling results show that the interfacial energy does not have any prominent effect on the character of precipitation.
- The mobility of interface and the diffusivity of alloying elements can be considerably influential. For example, when the parameter A_{ac} is very small, as is the case for coherent interfaces, especially in the beginning of ageing or for small precipitates of the size distribution the assumption of diffusion-controlled

4. A Mixed-Mode Precipitation Model for Al-Mg-Si Alloys

growth is doubtful. Also, when the diffusion rate is relatively high, for instance when the alloying elements are interstitial, the precipitation reaction becomes mixed-mode or even interface-controlled.

- Increasing diffusion rate, in the selected range, accompanied by an increase in the mean radius and decrease in the number density, decreases the yield strength.
- Increasing A_{ac} , in the selected range, accompanied by an increase in the mean radius and decrease in the number density, increases the yield strength.
- There is a certain radius below which precipitation character is always interface controlled for all values of the parameter A_{ac} . Of course the faster the diffusion rate, the higher this radius is.
- At higher ageing temperatures, in the beginning of ageing, more deviation from diffusion-controlled growth is expected. This is because of the higher value of equilibrium interfacial concentrations at higher temperatures.

References:

- [1] Kampmann R, Wagner R, in: P. Hassan, V. Gerold, R. Wagner, MF. Ashby, editors. Decomposition of alloys: the early stages, Oxford: Pergamon Press; 198. pp 91.
- [2] Robson JD, Jones MJ, Prangnell PB, Acta Mater 2003;51;1453.
- [3] Robson JD, Mater Sci Tech 2004;20;441.
- [4] Myhr OR, Grong Ø, Acta Mater 2000;48;1605.
- [5] Khan IN, Starink MJ, Yan JL, Mater Sci Eng A 2008;66;472.
- [6] van Leeuwen Y, Sietsma J, van der Zwaag S, ISIJ Int 2003;43;767.
- [7] Sietsma J, van der Zwaag S, Acta Mater 2004;52;4143; Bos C, Sietsma J, Scr. Mater. 2007; 57; 1085
- [8] Zener C, Applied Physics 1949;20;950.
- [9] Wu L, Ferguson WG, Int. Journal of Modern Physics C 2009;20;1113.
- [10] Doherty RD, Diffusive phase transformations in the solid state, Physical metallurgy 4th edition; 1996. pp 1364.
- [11] Samaras SN, Modelling Simul Mater Sci Eng 2006;14;1271.
- [12] Myhr OR, Grong Ø, Andersen SJ, Acta Mater 2001;49;65.
- [13] Robson JD, Acta Mater 2004;52;4669.
- [14] Edwards GA, Stiller K, Dunlop GL, Couper MJ, Acta Mater. 1998;11;3893.

4. A Mixed-Mode Precipitation Model for Al-Mg-Si Alloys

- [15] Marioara CD, Andersen SJ, Jansen J, and Zandbergen HW, *Acta Mater* 2001-49; 321:331.
- [16] Sadeghian AR, Private communication, Materials Engineering Department, Yazd University, Iran.

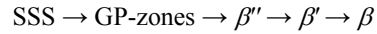
CHAPTER 5

Multi-Component Multi-Precipitate Modelling of Ageing Kinetics in Al-Mg-Si Alloys

An ageing model based on the assumption of maximum Gibbs free energy dissipation is applied to model the ageing kinetics of Al-Mg-Si alloys. The proposed model is a multi-component multi-precipitate model, which has been already applied to Fe-based alloying systems. In this modelling framework it is possible to consider simultaneous formation of GP-zones, β'' , β' , β , and free-Si. The model predicts that a large fraction of the nuclei of different precipitate species form during quenching from solutionizing temperature and during heating up to ageing temperatures. Besides, the model shows that the nucleation of all precipitates happen in a very fast rate, inferring the site saturation nucleation. The beginning of ageing is accompanied by the growth of the less stable precipitates, followed by their dissolution at some point in favor of more stable precipitates. In the end, only thermodynamically stable precipitates like β and free-Si remain in the alloy. This actually ends up the precipitation sequence. The outputs of the ageing model are used as inputs of strengthening model to predict the yield strength of the aged alloys. The total strength of the alloy has contributions from precipitation strengthening and solid solution hardening. The model shows that the most important precipitate in terms of strengthening is β'' phase, having a temperature-dependent interfacial energy in the range of 0.25 to 0.29 J/m².

5.1. Introduction

Al-Mg-Si alloys undergo a very complicated precipitation sequence during ageing. The precipitation sequence of Al-Mg-Si alloys is conventionally believed [1] to be:



Where SSS is the supersaturated solid solution, atomic clusters and GP-zones are Si and/or Mg colonies, β'' are needle-shaped precipitates oriented along $\langle 100 \rangle_{\text{Al}}$ with a monoclinic structure, β' is a metastable rod-shaped precipitate aligned in the $\langle 100 \rangle_{\text{Al}}$ direction, and β is the stable Mg_2Si precipitate [2]. Table 5.1 shows a rather complete overview of different precipitates in Al-Mg-Si system. The precipitation in Cu-containing Al-Mg-Si alloys has been traditionally considered to be analogous to ternary Cu-free Al-Mg-Si alloys, with the exception of the presence of a quaternary phase, Q and its metastable precursor, Q' [3]. The precipitate to nucleate in the beginning of ageing is not the equilibrium precipitate β even though it has the highest nucleation driving force as is shown schematically in Fig. 5.1. The precipitation starts with GP-zones due to their relatively low activation energy barriers for nucleation (see schematic Fig. 5.2). GP-zones are fully coherent precipitates having very low interfacial energy, whereas the β phase has a high-energy incoherent interface. The interfacial energies of other intermediate precipitates vary between these two extremes. Therefore, despite the fact that the driving force for precipitation of GP zones is less than for the equilibrium phase, the barrier to nucleation (ΔG^*) is still less due to the low value of interfacial energy, and GP-zones nucleate most rapidly. The value of interfacial energy is strongly dependent on the type of interface. For fully coherent precipitates (shown schematically in Fig. 5.3), where there are no broken bonds across the interface, the interface energy is only of chemical nature, because there is no structural difference. Fully coherent interface is expected whenever there is no or only very little mismatch. Especially GP-zones, having lattice parameter very close to that of aluminum matrix, have fully coherent interfaces. If the lattice parameters of precipitate and matrix differ, the lattice will be deformed elastically (see Fig. 5.4) resulting in coherency strain energy. If the coherency strain becomes large, it would be energetically more favorable for the system to replace the fully coherent interface with a semicoherent interface in which the strain in the interface is accommodated by dislocations. When the interfacial plane separates two very different atomic configurations in the precipitate and in the matrix, there is no possibility of good matching across the interface. In this case the interface is said to be incoherent. During ageing, small GP-zones will nucleate with fully coherent interfaces

5. Multi-Component Multi-Precipitate Modelling of Ageing Kinetics in Al-Mg-Si Alloys

and introduce only low elastic strain. During their growth to other precipitates, some interfaces can transform into semicoherent interfaces to reduce the elastic strain energy accompanied by the formation of misfit dislocations in the interface. By increasing the number of misfit dislocations or changing the crystal structure from FCC (GP-zones) to monoclinic (β'') and hexagonal (β'), the interface eventually becomes incoherent.

Table 5.1: Reported crystal structures of Al–Mg–Si–(Cu) precipitate phases [3]

Phase	Structure (Dimensions are in Å)	Mg/Si	Ref.
GP-zone	fcc based orthorhombic super cell Mg:Si=2:1, a=8.08, b=8.74, c=4.05	1.59	4
GP-zone	fcc based cubic (Mg:Si=1:1, a=4.05)	1.73	5
GP-zone	fcc based base-centered monoclinic (Al+Mg):Si=5:6, a=14.78, b=4.05, c=6.74, $\beta=106.8^\circ$	0.67	2
β''	Base-centered monoclinic (C2/m) Mg:Si=5:6, a=15.16, b=4.05, c=6.74, $\beta=105.3^\circ$	0.94	6
β''	Base-centered monoclinic Mg:Si=5:6, a=15.34, b=4.05, c=6.83, $\beta=106^\circ$	1.01	7
β''	Monoclinic Mg:Si=5:6, a=6.16, b=6.16, c=7.1 $\alpha=\beta=106^\circ, \gamma=82^\circ$	0.09	8
β''	Monoclinic Mg:Si=5:6, a=3.00, b=3.30, c=4.00 $\alpha=\beta=106^\circ, \gamma=71^\circ$	1.73	9
β''	Monoclinic Mg:Si=5:6, a=6.5, b=7.6, c=4.05, $\gamma=70^\circ$	1.54	10
β''	Monoclinic Mg:Si=5:6, a=6.5, b=7.6, c=4.05, $\gamma=70^\circ$	1.54	11
β''	Monoclinic (P2/m) Al:Mg:Si=3:1:6, a=7.7, b=6.7, c=2.03, $\gamma=75^\circ$	0.83	12
β'	Hexagonal (a=b=7.05, c=4.05)	1.73	9
β'	Hexagonal (Mg:Si=0.44:1, a=b=7.08, c=4.05)	1.73	13
β'	Hexagonal (Mg:Si=2:1, a=b=7.1, c=4.05)	0.83	14
β'	Hexagonal (a=b=7.15, c=4.05)	1.8	15
β'	Hexagonal (a=b=7.15, c=4.05)	1.8	15
β'	Hexagonal (P62m) (a=b=7.1, c=4.05)	1.54	16
Q'	Hexagonal	0.44	17
Q	Hexagonal	1.12	17
β	Cubic (Mg:Si=2:1, a=6.39)	1.73	18
β	Cubic (Mg:Si=2:1, a=6.4)	1.73	12

5. Multi-Component Multi-Precipitate Modelling of Ageing Kinetics in Al-Mg-Si Alloys

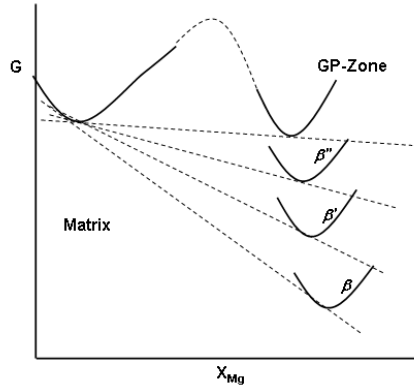


Figure 5.1: A schematic molar free energy diagram for the Al-Mg-Si system (assuming constant Si)

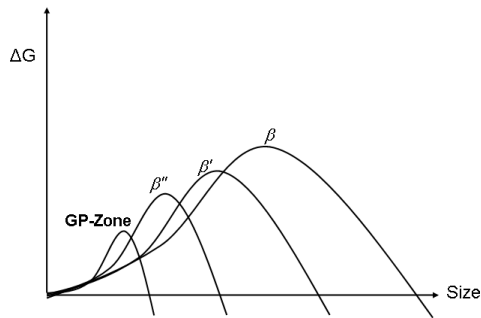


Figure 5.2: A schematic of the activation energy barriers to the formation of different precipitates in Al-Mg-Si alloys

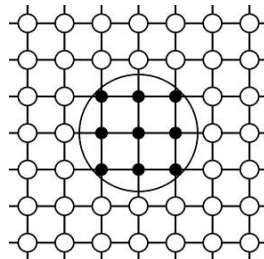


Figure 5.3: Fully coherent precipitates, no broken bonds [19]

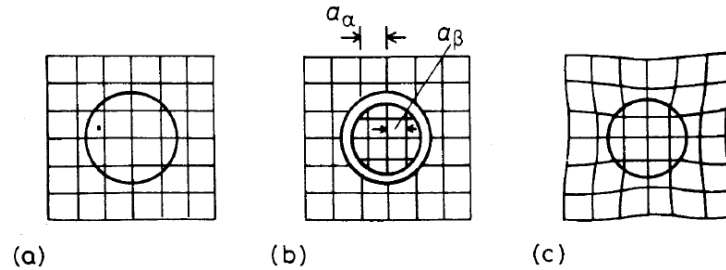


Figure 5.4: Coherency strain due to the difference in lattice parameter of precipitate and the matrix [20]

Modelling the precipitation kinetics in multi-component multi-precipitate alloys, knowing that nucleation, growth, and coarsening are likely to happen simultaneously, is very complicated. There is also the issue of dissolution of one type of precipitate in favor of more stable species. There are a number of approaches to model precipitation kinetics including extended Johnson–Mehl–Avrami model [21], Monte Carlo simulation [22], phase-field methods [23], or sharp interface models [24]. These approaches are either much too detailed for a comprehensive modelling (i.e. Monte Carlo method) or they are not developed for multi-precipitate systems. Recently, a theoretical model has been developed that describes the precipitates evolution in multi-component systems during ageing. The model is essentially based on the *Onsager* extremal thermodynamic principle, which postulates that a thermodynamic system evolves with a maximum Gibbs free energy dissipation [25–28]. This model simultaneously keeps the complexity and the most important features of the real microstructure. In this study, this previously developed model is applied to Al-Mg-Si system. Precipitates assumed to be available in Al-Mg-Si alloys are GP-zones, β'' , β' , β and free-Si. In this chapter, first the model is briefly described. Then the sensitivity of the model to the variation of interfacial energy of β'' phase is discussed. Using the chosen values for interfacial energies, the model is used to study the effects of ageing temperature and time on the precipitates number density, precipitates volume fraction, and precipitation sequence. The obtained microstructure data is used as input values of strengthening model to predict the yield strength of Al-Mg-Si alloys.

5.2. Multi-component multi-precipitate model

In aged Al-Mg-Si alloys, the system is a matrix in which precipitates of various sizes, chemical compositions, and crystal structures are distributed. Each precipitate is in

5. Multi-Component Multi-Precipitate Modelling of Ageing Kinetics in Al-Mg-Si Alloys

contact with the surrounding matrix. Assuming that there are S alloying elements in the system and N_{0i} ($i=1, \dots, S$) is the molar concentration of alloying element i . There are m spherical precipitates in the system, each of which having a different radius r_k ($k=1, \dots, m$). The number of moles of component i in the matrix is calculated from the mass-balance as follows

$$N_i = N_{0i} - \frac{4\pi}{3} \sum_{k=1}^m r_k^3 c_{ki}, \quad (5.1)$$

where c_{ki} is the concentration of alloying element i in the precipitate k . In such a system with S components and m precipitates, the total Gibbs energy is expressed as [26]

$$G_{tot} = \sum_{i=1}^S N_i \mu_i + \frac{4}{3} \pi \sum_{k=1}^m r_k^3 (\lambda_k + \sum_{i=1}^S c_{ki} \mu_{ki}) + 4\pi \sum_{k=1}^m r_k^2 \gamma_k, \quad (5.2)$$

where μ_i is the chemical potential of alloying element in the matrix, μ_{ki} is the chemical potential of alloying element in the precipitate, λ_k is the strain energy, and γ_k is the precipitate/matrix interface energy. It is important to note that the representation of the total free energy of the system in this model involves only mean quantities for the composition, meaning that concentration gradients from the matrix towards the precipitates are not taken into accounts. In the abovementioned total Gibbs free energy equation, the first term describes the Gibbs energy of the matrix by summing up the contributions from alloying elements in the matrix. The second energy term is due to the precipitates, where the specific quantities for the mechanical free energy contribution, λ_k , are also included. The third term takes into account the increase in the energy of system due to the formation of the precipitate–matrix interfaces. If the system is not in equilibrium, the radius of precipitates and the alloying elements concentrations evolve to decrease the Gibbs energy of the system. When a thermodynamic system evolves toward a stable thermodynamic state, the difference in free energy between the initial and the final state is dissipated [25]. Basically there are three different possibilities for Gibbs free energy dissipation during ageing. These are:

- Dissipation by the precipitate-matrix interface movement during growth-dissolution of precipitates
- Dissipation by diffusion of alloying elements inside the precipitate
- Dissipation by diffusion of alloying elements inside the matrix

The first dissipation mechanism is due to the interface opposition against the driving pressure. The character of this opposing force is like a friction force, which dissipates energy. The total dissipation rate due to the interface migration can be written as [27]

5. Multi-Component Multi-Precipitate Modelling of Ageing Kinetics in Al-Mg-Si Alloys

$$Q_1 = \sum_{k=1}^m \frac{4\pi r_k^2}{M_k} \left(\frac{dr_k}{dt} \right)^2, \quad (5.3)$$

where M_k is the mobility of interface. The rate of Gibbs energy dissipation due to diffusion inside the precipitate is given by the expression [28]

$$Q_2 = \sum_{k=1}^m \sum_{i=1}^S \frac{4\pi R T r_k^5}{45 c_i D_{ki}} \left(\frac{dc_{ki}}{dt} \right)^2, \quad (5.4)$$

where D_{ki} is the diffusion rate of alloying element i in the precipitate k . The third contribution is more difficult to obtain and can only be evaluated in an approximate manner. If it is assumed that the distance between the individual precipitates is sufficiently large, the energy dissipation by diffusion of alloying elements inside the matrix is given by [27]

$$Q_3 = \sum_{k=1}^m \sum_{i=1}^S \frac{4\pi R T r_k^3}{45 c_i D_i} \left(\frac{dr_k}{dt} (c_i - c_{ki}) + \frac{r_k}{3} \frac{dc_{ki}}{dt} \right)^2, \quad (5.5)$$

with c_i and D_i being the concentration and diffusion rate of alloying element i in the matrix. The total rate of Gibbs free energy dissipation, Q_{tot} , is therefore given as the sum of the individual contributions with

$$Q_{tot} = Q_1 + Q_2 + Q_3. \quad (5.6)$$

Based on the Onsager's thermodynamic extremal principle, a thermodynamic system will evolve toward equilibrium in such a way that it produces maximum entropy or the maximum Gibbs free energy dissipation rate [26]. The maximization of the Gibbs free energy dissipation rate necessitates

$$\frac{dG_{tot}}{dt} + Q_1 + Q_2 + Q_3 = 0. \quad (5.7)$$

Applying the thermodynamic extremal principle to the system containing precipitates, a set of equations can be obtained, in which the total Gibbs free energy of a system can be expressed by means of the state parameters and the rate of the total Gibbs energy dissipation. This results in

$$\frac{\partial G_{tot}}{\partial r_k} = -\frac{1}{2} \frac{\partial Q_{tot}}{\left(\frac{\partial^2 r_k}{\partial t^2} \right)} \quad (k = 1, \dots, m). \quad (5.8)$$

5. Multi-Component Multi-Precipitate Modelling of Ageing Kinetics in Al-Mg-Si Alloys

$$\frac{\partial G_{tot}}{\partial c_{ki}} = -\frac{1}{2} \frac{\partial Q_{tot}}{\left(\frac{\partial^2 c_{ki}}{\partial t^2}\right)} \quad (k = 1, \dots, m; i = 1, \dots, S). \quad (5.9)$$

The numerical way to solve these sets of linear equations is explained in the literature [25-28]. The nucleation rate of a family of precipitates of same shape, interface energy, and chemical composition is given in the model by

$$J = Z\beta^* N_c \exp\left(\frac{-\Delta G^*}{k_B T}\right) \exp\left(\frac{-1}{2Z^2 \beta^{*2} t}\right), \quad (5.10)$$

where the second exponential term is due to the transient nucleation rate. In this equation, Z is the Zeldovich factor, β is the atomic attachment rate for the critical nucleus, N_c is the number of available nucleation sites, k_B is the Boltzmann constant and ΔG is the nucleation energy barrier given by [28]

$$\Delta G^* = \frac{f\gamma_k^3}{F_k^2} \begin{cases} f = 16\pi/3 & \text{Homogeneous Nucleation} \\ f < 16\pi/3 & \text{Heterogeneous Nucleation} \end{cases}, \quad (5.11)$$

where F_k is the driving force for the formation of precipitates k , calculated from the chemical potentials derived from the thermodynamic data base as follows:

$$F_k = -\lambda_k - \sum_1^n C_{ki} (\mu_{ki} - \mu_{0i}). \quad (5.12)$$

In the case of a multi-component system, β can be calculated as [28]

$$\beta^* = \frac{4\pi r_c^2}{a^4 \Omega} \left[\sum_{i=1}^n \frac{(C_{ki} - C_i)^2}{C_i D_i} \right]^{-1}, \quad (5.13)$$

where a is the lattice spacing, Ω is the partial molar volumes of the alloying elements (considered to be the same for all components), and r_{cr} is the critical radius. The first factor in Eq. (5.13) represents the number of available atomic sites on the surface of the critical nucleus and the second factor corresponds to the mean exchange frequency of atoms between the matrix and the critical nucleus [28]. Critical radius, r_{cr} , is given by

$$r_{cr} = \frac{2\gamma_k}{F_k}. \quad (5.14)$$

5. Multi-Component Multi-Precipitate Modelling of Ageing Kinetics in Al-Mg-Si Alloys

In a multi-component system, assuming that the chemical composition of the precipitates is time invariant and the interface mobility is infinite, equations (5.8) and (5.9) lead to the growth rate of the precipitate k to be expressed as

$$\frac{dr_k}{dt} = \frac{F_k - \left(\frac{2\gamma_k}{r_k}\right)}{RT r_k} \left[\sum_{i=1}^n \frac{(C_{ki} - C_i)^2}{C_i D_i} \right]^{-1}, \quad (5.15)$$

The factor $F_k - \frac{2\gamma_k}{r_k}$ represents the balance between the driving force and the surface tension and therefore controls the evolution mode (growth or dissolution) of the precipitate.

5.3. Strengthening model

The microstructural data obtained from the multi-component multi-precipitate microstructure model, can be used as input parameters to predict the strength of the alloy. There are three major contributions to the yield strength of the alloy; i) the matrix, ii) the solid solution hardening and iii) the precipitate strengthening. The contribution from solid solution strengthening is calculated as [24]

$$\sigma_{ss} = \sum_{j=Mg, Si, Cu} k_j C_j^{2/3}, \quad (5.16)$$

where C_j is the concentration of alloying elements in the matrix and k_j is the corresponding constant.

The usual approach to treat the precipitation hardening phenomenon is to consider the particles as an array of obstacles interacting with dislocations. When a gliding dislocation encounters such set of obstacles, it bows out to some angle, ψ . By increasing the applied stress the bowing angle becomes smaller until it reaches a critical value, after which the obstacle is overcome, meaning that the dislocation moves on. Figure 5.5 shows the schematic of the interaction of a moving dislocation with an array of precipitates. In this figure l is the effective obstacle spacing along the dislocation line, R_c is the bowing curvature of dislocation, Γ is the line tension of dislocation, and F is the obstacle strength (the maximum force that the obstacle can sustain). The obstacle strength, F , is given by [29]

$$F = 2\Gamma \cos\left(\frac{\psi_c}{2}\right), \quad (5.17)$$

5. Multi-Component Multi-Precipitate Modelling of Ageing Kinetics in Al-Mg-Si Alloys

where ψ_c is the critical bowing angle, below which the obstacle is overcome. The obstacle strength determines the critical bowing angle. For a large ψ_c , F is small and hence the precipitates are sheared by moving dislocations, while for a small ψ_c , F is large and the obstacle imposes larger resistance to the moving dislocation before being overcome. For non-shearable precipitates, ψ_c is zero and a dislocation leaves a loop around the precipitate when it passes through (see Fig. 5.6).

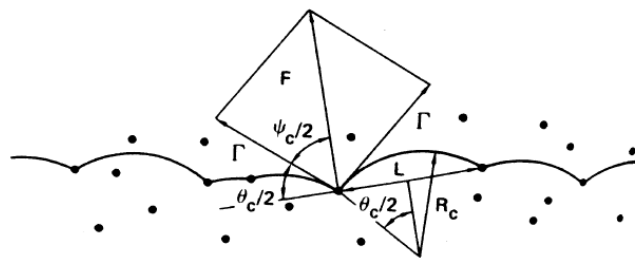


Figure 5.5: The interaction of dislocation with a random array of precipitates [29]

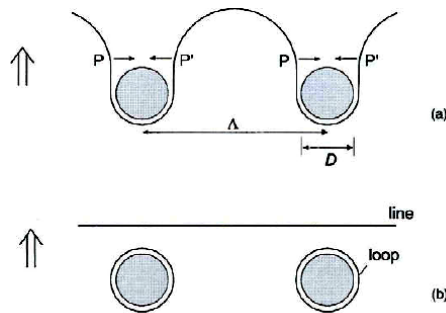


Figure 5.6: The Orowan mechanism, (a) the dislocation line bows between the obstacles until the segments at P and P' are parallel ($\psi_c = 0$). They then attract and meet (b) the line moves forward leaving Orowan loops around the obstacles [29]

The contribution of precipitation strengthening to the yield strength is given by [29]

$$\sigma_{ppt} = \frac{MF}{bl}, \quad (5.18)$$

where M is the Taylor factor and b is the Burgers vector. The effective obstacle spacing, l , is not the same value for weak and strong obstacles. For weak obstacles the dislocation

5. Multi-Component Multi-Precipitate Modelling of Ageing Kinetics in Al-Mg-Si Alloys

line is nearly straight and the mean obstacle spacing is larger than the mean center-to-center distance between the particles [29], while this value is smaller for strong obstacle, since the dislocations meet more precipitates when they bow. The obstacle-strength-dependent effective particle spacing is given by the so-called Friedel equation [30]

$$l = L \left(\cos \frac{\psi_c}{2} \right)^{-1/2}, \quad (5.19)$$

where L is the center-to-center precipitate distance, which is given by [30],

$$L = \left(\frac{2\pi r^2}{3f} \right)^{1/2}, \quad (5.20)$$

where r is the radius and f is the volume fraction of obstacles. Using the abovementioned equation and Eq. (5.17), the effective obstacle spacing is given by

$$l = \left(\frac{3f}{4\pi r^2} \frac{F}{\Gamma} \right)^{-1/2}. \quad (5.21)$$

The dislocation line tension is calculated by [24]

$$\Gamma = \beta G b^2, \quad (5.22)$$

where β is a constant close to 0.5 and G is the shear modulus. Putting l and Γ from Eqs. (5.21) and (5.22) into Eq. (5.18) yields

$$\sigma_{ppt} = \frac{M}{br} \left(\frac{3f}{2\pi} \right)^{1/2} (2\beta G b^2)^{-1/2} F^{3/2}, \quad (5.23)$$

where F is assumed to be a function of precipitate radius when precipitate is shearable ($r < r_{trans} = 5$ nm), and it is independent of radius when precipitate is non-shearable ($r \geq r_{trans} = 5$ nm). The relationship between the average obstacle strength for shearable precipitates and their average radius in the present system is approximated by [30]:

$$F \propto r^m. \quad (5.24)$$

Esmaili et al. [30] divided the whole ageing process into three parts: (i) underageing up to peak-age when precipitates are shearable, (ii) peak-age point to the transition point up to which precipitates are shearable, and (iii) from transition point on where precipitates all become non-shearable. The transition radius, r_{trans} , is defined as the radius where the strengthening mechanism is changing from shearing mechanism to bypassing

5. Multi-Component Multi-Precipitate Modelling of Ageing Kinetics in Al-Mg-Si Alloys

mechanism. Based on this explanation, the normalized mean obstacle strengths at these three stages are given as [30]

$$\begin{cases} F = \frac{r}{r_{PA}} F_{PA} & r < r_{PA} & (a) \\ F = \left(\frac{r}{r_{PA}}\right)^m F_{PA} & r_{PA} < r < r_{trans} & (b) \\ F = 2\Gamma & r_{trans} < r & (c) \end{cases} \quad (5.25)$$

Where F_{PA} is the mean obstacle strength for precipitates in the peak-age condition, r_{peak} is the radius of precipitate at peak-age, calculated by the microstructure model, and m is a constant close to 0.6 [30]. Knowing that F at the transition radius is given by

$$F_{trans} = 2\Gamma = 2\beta Gb^2, \quad (5.26)$$

F_{PA} is written as

$$F_{PA} = \left(\frac{r_{PA}}{r_{trans}}\right)^m F_{trans} = 2\beta Gb^2 \left(\frac{r_{PA}}{r_{trans}}\right)^m. \quad (5.27)$$

Using this equation for F_{PA} , Eq. (5.25) is rewritten as

$$\begin{cases} F = 2\beta Gb^2 \frac{r_{PA}^{m-1}}{r_{trans}^m} r & r < r_{PA} & (a) \\ F = 2\beta Gb^2 \left(\frac{r}{r_{trans}}\right)^m & r_{PA} < r < r_{trans} & (b) \\ F = 2\beta Gb^2 & r_{trans} < r & (c) \end{cases} \quad (5.28)$$

It is most likely that there are different types of precipitates available in the microstructure at any time. These precipitates might be either shearable or non-shearable. It is not really practical to linearly add the contributions from different precipitates. Superposition of the strengthening effects of different types of precipitates in Al-Mg-Si alloys is given by [30]

$$\sigma_{ppt}^\alpha = n_{GP}^{\alpha/2} \sigma_{GP}^\alpha + n_{\beta''}^{\alpha/2} \sigma_{\beta''}^\alpha + n_{\beta'}^{\alpha/2} \sigma_{\beta'}^\alpha + n_{\beta}^{\alpha/2} \sigma_{\beta}^\alpha + n_{Si}^{\alpha/2} \sigma_{Si}^\alpha, \quad (5.29)$$

where n is molar fraction. There is no existing model to calculate the parameter α depending on the distribution of obstacle types and therefore the solution corresponding

5. Multi-Component Multi-Precipitate Modelling of Ageing Kinetics in Al-Mg-Si Alloys

to the case of equal strength of all precipitate types is chosen, meaning α is taken equal to 2.0. It is important to note that the contributions of the matrix should be linearly added to that of precipitates.

5.4. Model implementation

The *MatCalc* software [25-28] is used to simulate the kinetics of ageing. This software evaluates the multi-component thermodynamics of the system from *CALPHAD* type databases and provides chemical potentials and driving forces of all phases as well as the diffusivities of all elements as a function of chemical composition and temperature. Figure 5.7 shows the schematic structure of the *MatCalc* precipitation model. *MatCalc* has the ability to simulate precipitation in different domains. This would be very useful for materials having a duplex microstructure. However, in Al-Mg-Si system there is only one matrix, in which precipitates of different compositions and structures are distributed. Different precipitate phases can be defined in *MatCalc*, each of which having their own interfacial energy, preferred nucleation sites, and nucleus composition. It is also possible to define two precipitates of the same composition nucleating on different sites. An array of size classes is assigned to each precipitate type. Each precipitate size class consists of a number of precipitates of the same radius. The number of these classes can be one or any higher number, depending on the type of simulation. However, usually, it is not necessary to consider more than 250 classes [25]. The total number of precipitate in each size class changes during ageing due to nucleation, growth, coarsening, and dissolution. In every time step, and for each precipitate phase, the nucleation rate is evaluated and newly formed precipitates are added to a size class. In the meantime, the growth/dissolution kinetics and the change in composition/numbers of precipitates in all existing size classes are evaluated. In the simulation, a variable time step is used, which is automatically controlled and redefined during ageing, in such a way that in the beginning it is smaller and becomes bigger when the ageing goes on [26]. During ageing, in reality, a diffusion field is developed around each growing precipitate with a composition gradient from matrix to the surface. It is assumed that there is no nucleation inside this diffusion fields. This diffusion field is assumed to be a spherical volume of radius 1-5 times higher than the precipitate radius [25].

5. Multi-Component Multi-Precipitate Modelling of Ageing Kinetics in Al-Mg-Si Alloys

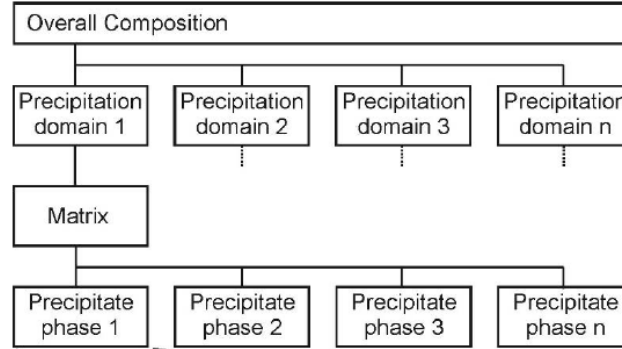


Figure 5.7: The schematic structure of the *MatCalc* precipitation kinetics model [25]

The rate at which the precipitates grow is assumed to be controlled by the rate at which atoms diffuse towards the particle/matrix interface. Bulk diffusion coefficient rates for Mg and Si used in the simulation are given by

$$\begin{cases} D_{Mg} = (5.7 \times 10^{-5} \text{ m}^2 / \text{s}) \exp\left(\frac{-112,5 \text{ kJ} / \text{mol}}{RT}\right) \\ D_{Si} = (1.4 \times 10^{-5} \text{ m}^2 / \text{s}) \exp\left(\frac{-126,7 \text{ kJ} / \text{mol}}{RT}\right) \end{cases} \quad (5.30)$$

Apart from the bulk diffusion coefficient of alloying elements, there is also another important parameter, which controls the rate of diffusion. This parameter, which is called the Matrix diffusion enhancement factor (*MDEF*), is accounting for the faster diffusion of alloying elements due to the presence of structure imperfections and mainly vacancies (the diffusion coefficient is simply multiplied by the *MDEF* parameter). No need to mention that quenched-in (excess) vacancies remaining in the matrix, do have effect on the diffusion rates of alloying elements. It is also important to note that most quenched-in vacancies are most likely consumed during the formation of initial precipitates like GP-zones and β'' and, therefore, they only have a small accelerating effect during formation of β' and β . Increasing *MDEF* parameter basically increases the kinetics of ageing by forming higher number density of precipitates with lower mean radius. There is also a coherency strain, which is important during nucleation and in the strengthening part of the model. This coherency strain originates from the difference between the matrix and precipitate lattice parameters. Knowing that the lattice parameter of GP-zone and that of the matrix are similar (see table 5.1), and assuming that the Si, β' , and β precipitates have nearly incoherent interfaces, one can assume that the coherency

5. Multi-Component Multi-Precipitate Modelling of Ageing Kinetics in Al-Mg-Si Alloys

strains for these precipitates are equal to zero. The coherency strain due to the semi-coherent interface of β'' /matrix is chosen to be 0.005. There are a number of available nucleation sites in the matrix, including grain interiors (homogeneous nucleation), grain boundaries, and dislocations. Each type of precipitate might nucleate on several nucleation sites at the same time. However, for the sake of simplicity, it is assumed that each kind of precipitate nucleates only on one type of nucleation site. On the grounds that GP-zones and β'' have coherent and semicoherent interfaces, their activation energy barriers for nucleation are relatively low compared to β' and β (see schematic Fig. 5.2). This means that, highest nucleation rates for these two precipitates are likely to be achieved when they nucleate homogeneously. For β' and β , nucleation is assumed to happen on dislocations. The model has been applied to the aging of solution treated AA6111 and another alloy, which is henceforward named alloy A, in the temperature range of 60–220 ° C. The experimental data used to validate the model is taken from the literature [30,31]. The chemical composition of the alloy AA6111 is (in wt%) 0.8Mg, 0.6Si, 0.7Cu, 0.25Fe, 0.2Mn, and balance Al, and that of the alloy A is (in wt%) 1.0Si, 0.5Mg, 0.03Cu, 0.2Fe, 0.1Mn, and balance Al. All samples have had a solution treatment of 10 minutes at 560 °C prior to water quenching. Knowing that a part of Si is consumed to form Fe and Mn-containing inclusions, the effective Si content in solid solution is given by [24]

$$C_{eff}^{Si} = C_0^{Si} - 0.33(C_0^{Fe} + C_0^{Mn}) . \quad (5.31)$$

This yields the effective Si value of 0.45 wt% for the alloy AA6111 and 0.9 wt% for the alloy A. So, basically, the alloy AA6111 is almost a balanced alloy with high Cu concentration, while the alloy A has some excess Si. The last input parameter to discuss is the interfacial energy, which is undoubtedly the most important and the most challenging parameter in models dealing with the kinetics of ageing. The way to estimate optimal values for the interfacial energy will be briefly explained.

- **Interfacial energy**

Unfortunately, in most cases a measured quantity for interfacial energy is not available due to the limitations and difficulties in direct experimental measurement methods. In most available models, interfacial energy has been treated as a fitting parameter [21, 24]. Since the aim of this project is to develop an age-hardening model considering precipitation sequence, it is not reasonable to choose one unique (fitted) value for interfacial energies of different precipitates. In recent years, many models, using first-

5. Multi-Component Multi-Precipitate Modelling of Ageing Kinetics in Al-Mg-Si Alloys

principle, ab-initio, and cluster dynamic approaches [25] have been developed to predict the interfacial energy. In this section, the simple and practical nearest-neighbor broken-band (NNBB) model is presented, which relates the interfacial energy to the formation enthalpy of precipitate. One has to bear in mind that the interfacial energy is sensitive to so many parameters like degree of coherency, solute segregation, misfit dislocations, coherency strains, and crystallographic misorientation. This means that the calculated values from the NNBB model are not necessarily precise values. However, the approximate values given by the model give an indication of the trends of interfacial energies. Consider two blocks of materials A and B of pure elements. If each block is divided into two sections, and half-blocks A are connected to half-blocks B (see Figs. 5.8 and 5.9), the energy of the newly formed A-B interfaces can be calculated as the sum of the energies of the new bonds in new blocks, minus the energy of the broken bonds in the original blocks as given below [25]

$$\gamma = E_{AB} - E_{AA} - E_{BB}, \quad (5.32)$$

where E_{AB} , E_{AA} , and E_{BB} are energy per unit area of interfaces and are obtained as follows

$$\begin{aligned} E_{AB} &= n_S z_S \varepsilon_{AB} \\ E_{AA} &= \frac{n_S z_S}{2} \varepsilon_{AA}, \\ E_{BB} &= \frac{n_S z_S}{2} \varepsilon_{BB} \end{aligned} \quad (5.33)$$

where ε is the bond energy, n_S is the number of surface atoms per unit area, and z_S is number of bonds across the interface per atom. Putting the values E_{AB} , E_{AA} , and E_{BB} from equation (5.33) into equation (5.32) gives

$$\gamma = n_S z_S \left(\varepsilon_{AB} - \frac{\varepsilon_{AA}}{2} - \frac{\varepsilon_{BB}}{2} \right). \quad (5.34)$$

Since it is not always easy to find values for bond energy, Turnbull [32] made the connection between the interfacial energy and the enthalpy of solution of the precipitate. Assuming a regular solution, the total bond energy of one mole of pure A atoms and one mole of pure B atoms and after mixing that of the solution are

5. Multi-Component Multi-Precipitate Modelling of Ageing Kinetics in Al-Mg-Si Alloys

$$\begin{aligned} E_{AA} &= \frac{zN}{2} \varepsilon_{AA} \\ E_{BB} &= \frac{zN}{2} \varepsilon_{BB} , \\ E_{AB} &= zN \varepsilon_{AB} \end{aligned} \quad (5.35)$$

where z is the coordination number and N is Avogadro number. Assuming that the difference between the bond energies of the pure substances and the mixture is the enthalpy of solution, ΔH_m , this value is obtained as [33]

$$\Delta H_m = zN \left(\varepsilon_{AB} - \frac{\varepsilon_{AA}}{2} - \frac{\varepsilon_{BB}}{2} \right). \quad (5.36)$$

Using the abovementioned equation, the interfacial energy from equation (5.34) is given as

$$\gamma = \frac{z_s}{z} \frac{n_s}{N} \Delta H_m , \quad (5.37)$$

where z_s/z factor is dependent on the crystallography of interface. The more bonds crossed across the interface (high value of z_s), the higher is the interfacial energy [25].

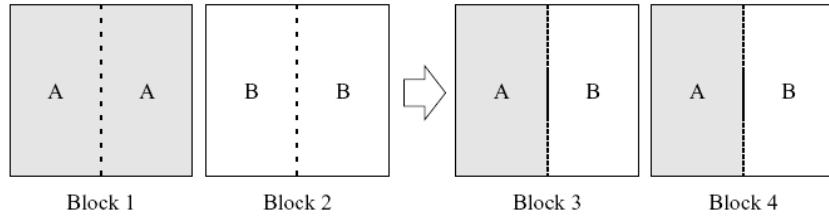


Figure 5.8: Formation of A-B interfaces [33]

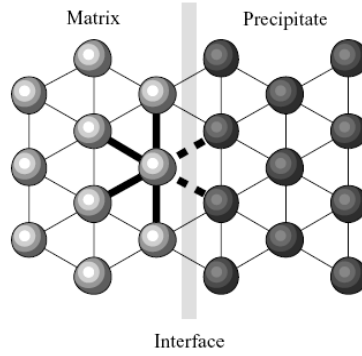


Figure 5.9: Two-dimensional coherent $A-B$ interface with nearest-neighbor broken bonds [33]

One of the basic assumptions of the NNBB model is the presence of a sharp interface between precipitate and the matrix. However, the interface in reality is mainly diffuse, meaning that the interface is a volume instead of a 2D layer. The interface is extended over a certain number of lattice planes, the width of which is temperature dependent [25]. The higher the temperature, the wider is the interface. Since, the diffuse interface has a lower energy compared to the sharp interface [33], the value obtained by the NNBB model is multiplied by a constant, which is less than unity,

$$\gamma = \alpha_D \frac{z_s n_s}{z N} \Delta H_m, \quad (5.38)$$

where α_D is the diffuse interface constant. α_D is assumed to be temperature-independent. The precipitates in Al-Mg-Si alloys have different crystal structure. Not all precipitates have the same orientation relationship with the matrix. Also, not all possible crossing bonds at the interface are linked in the real microstructure [25]. The atomic volume of the precipitate phase, V_a , is used to calculate the number of atoms on the surface, n_s , as follows (It is assumed that the atomic volume of precipitates is the same) [25]

$$n_s = \frac{1}{V_a^{2/3}}. \quad (5.39)$$

Table 5.2 shows the chosen input values, used in the model. It contains the interfacial energy for each precipitate calculated by *MatCalc* according to the NNBB model and, in the last column, the fitted values, which give more accurate results. Three interfacial

5. Multi-Component Multi-Precipitate Modelling of Ageing Kinetics in Al-Mg-Si Alloys

energy values for β'' precipitate are used to investigate the effect of the interfacial energy of this important precipitate on the kinetics of precipitation.

Table 5.2: Chosen input values for different precipitates

Type of precipitate	Stoichiometry	Coherency Strain	$MDEF$	γ (J/m ²) $NNBB$ (Eq. 37)	γ (J/m ²) Fitted
GP	$Mg_2Si_3Al_6$	-	100	0.13	0.10
β''	Mg_5Si_6	0.005	30	0.36	0.25, 0.27,0.29
β'	$Mg_{1.8}Si$	-	1	0.43	0.37
β	Mg_2Si	-	1	0.47	0.45
Free-Si	Si	-	1	0.50	0.50

5.5. Results

In this section, first the effects of interfacial energy on the ageing and hardening kinetics will be discussed and then the influence of ageing temperature on the precipitation behavior of different precipitate species will be shown.

- **Effects of interfacial energy**

Figure 5.10 shows the simulation of number density, volume fraction, and radius of β'' precipitate in the alloy AA6111, assuming three values of $\gamma_{\beta''}$ as is shown in table 2, aged at 180 °C as well as the yield strength of the alloy. The dashed line in the figures shows the applied heat treatment; solutionizing at 560 °C, quenching (with approx 50 °C/s), storing the alloy at room temperature for 10 s, increasing the temperature at a rate of 50 °C/s up to 180 °C, which is the ageing temperature, and finally holding the alloy at 180 °C. It is apparent that the interfacial energy of β'' precipitate has huge influences on the ageing kinetics and strength of the alloy AA6111. Figure 5.10a shows that the value of 0.25 J/m² gives the best prediction for β'' radius and for this value the first four experimental points are very well predicted. However, the model shows that at ageing time close to 1000 h (the fifth experimental point), β'' precipitates are already dissolved. As a matter of fact, the model shows that β'' precipitates disappear at around 250 hour, having the mean radius of 6 nm for the interfacial energy of 0.25 J/m². There are three distinguishable stages in the evolution of the mean radius of β'' precipitate; i) the initial increase of radius in the beginning of ageing from 0.5 to 2 nm, ii) a plateau in the value

5. Multi-Component Multi-Precipitate Modelling of Ageing Kinetics in Al-Mg-Si Alloys

of radius lasting until 5 h, and iii) the final increase in the radius until 250 h followed by an abrupt drop, showing the complete dissolution of β'' . The third stage, which is the final increase after the plateau, however, is not seen when the interfacial energy is increased from 0.25 to 0.27 or 0.29 J/m². In these cases, β'' precipitates reach a larger size and dissolve after the plateau. Figure 5.10b shows the effects of interfacial energy on the number density of β'' precipitates. The first notable feature is that no matter how much the value of interfacial energy is, almost all precipitates nucleate during cooling from solutionizing temperature and the nucleation rate at 180°C is very small. It is similar to a site saturation nucleation, in which all precipitates nucleate in the beginning of ageing. However, experimental measurement shows a smooth increase in the number density of precipitates during ageing up to a maximum at around one hour, followed by a decrease due to coarsening or dissolution. Figure 5.10b also shows that the maximum number density of β'' precipitates is very well predicted when the interfacial energy is 0.25 J/m². Figure 5.10c represents the prediction of the evolution of volume fraction of β'' precipitates together with experimental data. In this case, the model with 0.29 J/m² as the value of interfacial energy for β'' precipitate shows an excellent fit with the experiment, while when the interfacial energy is 0.27 or 0.25 J/m² one can see a faster increase of volume fraction of β'' precipitate to its maximum value. This excellent prediction of β'' volume fraction (when $\gamma_{\beta''}=0.29$ J/m²) obviously is not related to the correct predictions of number density and radius as is shown in Figs. 5.10a,b. This is happening because in this case the number density of β'' precipitates formed during cooling is comparatively small (see Fig. 5.10b), meaning that precipitates keep growing for a longer time until their size reaches a plateau, resulting in a smoother increase in the volume fraction of β'' precipitates. The comparison of figures 5.10a,b,c shows that, when the interfacial energy is 0.25 J/m², the initial fast and simultaneous increase of mean radius and volume fraction corresponds to the growth of β'' , and the following period with an approximately constant volume fraction corresponds to the coarsening of β'' . β'' dissolution starts around 70 h. However, experiment results show that β'' precipitates grow until 1 h. In the same way, although higher interfacial energies give much lower simulated density of β'' than experiment, the calculated volume fractions are larger than or equal to the experimental one. These results indicate that the growth rates predicted by the model are overestimated. Due to this overestimation of radius for $\gamma_{\beta''}=0.29$ J/m², the yield strength is underestimated by the model (see Fig. 5.10d). It is also apparent in Fig. 5.10d that when $\gamma_{\beta''}=0.25$ or 0.27 J/m², there is a fairly good agreement between the predicted and experimental peak-strength. Another notable feature is the abrupt increase in the yield strength in the underage regime, while in reality the yield strength increases

5. Multi-Component Multi-Precipitate Modelling of Ageing Kinetics in Al-Mg-Si Alloys

smoothly up to peak-age. This is a direct consequence of the very fast predicted nucleation rate during cooling and growth rate. In addition, in all three cases the modelling results show an underestimation of the yield strength of the alloy in the overaged regime coming from a relatively sudden dissolution of β'' precipitates. In reality, the yield strength during overageing decreases with a slower kinetics. Figure 5.11 shows radius, number density, and volume fraction of all precipitates in the alloy AA6111, predicted by the model assuming $\gamma_{\beta''}=0.25 \text{ J/m}^2$. As is seen, all GP-zones formed during heating and cooling before the beginning of isothermal ageing. Also, the model gives a very good prediction of β' radius (see Fig. 5.11a), whereas it underestimates the number density of β' . One can fit $\gamma_{\beta'}$ value in such a way that it gives reasonable predictions of both number density and radius of β' precipitate. However, this does change the predicted values for β'' precipitates. Since the β'' precipitate is more important in terms of strengthening, the model is decided to be fitted in such a way that it gives better predictions for size and number density of β'' rather than β' precipitate.

As it is already discussed, $\gamma_{\beta''}$ is a very influential parameter, and the model is very sensitive to the chosen value of interfacial energy. In order to check the validity of the model in other conditions, the model is applied to the alloy A, which has a different chemical composition. Among different values of the interfacial energy of β'' precipitate, the value 0.27 J/m^2 , which gives more reasonable results for both number density and mean radius of precipitates, is chosen. Figure 5.12 shows the calculated values of the mean radius and number density of precipitates in alloy A aged at $180 \text{ }^\circ\text{C}$, together with experimental data. The calculated mean radius of β'' is initially smaller than the measured one but the number density corresponds rather well to the experimental one. As for experiment, the model predicts higher density at the beginning of isothermal ageing in alloy A than in AA6111, showing that the model captures properly the effect of composition on the nucleation rate. Similar to the case of the alloy AA6111, a large proportion of precipitates nuclei form during cooling from solutionizing temperature or during heating up to the ageing temperature (note that the beginning of isothermal ageing in the curves is close to 0.01 h). All the GP-zones formed during cooling and heating are also dissolved before the beginning of isothermal ageing. It is also seen that β'' precipitates grow very rapidly before to start coarsening or dissolving at around 0.01 hour, and they completely disappear at 600 hours, while their mean radius at this time is more than 10 nm. β' , the other important precipitate, is stable only until 14000 hours, reaching the maximum radius of 40 nm. Only β and free-Si continue to exist after this time. Contrary to the alloy AA6111 in which the free-Si only exists until one hour (see

5. Multi-Component Multi-Precipitate Modelling of Ageing Kinetics in Al-Mg-Si Alloys

Fig. 5.11a), the free-Si in the alloy A remains in the structure as a stable precipitate. This is due to the difference in the chemical composition of alloy A and alloy AA6111; the former has excess Si, while the latter is a balanced alloy. It is also evident that in the alloy A there is a small hump in the mean radius of free Si located at around 100 hour (see Fig. 5.12a), which coincides with the extra nucleation of free-Si particles and the very last part of the existence of β'' precipitates in the structure. The dissolution of β'' precipitates releases Si and Mg atoms in the matrix. Since the concentration of Si needed to form β' precipitate is lower compared to that needed to form β'' precipitate (due to their different stoichiometries), a large proportion of this released Si will enrich the aluminium matrix while Mg atoms are immediately used to form β' (Fig. 5.13b). These Si solutes nucleate as new particles of free Si. These small newly formed free Si nuclei temporarily decrease the average size of free Si particles, turning out like a hump in Fig. 5.12a.

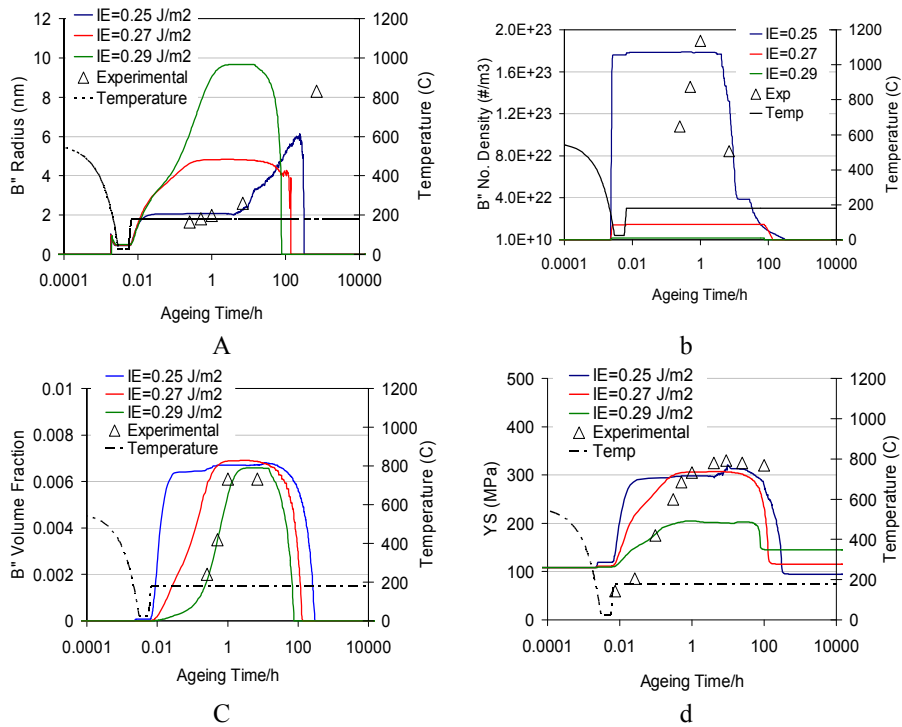
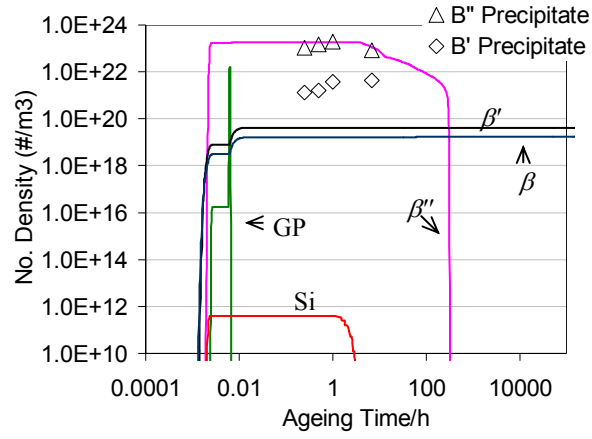
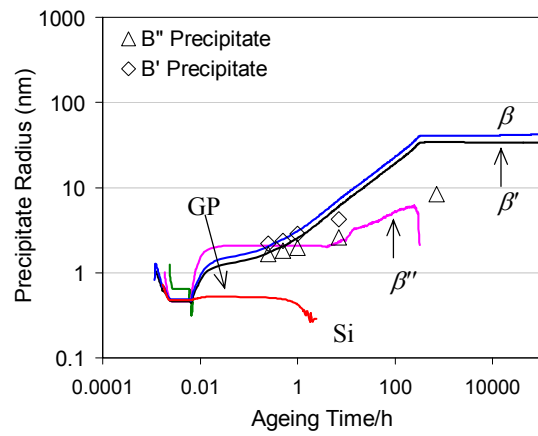


Figure 5.10: Prediction of a) the radius, b) number density, and c) volume fraction of β'' precipitate as well as d) the strength of the alloy AA6111 aged at 180 °C for three chosen values of $\gamma_{\beta''}$. (Note that IE is interfacial energy)

5. Multi-Component Multi-Precipitate Modelling of Ageing Kinetics in Al-Mg-Si Alloys



(a)



(b)

Figure 5.11: Prediction of a) radius and b) number density of all precipitates in the alloy AA6111 aged at 180 °C for $\gamma_{\beta''}=0.25 \text{ J/m}^2$ (Note: the beginning of isothermal ageing is close to 0.01 h)

5. Multi-Component Multi-Precipitate Modelling of Ageing Kinetics in Al-Mg-Si Alloys

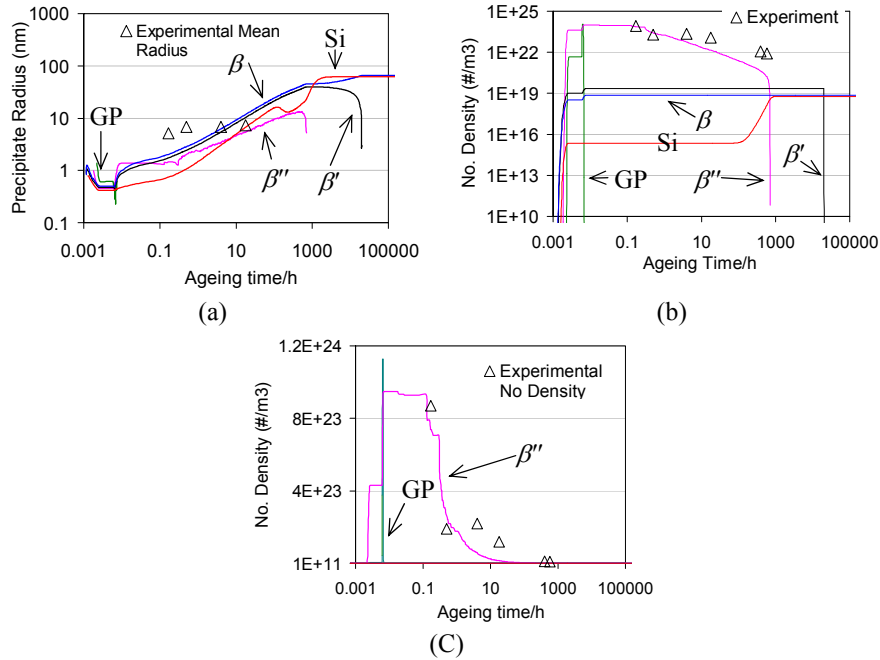


Figure 5.12: Prediction of a) radius, b) number density (in Log-scale), c) number density (in linear scale), and d) yield strength of the alloy A aged at 180 °C (Note: the beginning of isothermal ageing is close to 0.01 h) ($\gamma_{\beta''}=0.27$ J/m²)

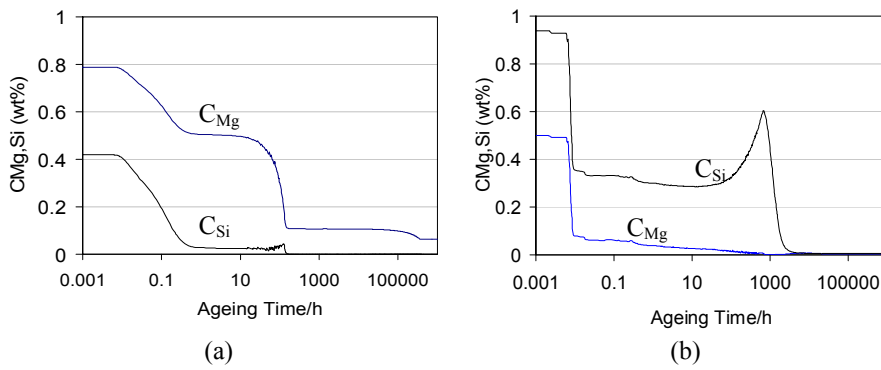


Figure 5.13: Evolution of the concentration of Mg and Si in the matrix of the alloy a) AA6111 and b) A during ageing at 180 °C ($\gamma_{\beta''}=0.27$ J/m²)

- **Effects of ageing temperature**

Figures 5.14 shows the evolution of volume fractions of different precipitates formed in alloy AA6111 and alloy A during ageing at 60, 140, and 220 °C. For these simulations a common value of 0.27 J/m² is used for the interfacial energy of β'' . In both alloys GP-zone phase is only present during isothermal ageing at 60 °C and there is no GP-zone at ageing temperatures 140 and 220 °C. At all temperatures, the volume fraction of β'' increases in the beginning of isothermal ageing, then remains constant for a period of time before to decrease at 140 and 220 °C. This evolution corresponds to the sequence of growth, coarsening and dissolution of β'' precipitates. The existence range of β'' precipitates increases by decreasing the ageing temperature. At 220 °C, β'' precipitates are present in the structure only until 20 h and 10 h in respectively AA6111 and alloy A. At ageing temperatures 60 °C, the stability of this important phase is not terminated by other more stable precipitates (β' and β) even until 10⁹ h. Similar evolutions are observed successively for β' and β precipitates. As it was already observed at 180 °C the amount of free Si (Si diamond) formed in the alloy AA6111 is negligible at every temperature, while considerable amounts of free Si exist in the alloy A. It is also evident that in the alloy A there is a kind of temperature-dependent competition between free Si and β' (and β) precipitate to grow during and after dissolution of β'' precipitates. This effect is related to the nucleation rate and will be discussed later. It seems that at 220 °C, pre-existing nuclei of β' and β start growing prior to free Si particles. At 140 °C, these three precipitates start growing at the end of the stability of β'' precipitates almost simultaneously. At temperatures lower than 100 °C, free Si particles, however, are clearly the only winners of this competition, since there is no indication of the growth of β' and β precipitates during the simulated time (Figs. 5.14b). The last difference to mention between the alloy AA6111 and alloy A is the noticeable difference of maximum volume fractions of GP-zone and β'' precipitates at a given temperature. It is apparent that the maximum volume fraction of GP-zone and β'' precipitates in the alloy A are two times higher than those in the alloy AA6111, whereas the maximum volume fractions of β' and β precipitates in the two alloys are nearly close together. The reason is related to the stoichiometry of different precipitates and the initial concentration of Si and Mg in the matrix. In AlMgSi alloys it can be assumed as a first approximation that the molar volume and molar mass of Mg_xSi_yAl_z precipitates are equal to the matrix ones. In that case the maximum volume fraction of each precipitate type that can be formed is given by:

5. Multi-Component Multi-Precipitate Modelling of Ageing Kinetics in Al-Mg-Si Alloys

$$f_k \approx \frac{C_0}{C_k}, \quad (5.33)$$

where C_0 is the initial solute concentration and C_k the concentration in the precipitate of type k of the default alloying element. The default alloying element, whatever the considered precipitate type, is Si for AA6111 and Mg for alloy A. Table 5.3 gives the maximum volume fraction and the corresponding amount of excess alloying element remaining in the matrix in alloys AA6111 and A.

Table 5.3: Maximum possible volume fraction of different precipitate type and remaining concentration of excess element in AA6111 and alloy A.

Type of precipitate	Stoichiometry	$f-6111$ (-)	$f-A$ (-)	$C_{Mg}-6111$ (wt%)	$C_{Si}-A$ (wt%)
GP	$Mg_2Si_3Al_6$	0.016	0.031	0.55	0.04
β''	Mg_5Si_6	0.008	0.012	0.48	0.21
β'	$Mg_{1.8}Si$	0.012	0.009	0.10	0.58
β	Mg_2Si	0.013	0.008	0.02	0.61

The calculated volume fractions are in good agreement with the ones observed in figure 5.14 and demonstrate that the differences in volume fraction of GP-zone and β'' precipitates between the two alloys stem from the alloy composition and precipitate stoichiometry. Table 3 is also an extra support for the previously presented argument about the presences of free-Si particles in the alloy A. Clearly, the amount of excess Si remaining in the matrix in alloy A increases during the precipitation sequence. These Si atoms can precipitate as free-Si particles.

5. Multi-Component Multi-Precipitate Modelling of Ageing Kinetics in Al-Mg-Si Alloys

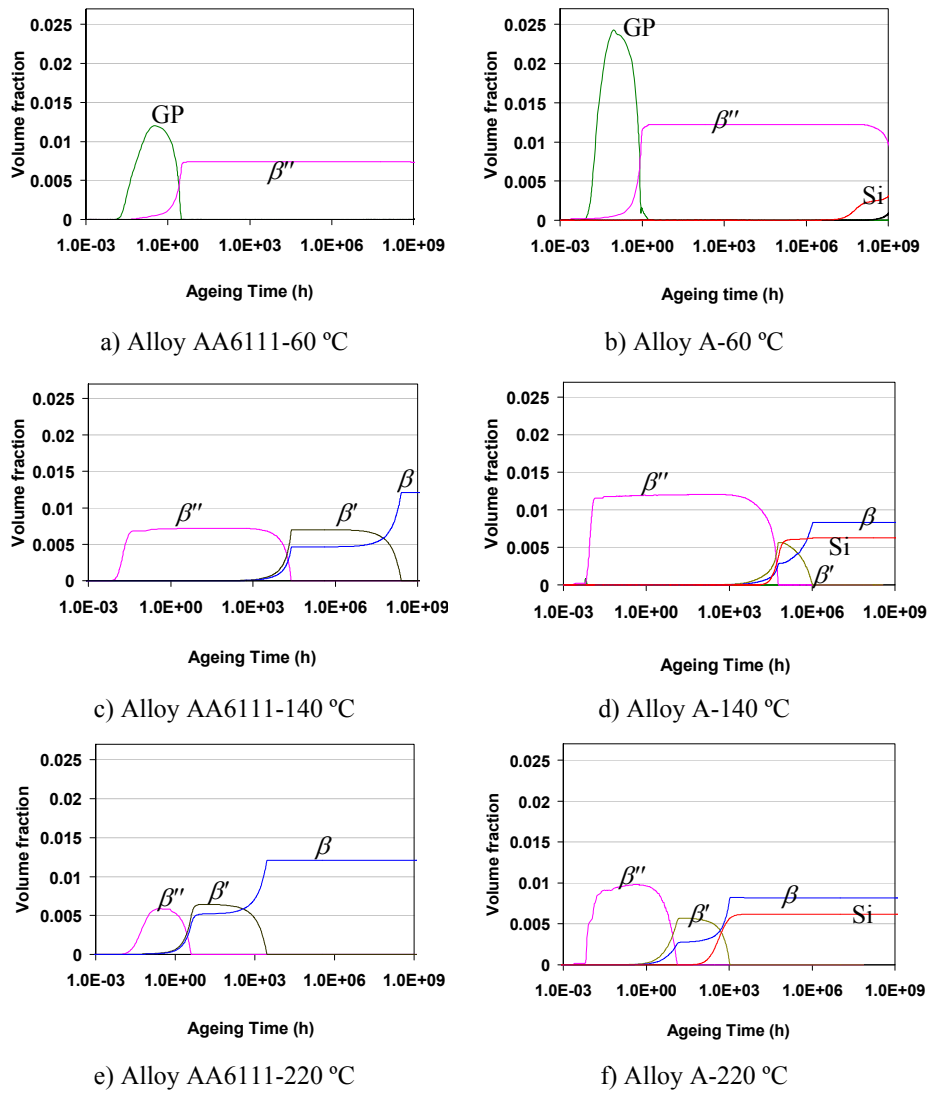


Figure 5.14: The evolution of the volume fractions of different precipitates formed in alloys AA6111 and A during ageing at different temperatures with 0.27 J/m^2 as the chosen value for $\gamma_{\beta''}$ (Note: the beginning of isothermal ageing is close to 0.01 h)

5. Multi-Component Multi-Precipitate Modelling of Ageing Kinetics in Al-Mg-Si Alloys

Figures 5.15 and 5.16 show the number density and the radius of different phases in alloys A and AA6111 at 60, 140, and 220 °C. The evolution of number density and size of different precipitates is discussed in more detail as follows:

- **GP-zones:** the model shows that the number density of GP-zones increases in two steps. The number density of GP-zones initially increases during cooling from solutionizing temperature, followed by a small plateau, corresponding to holding time between quenching and heating. The second increase in the number density of GP-zones takes place during heating to the ageing temperature. At the ageing temperature of 60 °C, GP-zones continue to nucleate and grow in the beginning of ageing up to the moment when the volume fraction of β'' becomes significant and they dissolve. At 140 or 220 °C all GP-zones, formed during quenching or heating, dissolve before the beginning of isothermal ageing. So, obviously depending on the ageing temperature, GP-zones might or might not appear in the beginning of isothermal ageing. It is also worth noting that the number density of GP-zones formed during cooling in the alloy A is 10^8 times higher than that formed in the alloy AA6111. This is due to the higher Si content in alloy A as explained before. It seems that in the case of ageing at 140 or 220 °C the size of GP-zones nuclei initially decreases, followed by a plateau, which persists until approximately 0.1 h, and a complete dissolution before isothermal ageing starts. However, when ageing temperature is 60 °C, GP-zones grow in the beginning of ageing. The initial decrease taking place during cooling is certainly not due to the dissolution of GP-zone. As a matter of fact, the critical radius of precipitates decreases during cooling, giving the chance to smaller nuclei to form. Since what is given in Fig. 5.15 is the mean radius, these smaller nuclei decrease the average size of GP-zones (and other precipitates as well) until the cooling is over. At the end of plateau at around 0.1 h, the second population of GP-zone nucleates (see Figs. 5.15), which yet again momentarily decreases the mean radius of GP-zones.
- **β'' Precipitates:** the model shows that in all cases, a proportion of β'' precipitates forms during cooling. In case when GP-zones are present at the beginning of isothermal ageing (i.e. 60 °C), the number density of β'' precipitates also increases continuously during ageing up to the time of complete dissolution of GP-zones. In the alloy AA6111, this (intermediate) increase in the number density of β'' during ageing at 60 °C is by a factor of 10^3 (see Fig. 5.15a), while in case of alloy A it is by 1 order of magnitude. However, when the ageing temperature is high (i.e. 220 °C), there is no such intermediate increase in the number density of β'' precipitates

5. Multi-Component Multi-Precipitate Modelling of Ageing Kinetics in Al-Mg-Si Alloys

during isothermal ageing. It can be seen that during the coarsening period of β'' precipitates (constant volume fraction), the number density decreases and the mean radius increases as it is expected (for instance Fig. 5.15d and Fig. 5.16d). In some cases, however, the number density and mean radius remain first constant (for instance Fig. 5.15c and Fig. 5.16c). This is also the case during ageing of alloy AA6111 at 180 °C between 1 and 10 h (Fig. 5.10, for $\gamma_{\beta''} = 0.27 \text{ J/m}^2$).

- **β' and β precipitates:** these precipitates show a relatively straightforward behavior. They nucleate during cooling and also at the beginning of ageing when the ageing temperature is high enough. The number density and mean radius of these two precipitates are in the same order of magnitude. At some point, as a result of the competitive coarsening between β' and β , the β' precipitates dissolve and only β precipitates continue to grow and coarsen.
- **Free-Si particles:** the negligible volume fraction of free Si particles observed in alloy AA6111 (Fig. 5.14a,c,e) is related to a very small number density and mean radius (the reason is already explained). The temperature-dependent competition between free Si and β' (and β) precipitates mentioned earlier for alloy A seems to be related to the time at which an intermediate increase in the number density of free Si particle takes place. At low temperature (60 °C) extra nucleation of free Si particles takes place during coarsening of β'' and comes from the excess Si present in the matrix (Table 5.3). However the volume fraction of free Si remains negligible until this phase can grow further when β'' precipitates start dissolving. At 140 °C, the Si atoms released by the dissolution of β'' is used for simultaneous extra nucleation and growth of free Si particles. At 220 °C, however, the extra nucleation and growth of free Si particles take place after the complete dissolution of β'' . The dissolution of β'' and significant growth of β' , on the other hand, are always concurrent processes, suggesting that β'' dissolution is related to the growth of β' precipitates. Therefore it appears that increasing the ageing temperature increases the kinetics of free Si particle nucleation and growth to a lesser extent than the kinetics of coarsening and dissolution of β'' and growth of β' . These different temperature dependent kinetics also explain why there is no hump in the radius of free Si particles when the alloy is aged at 65 and 140 °C (Figs. 5.16b,d), while there is evidently a hump when the alloy is aged at 180 °C (see Fig. 5.12a) or at 220 °C (Fig. 5.16f). At lower ageing temperatures, the slower kinetics of β'' dissolution results in a slower kinetics of intermediate free

5. Multi-Component Multi-Precipitate Modelling of Ageing Kinetics in Al-Mg-Si Alloys

Si particles nucleation, averting the rapid formation of a high density of small free Si particles, and eventually avoiding the temporary decrease of the mean size of free Si particles.

In order to have a better perspective of the evolution of number density of precipitates, the size distribution of β'' precipitates in the alloy AA6111 during ageing at 180 °C is shown in Fig. 5.17. The size distribution shortly after nucleation (0.05 h) is sharper than usually observed. This is a consequence of the short nucleation period and confirms that site saturation nucleation is not a fully accurate description. It can also be seen that, initially, the whole size distribution moves to larger radius, meaning that β'' precipitates are growing. At ageing time around 10 h, β'' precipitates have already started dissolving, which is accompanied by an increase of the size distribution width towards smaller radii. However, the largest precipitates still slowly grow, which shows that solutes released by the dissolution of small β'' precipitates are both used for the growth of β' and β and coarsening of β'' . This would finally result in a complete dissolution of β'' precipitates and further growth of β' and β .

5. Multi-Component Multi-Precipitate Modelling of Ageing Kinetics in Al-Mg-Si Alloys

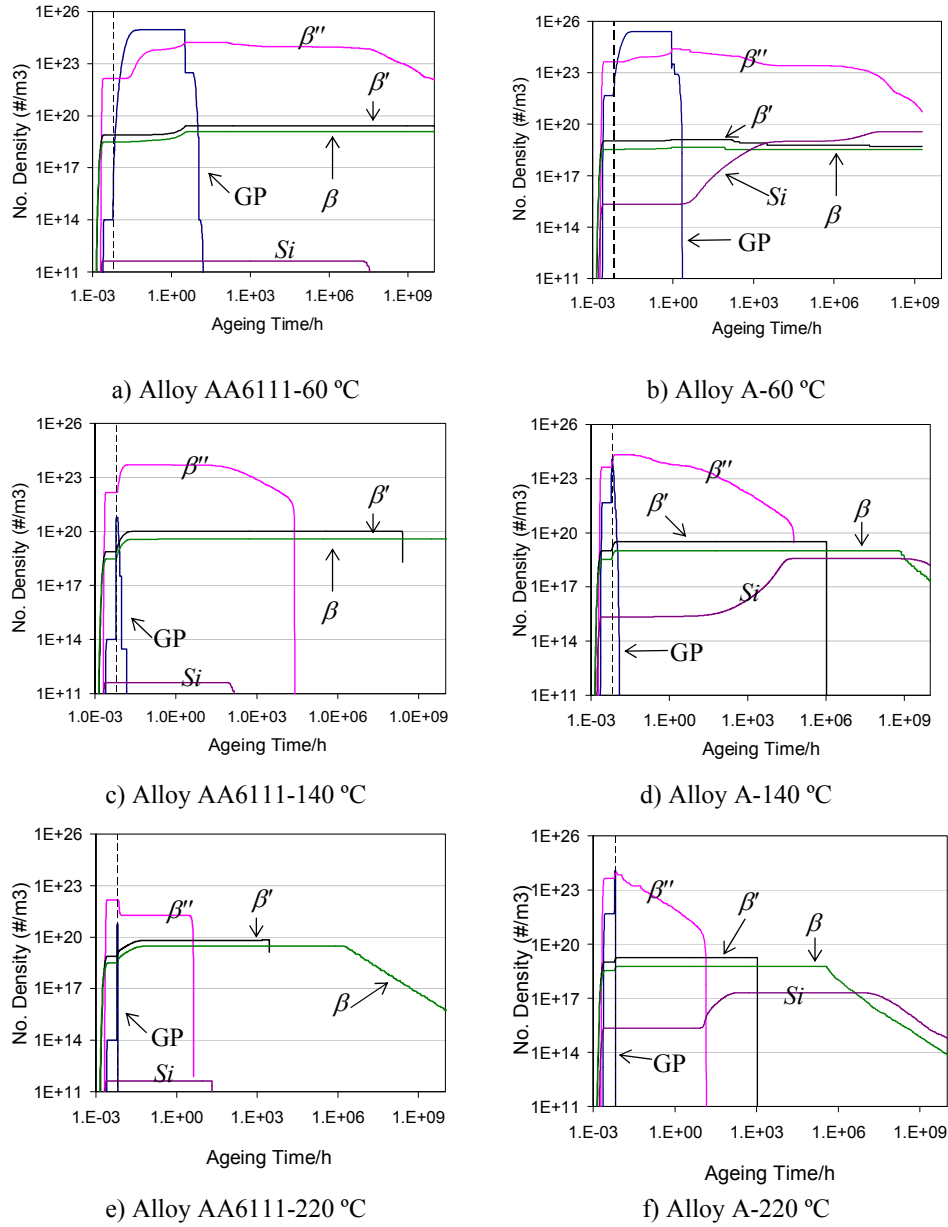


Figure 5.15: Effects of temperature on the number density of different precipitates in the alloy AA6111 (left) and alloy A (right) with 0.27 J/m^2 as the chosen value for $\gamma_{\beta''}$

5. Multi-Component Multi-Precipitate Modelling of Ageing Kinetics in Al-Mg-Si Alloys

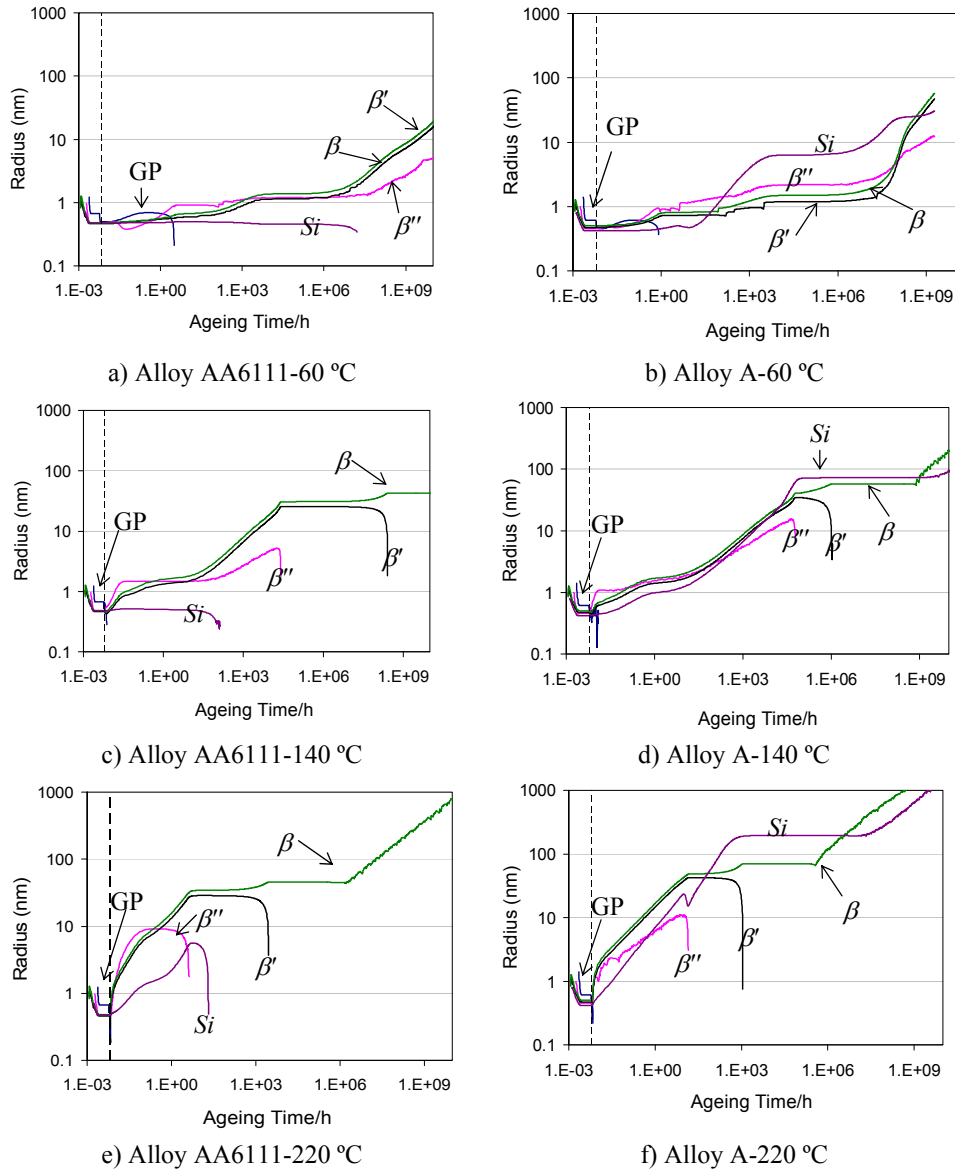


Figure 5.16: Effects of temperature on the radius of different precipitates in the alloy AA6111 (left) and alloy A (right) with 0.27 J/m^2 as the chosen value for $\gamma_{\beta''}$

5. Multi-Component Multi-Precipitate Modelling of Ageing Kinetics in Al-Mg-Si Alloys

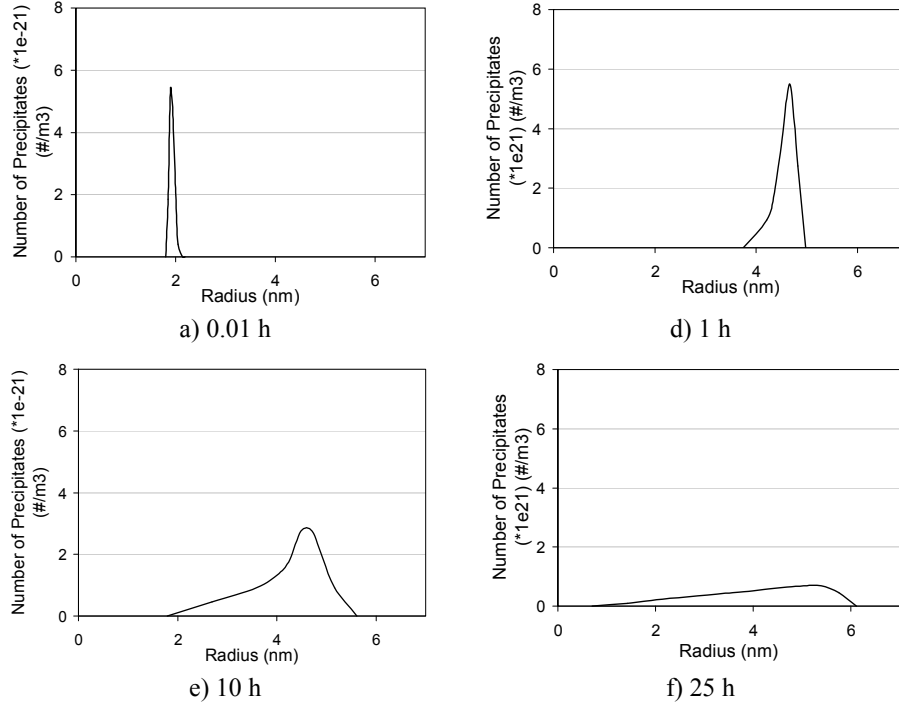


Figure 5.17: Size distribution of β'' precipitates in the alloy AA6111 during ageing at 180 °C with $\gamma_{\beta''} = 0.27 \text{ J/m}^2$.

- **Yield strength**

Figure 5.18 shows the calculated yield strength of the alloy AA6111 aged at different temperatures together with experimental data [30]. In fact, it is not possible to obtain a correct fit of the peak strength at all temperatures with a constant interfacial energy. In order to adjust the peak strength, one has to reduce the interfacial energy of β'' precipitate in the range of 0.25-0.29 J/m^2 with increasing temperature. Apart from 200 °C, clear differences still exist between the model results and experimental data, especially in the overage regime, where the model shows a faster kinetics. In order to check different factors affecting the yield strength of the alloy AA6111, different contributions to the yield strength of the alloy aged at 200 °C are plotted in Fig. 5.19. Clearly, the strength in the very beginning of ageing is due to the solid solution hardening. The solid solution hardening due to the presence of Si and Mg atoms in the matrix diminishes during ageing, while the contribution of Cu is constant. The

5. Multi-Component Multi-Precipitate Modelling of Ageing Kinetics in Al-Mg-Si Alloys

contribution of three existing precipitates at this temperature is shown in Fig. 5.19b. As is seen β'' precipitates form the major source of hardening in the alloy. Two other precipitates, β' and β , mainly determine the yield strength of the alloy in the overage regime.

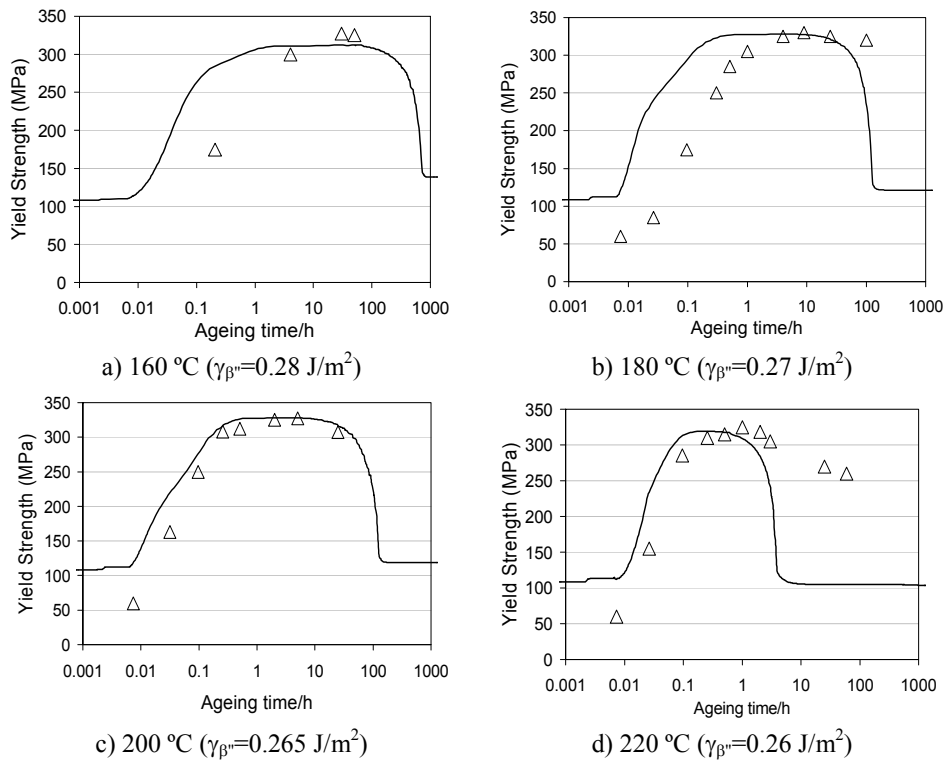
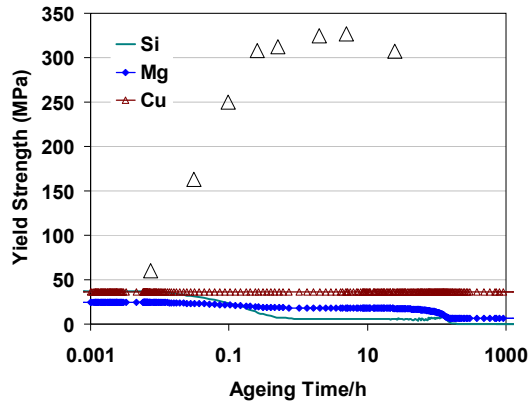
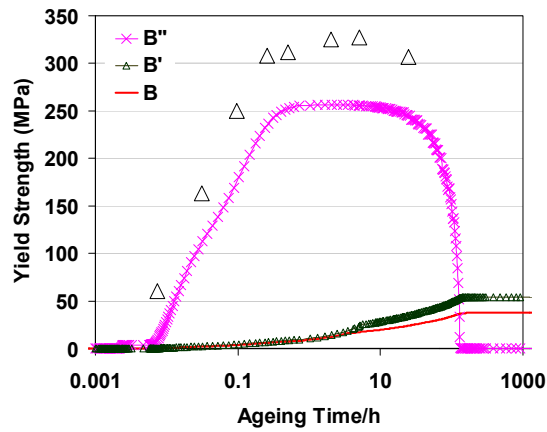


Figure 5.18: The prediction of the yield strength of the alloy AA6111, aged at different temperatures together with experimental data

5. Multi-Component Multi-Precipitate Modelling of Ageing Kinetics in Al-Mg-Si Alloys



(a)



(b)

Figure 5.19: Contributions of a) solid solution hardening and b) precipitation hardening to the yield strength of the alloy AA6111, aged at 200 °C.

5.6. Discussion

The MatCalc model has been used for the first time to simulate ageing in Al-Mg-Si alloys considering the possibility of simultaneous nucleation, growth, dissolution,

5. Multi-Component Multi-Precipitate Modelling of Ageing Kinetics in Al-Mg-Si Alloys

and coarsening of different precipitates in the matrix. The model is essentially based on the *Onsager* thermodynamic principle, which states that the system evolves with a maximum *Gibbs* free energy dissipation rate [25-28]. There are different nomenclatures used by different authors to introduce the first group of precipitates formed in the very beginning of ageing. These are named atomic clusters [34], GP-zones [35], or GP-I zones [36]. In the current model, the first group of precipitates believed to nucleate in the early stage of ageing is named GP-zones. GP-zones nucleate when the alloy is stored at room temperature (natural ageing), or when it is aged at very low temperatures. They normally consume excess vacancies, Mg, and Si, decreasing the precipitation kinetics of β'' precipitates [37]. Apart from GP-zones, there are three other major precipitates available in the Al-Mg-Si alloys namely β'' , β' , and β . Free-Si particles are formed only when there is excess Si in the composition of the alloy. It has been found that the addition of Cu can have a marked effect on the artificial aging, i.e. enhancing the precipitation hardening kinetics, refining precipitate size, and changing the precipitation sequence [35]. This for example means that Cu-containing precipitates such as Q' and Q might appear in the precipitation sequence. In the current model Q' and Q precipitates have not been considered. Therefore, it is assumed that Cu atoms do not leave the solid solution. Results of ageing simulation show that the investigated parameters, interfacial energy, alloy composition, and temperature, mainly influence the precipitation kinetics and the relative amount of different phases but the precipitation sequence remains qualitatively unchanged. During cooling a low density of GP zones, β' and β precipitates nucleate while a more significant number of β'' precipitates are formed. Their volume fraction remains low so that the supersaturation of Si and Mg is not decreasing significantly. During heating to the ageing temperature, additional nucleation of GP zones takes place. At temperatures higher than 100 °C these GP-zones dissolve very rapidly. At the beginning of isothermal ageing β'' precipitates start to grow. At low temperature, extra nucleation of β'' and simultaneous growth and dissolution of GP-zones is also predicted. At the same time, β' and β nucleate and grow, while Si particles just grow. The growth of β'' is then followed by a coarsening period of β'' . During this entire first period of isothermal ageing the volume fraction of β' , β and Si, however, remains negligible. When the volume fraction of β' and β precipitates starts to become significant the competition with β'' becomes visible; β'' dissolves and the released Mg and especially Si concentrations cause further growth of β' and β precipitates. Once all β'' precipitates have dissolved, coarsening of β' begins while β continues to grow. Once again, when the volume fraction of β precipitates reaches a certain amount, the competition with β' becomes visible and β' precipitates dissolve. After full dissolution of

5. Multi-Component Multi-Precipitate Modelling of Ageing Kinetics in Al-Mg-Si Alloys

β' precipitates, β precipitates start to coarsen. In the alloy containing excess Si, nucleation and growth of free Si particles also takes place during or after dissolution of β'' . For all ageing treatments, the higher number density of β'' precipitates formed during cooling (Fig. 5.15) shows that the nucleation rate of β'' precipitates is faster than the ones of β' and β . As expected, this illustrates that the effect of a higher MDEF parameter and lower interfacial energy for β'' precipitates dominates over the effect of a smaller driving force on the nucleation rate (Eqs. (5.10) and (5.11)). During isothermal ageing at high enough temperature, the model also predicts very short nucleation period of all precipitates, except free Si in alloy A, a situation which is very close to site saturation nucleation. The site saturation nucleation, as one of the major outcomes of the model, however, is certainly not an appropriate prediction of the nucleation kinetics (see Fig. 5.10b). Besides, there is no indication that β' and β precipitates are present in the underaged alloy [30]. It is expected that β' and β are forming in a sequential order after β'' . The formation mechanism of β' , as a case in point, could be the simultaneous dissolution of β'' and re-nucleation of β' , or the gradual transformation of β'' to β' . Although the site saturation nucleation of β'' has a strong effect on the underaged part of the precipitation kinetics, the site saturation nucleation of β' and β has less consequences for the current simulations. The number density of β' and β precipitates formed in the beginning of ageing is several orders of magnitude lower than usually observed (see Fig. 5.11b) and therefore the initial volume fraction of these precipitates is negligible. Only when these precipitates start to grow significantly, the competitive coarsening between β' , β , and β'' becomes relevant. β'' dissolves and the volume fraction of β' and β increases. This process can be considered as a good approximation of the sequential precipitation of β'' , β' and β .

The comparison of simulation and experimental results has shown that the predicted nucleation rate of β'' precipitates is overestimated around 150 °C and underestimated at higher temperatures. The model also overestimates the growth and dissolution rates. It was found that in order to obtain a good fit of the precipitation kinetics at all temperatures, the change in the interfacial energy is needed. Changing the interfacial energy has clear effects on the nucleation rate but has little effect on the growth rate. The diffusion coefficients used in the model are the ones for bulk diffusion. They are therefore already a lower bound and cannot be decreased further to slow down the nucleation and growth rates. This suggests that other model parameters need to be adjusted. The most probable one is the chemical driving force or the chemical potentials.

5. Multi-Component Multi-Precipitate Modelling of Ageing Kinetics in Al-Mg-Si Alloys

These parameters are, however, difficult to estimate, especially for metastable phases, and additional study would be required.

From the presented results, one can also see the importance of different precipitates in terms of strengthening, among which the β'' precipitates is the main source of strengthening. Both the kinetics of ageing (see Fig. 5.10) and the age-hardening (see Fig. 5.18) are very much dependent on the interfacial energy for the β'' phase. Since there is no experimentally measured value for this parameter, the interfacial energy is therefore obtained by fitting the model predictions to the experimental results. However, it is found that a constant interfacial energy for the β'' phase does not give correct predictions in all ageing temperatures. If this value is assumed to be constant, the predicted peak-strength decreases significantly with the increase in temperature due to a decrease in the maximum number density of β'' precipitates, which is in contradiction with the experimental data, which shows very small changes in the peak strength as a function of ageing temperature. The only way in which the developed model can describe the observed peak-strength is by changing the interfacial energy of β'' phase with temperature in the range 0.25-0.29 J/m². Khan and his colleagues [38] presented the following equation to consider the temperature dependency of the interfacial energy of precipitate

$$\gamma = \gamma_0 - \alpha T^3, \quad (5.34)$$

with α and γ_0 being fitting parameters. The reason that $\gamma_{\beta''}$ decreases with increasing temperature is the easier diffusion of atoms at the interface, making the interface more diffusive than sharp [25]. This is not only the case for β'' precipitates, but also for other precipitates one can expect a temperature-dependent variation of interfacial energy. However, for other precipitates the interfacial energy is assumed to be constant, since the variation in their interfacial energy does not have a strong effect on the kinetics of ageing and strengthening.

5.7. Summary

A multi-precipitate multi-component model based on the maximum Gibbs free energy dissipation is presented to model the ageing kinetics and age-hardening of Al-Mg-Si alloys. Five major precipitates are considered in the model: GP-zones, β'' , β' , β , and free Si. Based on the presented results one can draw the following conclusions regarding the developed model:

5. Multi-Component Multi-Precipitate Modelling of Ageing Kinetics in Al-Mg-Si Alloys

- The modelling results show that there is a concurrent nucleation of different precipitates taking place mostly before the beginning of ageing. A large fraction of precipitates nuclei form during quenching and heating to ageing temperature. The model also shows that in the beginning of ageing only less stable precipitates grow initially and at some point these precipitate dissolve in favor of more stable precipitates. In the end, only thermodynamically stable precipitates like β and free Si remain in the alloy. This actually forms the precipitation sequence. The modeled precipitation sequence and its dependence with temperature are semi-qualitatively in agreement with experimental data.
- The results show that nucleation for all precipitates is more like site saturation than a gradual increase in the number of nuclei during ageing.
- In the alloy A, which contains excess Si, there is an intermediate free Si particles nucleation at the very end of the stability of β'' precipitates. This is attributed to the dissolution of β'' and growth of β' . Since the latter precipitate needs less Si, the remaining excess Si nucleates as free-Si particles.
- The predicted nucleation, growth and dissolution rates are too fast and a good quantitative fitting of the precipitation kinetics could not be obtained with only one set of interfacial energy and MDEF parameters. The influence of other parameters, i.e. chemical driving force, needs to be considered.
- Prediction of the alloy yield strength at different temperatures is only possible by changing the interfacial energy in the range 0.25-0.29 J/m², in a way that by increasing temperature, this value decreases.
- When it comes to strengthening, β'' phase is certainly the most important precipitate, comprising around 80% of the total strength of the alloy.
- The yield strength in the underaged regime is controlled by the solid solution hardening; while in the overaged regime it is mainly controlled by β' and β precipitates.

5. Multi-Component Multi-Precipitate Modelling of Ageing Kinetics in Al-Mg-Si Alloys

References:

- [1] Andersen SJ, Zandbergen HW, Jansen J, Treholt C, Tundal U., Reiso O., *Acta Mater* 1998;46:3283:3294.
- [2] Marioara CD, Andersen SJ, Jansen J, and Zandbergen HW, *Acta Mater* 2001;49: 321:331.
- [3] Ravi C, Wolverton C, *Acta Mater* 2004;52;4213:4227.
- [4] Thomas G. *J Ins Metals* 1961–62;90:57.
- [5] Matsuda K, Gamada H, Fujii K, Uetani Y, Sato T, Kamio A, et al. *Metal Mater Trans* 1998;29A:1161.
- [6] Zandbergen HW, Andersen SJ, Jansen J. *Science* 1997;277:1221.
- [7] Edwards GA, Stiller K, Dunlop GL, Couper MJ. *Acta Mater* 1998;46:3893.
- [8] Wahi RP, von Heimendahl M. *Phys Status Solidi A* 1974;24:607.
- [9] Lynch JP, Brown LM, Jacobs MH. *Acta Metall* 1982;30:1389.
- [10] Sagalowicz L, Hug G, Bechet D, Sainfort P, Lapasset T. In: Sanders Jr TH, Starke Jr EA, editors. *Proceedings of the 4th International Conference on Aluminium Alloy*, Vol. 1. Atlanta: Georgia Institute of Technology; 1994. p. 636.
- [11] Matsuda K, Naoi T, Fujii K, Uetani Y, Sato T, Kamio A, et al. *Mater Sci Eng* 1999;A262:232.
- [12] Jacobs MH. *Phil Mag* 1972;26A:1.
- [13] Matsuda K, Tada S, Ikeno S. *J Electron Microsc* 1993;42:1.
- [14] Vissers R, Jansen J, Zandbergen HW. National Centre for HREM, Delft University of Technology, The Netherlands, (private communication); 2004.
- [15] Cayron C, Buffat PA. *Acta Mater* 2000;48:2639.
- [16] Miao WF, Laughlin DE. *Metal Mater Trans* 2000;31A:362.
- [17] Arnberg L, Aurivillius B. *Acta Chem Scand A* 1980;34:1.
- [18] Geisler AH, Hill JK. *Acta Cryst* 1948;1:238.
- [19] Martin JW, Doherty RD, Cantor B, *Stability of microstructure in metallic Systems*, 2nd edition, Cambridge Univ. Press, 1997, Cambridge UK.
- [20] Porter DA, Easterling KE, *Phase transformation in metals and alloys*, 2nd editions, Chapman & Hall Press, 1992:156.
- [21] Robson JD, Bhadeshia HKDH. *Mater Sci Tech*, 1997;13:631.
- [22] Fratzl P, Penrose O, Lebowitz JL, *Stat J. Phys* 1999;95:1429.
- [23] Chen LQ *Annual Rev Mater Res* 2002;32:113.
- [24] Myhr OR, Grong O, Andersen SJ. *Acta Mater* 2001;49:65.

5. Multi-Component Multi-Precipitate Modelling of Ageing Kinetics in Al-Mg-Si Alloys

- [25] Rajek HJ, Computer simulation of precipitation kinetics in solid metals and application to the complex power plant steel CB8, PhD thesis, Graz University of Technology, Austria, November 2005, pp. 46-48.
- [26] Kozeschnik E, Svoboda J, Fratzl P, Fischer FD. *Mater Science Eng A*. 2004;385:157–165.
- [27] Kozeschnik E, Svoboda J, Fischer FD. *Computer Coupling of Phase Diagrams and Thermochemistry*. 2004;28:379–382
- [28] Kozeschnik E, Svoboda J, Fratzl P, Fischer FD. *Mater Science Eng A*. 2004;385:166–174.
- [29] Ardell AJ. *Acta Metall*. 1967;15:1772.
- [30] Esmaili S, Precipitation hardening behavior of AA6111, PhD thesis, The University of British Columbia, Canada, 2002, pp. 25-86.
- [31] Zandbergen MW, Study of Early-Stage Precipitation in Al-Mg-Si(- Cu) Alloys by 3D Atom Probe, PhD thesis, University of Oxford, 2008.
- [32] Turnbull D. *Impur. Imperf*. 1955;121:43.
- [33] Janssens K, Raabe D, Kozeschnik E, *Computational Mater Eng an Introduction to Microstructure Evolution*, Elsevier Inc., 2007;194:196.
- [34] Wang X, Poole WJ, Esmaili S, Lloyd DJ, Embury JD, *Metal Mater Trans*. 2003;34A: 2913.
- [35] Miao WF, Laughlin DE, *Scripta Mater*. 1999;40:873–878.
- [36] Dutta I, Allen SM, *Mater Science Letter*. 1991;10:323-328.
- [37] Saga M, Sasaki Y, Kikuchi M, Yan Z, Matsuo M, *Proc. 5th Int. Conf. on Al Alloys*, Gronebel, France, 1996, pp. 821.
- [38] Khan IN, Starink MJ, Yan JL, *Mater Science Eng A*. 2008;472;66–74.

5. Multi-Component Multi-Precipitate Modelling of Ageing Kinetics in Al-Mg-Si Alloys

CHAPTER 6

Interrupted Ageing in Al-Mg-Si alloys

The effects of secondary precipitates, induced by interrupted ageing, on the age hardening of Al-Mg-Si alloys have been studied. The so-called interrupted ageing was carried out in three steps: (i) underageing the alloy at 170 °C for 15 min, (ii) quenching and holding the alloy at different temperatures from room temperature (RT) to 85 °C for one week, and (iii) re-ageing the alloy at 170 °C for various times. From the results it appears that the influence of secondary precipitates is highly dependent on the interruption temperature. Secondary precipitation stimulated by interruption at temperatures below 50 °C has almost no influence on the alloy strength, while when the interruption temperature is above 50 °C, it increases the hardness significantly. The proposed scenario to explain this behavior is based on the temperature-dependent competitive growth of GP-I and GP-II precipitates. According to this model, interruption temperature below 50 °C stimulates the formation of GP-I zones, which have a very slow kinetics of transformation and therefore they have almost no influence on the mechanical properties. On the other hand, when the alloy is interrupted at temperatures above 50 °C, the formation of GP-II zones is more likely to happen, consequently resulting in the higher density of β'' precipitates during re-ageing and better mechanical properties.

6. Interrupted Ageing in Al-Mg-Si alloys

6.1. Introduction

There is a growing interest in the application of light-weight heat treatable Al-Mg-Si alloys in automotive and aerospace industries. These alloys have a high potential for improving strength/weight ratio, corrosion resistance, and fuel efficiency [1-3]. Precipitates in Al-Mg-Si alloys are major contributors to the mechanical and physical properties. They are very influential in the slip and deformation behavior of Al-Mg-Si alloys and consequently they control the strength, hardness, ductility, and crashworthiness of these alloys. A great number of experiments have been carried out to modify the type, size, and volume fraction of precipitates [4-11]. Liu *et al.* [8] showed that if one can simultaneously increase the volume fraction of precipitates and decrease their size, it is possible to enhance both formability and yield strength. This can be achieved via interrupted ageing. Lumley *et al.* [12-14] showed that interrupted ageing is a way to modify both precipitate density and size. They showed that “if age hardenable aluminum alloys are first underaged at an elevated temperature, quenched and then exposed to a lower temperature (eg. 25-65 °C), and aged again at elevated temperatures, simultaneous increase in tensile properties and fracture toughness are possible”. A series of different interrupted ageing tempers have now been developed, which are summarized in Table 6.1. Among different interrupted ageing treatments, T6I4 and T6I6 are more important and they are briefly explained.

Table 6.1: Interrupted aging temper variants [12-14]

Temper	Process
T6I4	Solution treat, quench, underage, quench, age at 25-65°C
T6I6	Solution treat, quench, underage, quench, interruption at low temperature, re-age at artificial aging temperature
T8I6	Solution treat, quench, cold work, underage, quench, interruption at low temperature, re-age at artificial aging temperature
T9I6	Solution treat, quench, underage, cold work, interruption at low temperature, re-age at artificial aging temperature

6. Interrupted Ageing in Al-Mg-Si alloys

- **T6I4 Temper**

Secondary ageing may occur if age hardenable aluminum alloys are first underaged at an elevated temperature (e.g. 150 °C), quenched and then exposed to a lower temperature (e.g. 25-65 °C) [13]. At these lower temperatures, nucleation of fine precipitates occurs that depletes the matrix of solute elements and gives rise to additional strengthening. This treatment has been designated the T6I4 temper (I= interrupted). The T6I4 temper utilizes secondary precipitation after a short period of underageing at an elevated temperature to achieve the properties of the T6 temper or even higher.

- **T6I6 Temper**

The T6I6 temper is completed when an alloy that has undergone a complete or partial T6I4 temper is re-aged at an elevated temperature for a time to reach peak strength. This kind of interrupted ageing provides a means for modifying the size, composition, morphology, and distribution of precipitate particles in aged aluminum alloys. Also, typically, average improvements of 10-15% to hardness, yield strength and tensile strength occur during this ageing procedure with simultaneous improvements of fracture toughness in most alloys [12-14]. In some cases (e.g. 6061), fracture toughness may be increased by 60% [14]. Buha *et al.* [15] compared the size, shape, and distribution of precipitates obtained by isothermal and interrupted ageing. They showed that the interruption increases the number density and decreases the size of precipitates at peak-age. Lumley *et al.* [12-14] concluded that the mechanical properties and microstructural modifications are due to the secondary precipitation during interruption. According to their analysis, during interruption at lower temperatures the density of GP-zones increases. The GP-zones act as nucleation sites, facilitating an increased density of β'' precipitates during the re-ageing stage at higher temperatures. Yet, the increased number of GP-zones is not necessarily associated with the enhanced mechanical properties. As a case in point, keeping the alloy at room temperature before isothermal ageing, even though increases the number density of GP-zones [5], it degrades mechanical properties [16]. Therefore, the current scenario for improvement of mechanical properties due to secondary precipitation, which is mainly based on the evolving of secondary GP-zones into β'' precipitates requires further study. Unfortunately, because of their size at the nanometer scale and their chemical similarity with the matrix (low Z-contrast), it is extremely difficult to characterize secondary precipitates with direct characterization methods (e.g. TEM) [5]. It seems that indirect

6. Interrupted Ageing in Al-Mg-Si alloys

characterization techniques like electrical resistivity and DSC are more efficient compared to direct ones owing to the fact that the clustering or precipitation of GP zones leads to large changes of these properties [16-19]. This chapter aims to study the effects of temperature on the secondary precipitation phenomenon in Al-Mg-Si alloys, mainly focusing on the effect of this phenomenon on the evolution of electrical resistivity, DSC, and hardness.

6.2. Materials and methods

The alloy used for this study was 1-mm thick AA6061 (Al-0.95wt%Mg-0.62wt%Si-0.2wt%Cu) sheet, delivered in T4 condition. The samples were solution-treated in an air furnace for 20 min at 560 °C, water-quenched, underaged at 170 °C for 15 min, kept at room temperature, 45, 65, and 85 °C for 7 days, and then re-aged at 170 °C for various times. The time interval between water-quench and underageing was less than 2 min. Figure 6.1 shows a schematic view of interrupted ageing. The resistivity of the alloy AA6061 during isothermal ageing and interrupted ageing was measured by the eddy currents technique. The measurements were conducted by a Sigmatest D 2.068 at room temperature at a rate of 60 Hz. The effects of different ageing heat treatments on the hardness of the alloy AA6061 were monitored by Vickers hardness measurements with 300-gr load. The accuracy of hardness measurements was ± 4 VHN. DSC tests were conducted at 10 °C/min using a NETZSCH 404C calorimeter in He atmosphere. The baseline subtraction was done for all tests. The time scale is defined as cumulative time at ageing and re-ageing, not including the interruption time.

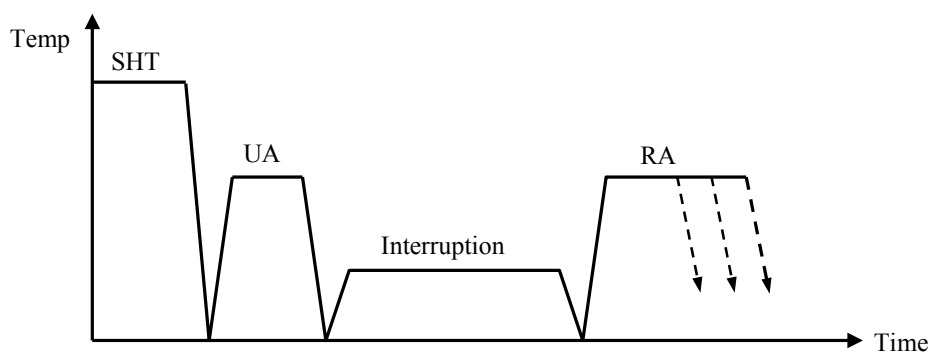


Figure 6.1: Schematic view of interrupted ageing (SHT: solution heat treatment, UA: underageing, and RA: re-ageing)

6. Interrupted Ageing in Al-Mg-Si alloys

6.3. Results

The electrical resistivity evolution of the alloy AA6061 during isothermal ageing at 170 °C is shown in Fig. 6.2. During ageing at 170 °C, the resistivity slightly increases at the beginning, reaches a peak in a few minutes, followed by a smooth decrease. The drop in the resistivity is explained by the solute depletion due to the formation of β'' precipitates [16]. The initial peak in the beginning of ageing is named resistivity anomaly, since this increase is happening when the matrix is being depleted due to precipitation. Figure 6.3 shows the effects of the interruption temperature on the resistivity evolution of the alloy AA6061 underaged at 170 °C for 15 min. It is seen that treating the alloy at RT, 45, 65, and 85 °C for a long time (7 days) results in a resistivity increase, hereafter named the secondary resistivity anomaly. From this figure it is seen that the intensity of secondary resistivity anomaly strongly depends on the interruption temperature. The lower the interruption temperature, the larger the secondary resistivity anomaly is. The appearance of the secondary resistivity anomaly due to interruption is an indication that the formation of small atomic clusters/GP zones is the governing phenomenon during interruption [20].

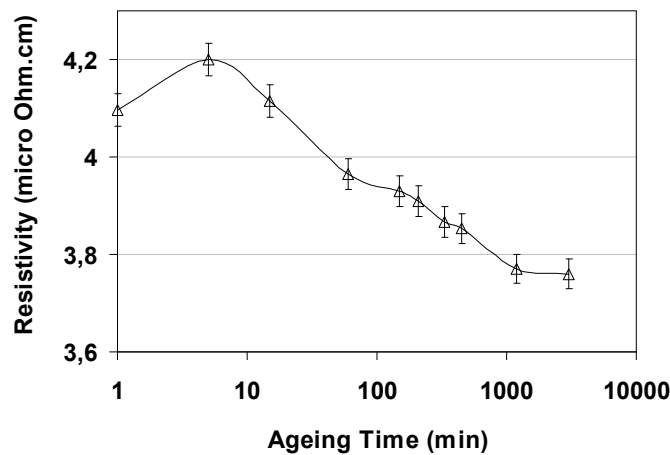


Figure 6.2: The electrical resistivity evolution of the alloy AA6061 aged at 170 °C

6. Interrupted Ageing in Al-Mg-Si alloys

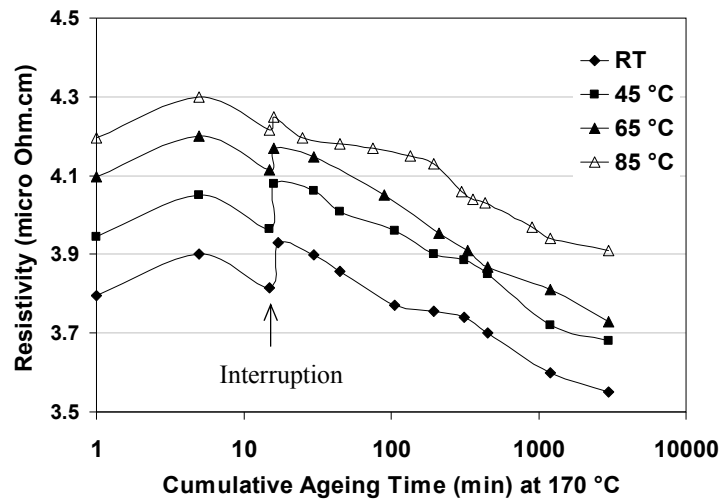


Figure 6.3: The effects of one week interruption temperature on the electrical resistivity evolution of the alloy AA6061 during ageing at a) 170, and b) 190°C (The error is the same as Fig. 6.2). The curves have been offset by multiples of 0.15 $\mu\Omega\cdot\text{cm}$ for clarity

Figure 6.4 shows a comparison between the hardness evolution of the alloy AA6061 with and without interruption, aged at 170 °C. It is seen that depending on the interruption temperature, the secondary precipitation may have significant effects on the age hardening behavior of the alloy. This figure suggests the presence of two distinctive secondary precipitation regimes at low (below 50 °C) and high temperatures (above 50 °C), hereafter termed low temperature and high temperature secondary precipitation. Low temperature secondary precipitation (RT and 45 °C interruption temperatures) does not have a positive contribution to the mechanical properties. However, high temperature secondary precipitation enhances the mechanical properties significantly.

6. Interrupted Ageing in Al-Mg-Si alloys

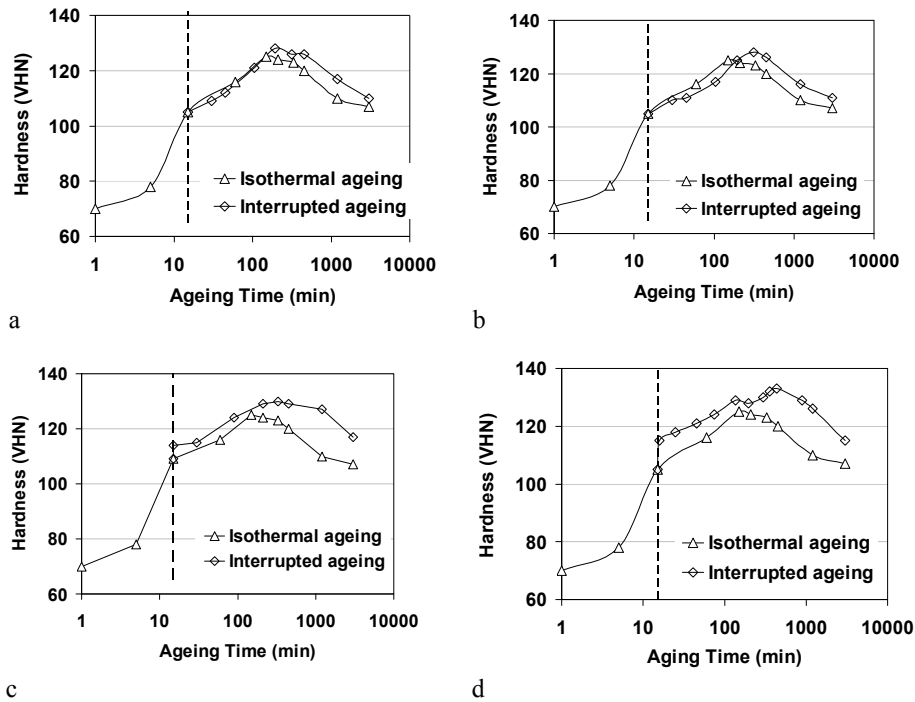


Figure 6.4: The hardness evolution of the alloy AA6061 during isothermal ageing (170 °C) and interrupted ageing at different interruption temperatures; a) RT, b) 45, c) 65, and d) 85 °C (Note that The time scale is defined as cumulative time at ageing and re-ageing, not including the interruption time) the dashed line shows the time of interruption

Figure 6.5 shows the DSC thermogram of as-solutionized material. The first peak corresponds to the precipitation of GP-I zone [7], the second peak to GP-II/ β'' [4], the third peak to β' , and the last one to β [12]. Figure 6.6 shows a comparison between the DSC curves of the alloy AA6061 after being underaged at 170 °C for 15 min and then aged at interruption temperature RT or 65 °C for one week. Obviously, when the alloy is interrupted at 65 °C there is no evidence of GP-II/ β'' peak in the thermogram, while when the interruption is at RT, GP-II/ β'' form during DSC test.

6. Interrupted Ageing in Al-Mg-Si alloys

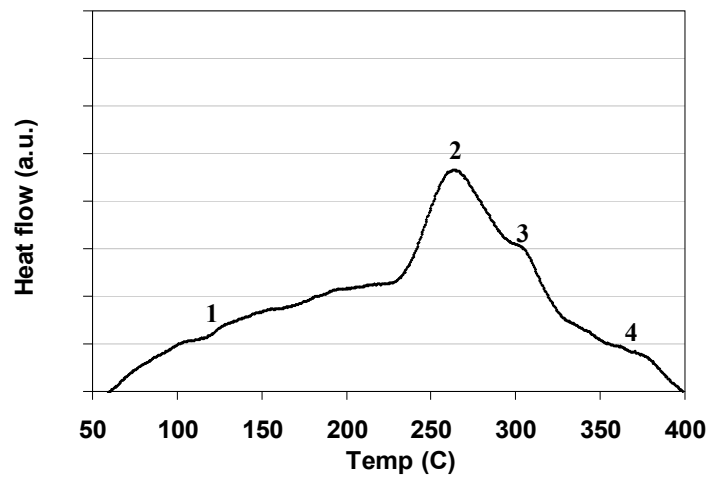


Figure 6.5: DSC thermogram of as-quenched alloy AA6061

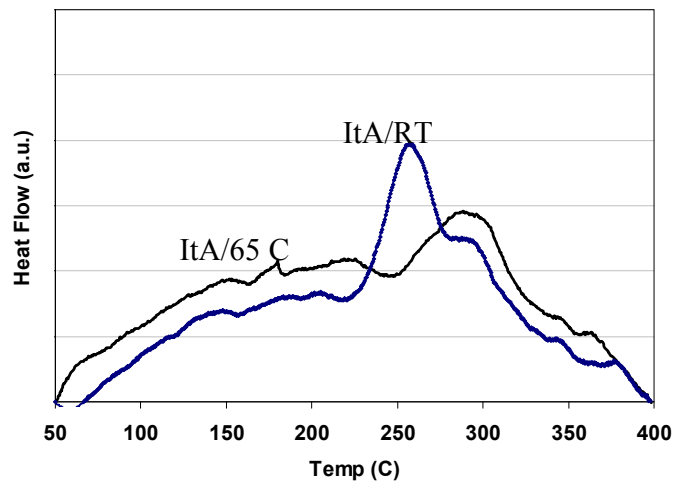


Figure 6.6: A comparison between the DSC curves of the alloy AA6061 after being underaged at 170 °C for 15 min and then aged at interruption temperature RT and 65 °C for one week

6. Interrupted Ageing in Al-Mg-Si alloys

6.4. Discussion

In this investigation the effects of secondary precipitation on the resistivity and mechanical properties of Al-Mg-Si alloys have been studied. In order to study the secondary precipitation phenomenon, the AA6061 alloy was underaged at 170 °C for 15 min, then kept at RT, 45, 65, and 85 °C for one week and then re-aged at 170 °C for various times. The anomalous increase in the resistivity of the alloy during interruption is attributed to the formation of fine secondary precipitates (see Figs. 6.3). It is anomalous because contrary to the Matthiessen's law [18] the solute depletion due to the formation of secondary precipitate is associated with an increase in resistivity. According to the Matthiessen's law [18], alloying elements in the solid solution have a very strong contribution to the overall resistivity, meaning that the depletion of alloying elements due to the formation of secondary precipitates is expected to decrease the total resistivity. The fact that secondary small coherent atomic clusters and/or GP-zones increase the resistivity cannot be explained by Matthiessen's law. Such effect has been also reported in Al-Ag, Al-Zn, Al-Cu, Cu-Be, and Al-Mg-Si systems [19]. The resistivity anomaly phenomenon is not yet completely understood, but it is generally ascribed to the formation of very fine (~10 Å [20]) atomic clusters or GP-zones [16,19,21]. There are three main propositions explaining the resistivity anomaly given as follows:

- a) **Coherency strain theory:** According to this theory the anomalous peak is due to the coherency strain around atomic clusters and/or GP-zones [22,23]. According to this hypothesis, the formation of GP-zones is accompanied with the collapse of matrix and introduction of strain to the matrix, which changes the lattice parameters and electronic structure of material and consequently results in the resistivity anomaly.
- b) **Interface dislocations theory:** In this theory the resistivity anomaly is attributed to the geometrically necessary dislocations (GNDs) around GP-zones [24]. This theory is not comprehensive enough to explain the observed resistivity anomaly in all metallic systems. As a case in point, the resistivity anomaly has been observed in Al-Ag and Al-Zn alloys [19] where the GP-zones have a negligible misfit with the matrix and consequently have a negligible density of GNDs.
- c) **Cluster size theory:** Based on this theory the resistivity anomaly is essentially due to the small size of the zones [25,26]. It is seen that when the cluster size

6. Interrupted Ageing in Al-Mg-Si alloys

reaches a critical and definite value, equal to the wavelength of conduction electrons at the Fermi level, clusters then cause strong scattering, resulting in the anomalous resistivity increase. The critical size of clusters and/or GP-zones is only dependent on the chemical composition of the alloying system [19,25,27,28].

The precipitation sequence in the AA6061 alloy (like other Al-Mg-Si alloys) is a very controversial topic [4-7,29]. The main discrepancy in the precipitation sequence of Al-Mg-Si alloys is related to the initial stage of ageing. Initial precipitates are spherical and coherent and because of their negligible pinning force they are least effective for strengthening the alloys. One can find different names for initial spherical precipitates in the literature i.e. clusters [5], co-clusters [6], or GP-I [4] zones. Regarding the chemical composition and crystallographic structure of initial spherical precipitates, Dutta and Allen [4] proposed that these precipitates are disordered colonies of Si atoms. However, Buha *et al.* [5] proposed that GP-I zones are clusters of Mg and Si alloys. In a relatively new study, Edwards *et al.* [6], using atom probe field ion microscopy (AFIM), showed that the initial precipitates are clusters/co-clusters of Mg and Si which form by the following three successive reactions:

SSS → Clusters of Si and/or Mg → Dissolution of Mg clusters → Mg/Si co-clusters

Contrary to the conventional notion indicating that spherical GP-I zones are disorder, Chen *et al.* [29] concluded that these precipitates have the stoichiometry of $Mg_2Si_2Al_7$ with a monoclinic lattice. Apart from GP-I zones, which are spherical precipitates [30], some researchers reported that GP-zones are needle-like [31,32]. Today, it has been proved that there are two kinds of GP-zones in Al-Mg-Si alloys [4]; GP-I and GP-II zones. GP-II zone is a needle-like precipitate with a structure resembling that of β'' but with different positions for some of the Mg atoms along the needle direction [10]. Formation of GP-II zone is a preliminary stage for the formation of β'' precipitates. The initial fast increase in the hardness of Al-Mg-Si during ageing could be related to the formation of GP-II zones. It is proposed [29] that initial needle-like GP-II zones have the composition of $Mg_{2+x}Si_{2+y}Al_{7-x-y}$. These precipitates have the tendency to distort the surrounding matrix and to inhibit the movement of dislocations. Saga [33] and Dutta and Allen [4] studied the effects of temperature on the formation of GP-zones. They concluded that the formation of GP-I and/or GP-II zones is a parallel, competitive process which is highly dependent on the temperature. Saga [33] showed that temperatures below 67 °C are more favorable for precipitation of GP-I, while

6. Interrupted Ageing in Al-Mg-Si alloys

temperatures above 67 °C are more favorable for precipitation of GP-II [33]. Based on this argument and experimental data, the secondary precipitation can be divided to low and high temperature regimes. Low temperature regime is mainly associated with the formation of GP-I zones, while the high temperature one is associated with the formation of GP-II zones. Secondary GP-I zones formed during interruption at RT and 45 °C are spherical and coherent and they can be easily sheared by moving dislocations and therefore they have a negligible influence on the mechanical properties (see Fig. 6.4). Regarding the behavior of secondary GP-I during re-ageing, some researchers believe that GP-I zones are unstable precipitates and they act as nucleation sites for other more stable precipitates and they eventually transform to GP-II and β'' precipitates [12,34]. However, Panseri *et al.* [20] showed that initial GP-I zones dissolve during re-ageing. Suzuki *et al.* [34], Zhen *et al.* [35] and Thomas *et al.* [36] showed that atomic clusters (GP-I zones) precipitated during pre-ageing at low temperatures do not easily transform into other precipitates during final aging and remain almost unchanged for a prolonged time. It is wise to consider the possibility of all the abovementioned phenomena happening simultaneously. Recently, it has been proposed [37] that some of GP-I zones transform to β'' while the others remain stable during ageing. The experimental results show that the amounts of low-temperature GP-I zones, transforming to β'' , is negligible, since there is no improvement of mechanical properties during re-ageing (see Fig. 6.4). By increasing the interruption temperature to temperatures higher than 50 °C, the volume fraction of GP-II zones increases significantly, having a positive contribution to the mechanical properties, and hence increasing the hardness of the alloy AA6061. Figure 6.6 shows that when the alloy is interrupted at 65 °C, almost all GP-II zones and β'' nuclei are formed during interruption, since there is no GP-II/ β'' formed during DSC test. It is reasonable to suggest that during re-ageing, initial and secondary GP-II zones continue their transformation on the expense of the remaining supersaturated solutes, resulting in an improvement in mechanical properties.

6.5. Conclusions

An investigation has been conducted on the effects of interrupted ageing on the resistivity and hardness evolutions in the alloy AA6061. The results indicate that:

6. Interrupted Ageing in Al-Mg-Si alloys

- The resistivity measurements during interrupted ageing show that there is an anomalous resistivity peak after interruption. The anomalous peak is related to precipitation of secondary GP-zones.
- The secondary precipitation mechanism could be divided into two regimes, i.e. low temperature secondary precipitation and high temperature one.
- Low temperature secondary precipitation mainly results in the formation of GP-I zones. During re-ageing these secondary GP-I zones do not have a significantly positive contribution to mechanical properties.
- High temperature secondary precipitation mainly results in the formation of GP-II zones. These precipitates have a positive contribution to the mechanical properties and they can increase the mechanical properties significantly.
- Based on the results of this study, the current theory of secondary precipitation is reviewed. The current theory indicates that secondary GP-zones can act as nucleation sites of other precipitates and because they are very small and densely dispersed, they finally result in a finer microstructure and better properties. But, the experimental evidence obtained in this study show that only secondary GP-II zones precipitated at temperatures higher than 50 °C can act as nucleation sites of other precipitates and finally they increase strength.

References:

- [1] X. Wang, W.J. Poole, S. Esmaeili, D.J. Lloyd, and J.D. Embury, *Metall Mater Trans* 34A (2003) 2913.
- [2] S. Esmaeili, X. Wang, W.J. Poole, and D.J. Lloyd, *Metall Mater Trans* 34A (2003) 751.
- [3] W.F. Miao and D.E. Laughlin, *Scripta Mater* 40 (1999) 873.
- [4] I. Dutta and S.M. Allen, *J. Mat Sci Lett* 10 (1991) 323.
- [5] J. Buha, R.N. Lumley, and A.G. Crosky, *J. Mater Metall Trans* 37A (2006) 3119.
- [6] G. A. Edwards, K. Stiller, G. L. Dunlop, and M. J. Couper, *Acta Mater.* Vol. 46, No. 11 (1998) 3893.
- [7] L.C. Doan, Y. Ohmori, and K. Nakai, *Mater Trans, JIM* 41 No. 21 (2000) 300.

6. Interrupted Ageing in Al-Mg-Si alloys

- [8] G. Liu, G.J. Zhang, X.D. Ding, J. Sun, and K.H. Chen, *Metall Mater Trans* 35A (2004) 1725.
- [9] S. J. Andersen, H.W. Zandbergen, J. Jansen, C. Treholt, U. Tundal, and O. Reiso, *Acta Mater* 46 (1998) 3283.
- [10] C.D. Marioara, S.J. Andersen, J. Jansen, and H.W. Zandbergen, *Acta Mater* 49 (2001) 321.
- [11] J.D. Bryant, *Met Mat Trans* 30A (1999) 1999.
- [12] J. Buha, R.N. Lumley, A.G. Crosky, and K. Hono, *Acta Mater* 55 (2007) 3015–3024.
- [13] R.N. Lumley, I.J. Polmear, and A.J. Morton, *Mater Sci Forum* 426-432 (2003) 303-308.
- [14] R.N. Lumley, I.J. Polmear, and A.J. Morton, *Mater Sci Forum* 396-402 (2002) 893-898.
- [15] J. Buha, R. N. Lumley, P. R. Munroe, and A. G. Crosky, *Proc. 9th Int Conf on Aluminium Alloys* (2004) 1167-1172.
- [16] S. Esmaeili, DJ. Lloyd, and W.J. Poole, *Mater Letters* 59 (2005) 575.
- [17] V. Massadier, T. Epicier, and P. Merlle, *Acta Mater* 48 (2000) 2911-2924.
- [18] Z.J. Lok, A.J.E. Feleming, R.Hamerton, and S. vab der Zwaag, *Mater Sci Forum* 396-402 (2002) 457-462.
- [19] A. Kelly and B. Nicholson, *Precipitation hardening, Prog. Mater. Sci.* 10 (1963) 149.
- [20] C. Panseri and T. Federighi, *J. Inst. Metals*, 94 (1966) 99.
- [21] S.K. Mehrotra, U. Ghosh, and S.K. Mukherjee, *Study of electrical conductivity of an Al-Mg-Si alloy*, internal report, Bharat Aluminum Co. Ltd.
- [22] A.H. Geisler, *Phase Transformation In Solids*, p 187, John Wiley 1951.
- [23] J. M. Pelletier, G. Vigier, J. Merlin, P. Merle, F. Fouquet, and R. Borrelly, *Acta Metall.* 32, No. 7 (1984) 1069.
- [24] M.E. Fine, *Acta Metall* 7 (1959) 228.
- [25] N.F. Mott, *J. Inst. Metals* 60 (1937) 267.
- [26] G. M. Raynaud, and P. Guyot, *Acta Metall* 36, No. 1 (1988) 143.
- [27] H. Herman and J.B. Cohen, *J. Nature* 190 (1961).
- [28] W.F. Miao and D.E. Laughlin, *Met Mat Trans* 31A (1999) 31.
- [29] J.H. Chen, E. Costan, M.A. Van Huis, Q. Xu, and H.W. Zandbergen, *Science* 312 (2006) 416.
- [30] H. Cordier and W. Gruhl, *Z. Metallkde* 56 (1956) 669.

6. Interrupted Ageing in Al-Mg-Si alloys

- [31] H.J. Rack and R.W. Krenzer, *Met Trans* 8A (1977) 335.
- [32] G. Thomas, *J. Inst Metals* 26 (1961) 1.
- [33] M. Saga, Y. Sasaki, M. Kikuchi, Z. Yan, and M. Matsuo, *Proc. 5th Int. Conf. on Al Alloys*, Gronebel, France, 1996, pp. 821.
- [34] H. Suzuki, M. Kanno, and G. Itoh, *Journal of Japan Institute of Light Metals*. Vol. 30, no. 11, pp. 609-6616. Nov. 1980
- [35] L. Zhen and S.B. Kang, *Scripta Mat* 36 (1997) 1089.
- [36] G. Thomas *J. Inst Metals* 90 (1961) 57.
- [37] T. Sato and S. Hirose, *Mat Scie. Forum* 475-479 (2005) 337-342.

CHAPTER 7

Strain Hardening of Al-Mg-Si alloys

In this chapter, the evolution of work-hardening and dynamic recovery rates vs. the flow stress increase ($\sigma - \sigma_y$) in Al-Mg-Si alloys is presented. The experimental data have been extracted from stress-strain curves. All curves show an initially very rapid decrease in slope of σ - ε curve, which is associated with the elastic-plastic transition. After elastic-plastic transition there are typically two distinctive behaviors. For underaged alloys, there is an approximately linear decrease of work-hardening rate as $(\sigma - \sigma_y)$ increases. However, for overaged alloys after elastic-plastic transition, there is a plateau in the work-hardening rate followed by an almost linear decrease. The maximum work-hardening and dynamic recovery rates are found to be dependent of the ageing state. In order to investigate these phenomena, a model has been employed to simulate the work-hardening behavior of Al-Mg-Si alloys. The model is based on a modified version of Kocks-Mecking-Estrin (KME) model, in which there are three main components; i) hardening due to forest dislocations, grain boundaries, and sub-grains, ii) hardening due to the precipitates, and iii) dynamic recovery. The modeling results are discussed and compared with the experimental data.

7. Strain Hardening of Al-Mg-Si alloys

7.1. Introduction

The influence of ageing on mechanical properties of Al-Mg-Si alloys is often viewed for its effect on yield strength. The influence of ageing on the work-hardening behavior is, however, also very important from industrial and scientific viewpoints. Understanding the behavior of materials during deformation is essential in optimizing production processes, which are based on forming, i.e. deep drawing and rolling. There are mainly two aspects in work-hardening; dislocation accumulation and dislocation annihilation [1-6]. Modeling and interpreting the work-hardening behavior of Al-Mg-Si alloys is much more complex compared to single phase alloys. This complexity is due to the presence of precipitates and their related solute distribution. Precipitates alter the mean free path of dislocations. They can also actively act as sites where dislocations are pinned and accumulated. Another important effect of precipitates is their influence on the solute content in the matrix. Alloying elements in solid solutions are known to decrease the dynamic recovery rate by changing stacking fault energy or causing solute drag effects [7]. The work-hardening behavior of Al-Mg-Si alloys is also influenced by the nature of precipitates. Shearable precipitates, for example, might lead to flow localization on the glide planes, where the precipitate strength is decreased because of shearing during deformation. Non-shearable precipitates, on the other hand, might store both elastic energy and dislocations, leading to larger hardening rates compared to single phase alloys. In addition to the effects of the nature of precipitates, their morphology can also be very important. Lath-shaped precipitates, for example, support larger local elastic stresses which give higher contribution to the hardening of alloys as compared to the precipitates of spherical morphology [8]. Several physically based approaches have been proposed to model work-hardening of metallic materials, from simple one-variable models, like the Kocks Mecking and Estrin, KME, model [9], to models including a more refined description of the microstructure [3]. Application of these models to simulate work-hardening of Al-Mg-Si alloys has been reported [6-12]. These applications used numerical methods to calculate the microstructure and flow stress change with deformation. In this chapter, we derive a simple analytical work-hardening model, based on the KME approach, coupled with a precipitation model and applicable to Al-Mg-Si heat-treatable alloys. In section 7.2 the modified KME is introduced and the parameters, used in the model to make it more applicable for precipitation-hardened systems, will be discussed. Then the experimental results will be presented and

7. Strain Hardening of Al-Mg-Si alloys

compared with modeling results in section 7.3 and the results will be discussed in section 7.4.

7.2. Kocks-Mecking-Estrin (KME) model

The modelling approach is similar to the one used by Cheng et al. [7] and also includes the solution by Simar [12] for the transition between precipitate shearing and bypassing domains. The evolution of the dislocation density, ρ , during deformation is dependent on the dislocation storage and dislocation annihilation [9] as is given below:

$$\frac{d\rho}{d\varepsilon} = \left. \frac{d\rho}{d\varepsilon} \right|_h - \left. \frac{d\rho}{d\varepsilon} \right|_s, \quad (7.1)$$

with ε the plastic true strain. The first term (indexed h) is due the dislocation accumulation and second term (indexed s) is due to dynamic recovery. These two terms are related to the dislocation density as follows [9]:

$$\begin{cases} \left. \frac{d\rho}{d\varepsilon} \right|_h = k_1 \sqrt{\rho} \\ \left. \frac{d\rho}{d\varepsilon} \right|_s = k_2 \rho \end{cases}, \quad (7.2)$$

where k_1 and k_2 are two proportionality parameters. Putting these equations into Eq. (7.1) and adding a term corresponding to dislocation storage around non-shearable precipitates yields:

$$\frac{d\rho}{d\varepsilon} = k_1 \sqrt{\rho} - k_2 \rho + k_D, \quad (7.3)$$

where k_D is the additional storage term due to dislocation-precipitate interaction. The value of k_D is related to the precipitate distribution as follows [10]:

$$k_D = \alpha_D \frac{M}{bL}, \quad (7.4)$$

where α_D is a constant close to 0.3 [10] and L is the precipitate spacing given by:

$$L = \left(\frac{2\pi}{f} \right)^{1/2} \langle r \rangle, \quad (7.5)$$

with f and $\langle r \rangle$ being the volume fraction and mean radius of precipitates, respectively. The stress increase due to dislocation hardening is related to the dislocation density using the Taylor equation as follows:

7. Strain Hardening of Al-Mg-Si alloys

$$\sigma_h = \alpha M G b \sqrt{\rho}, \quad (7.6)$$

where M is the Taylor factor, α is a constant in the range 0.2-0.5, G is the shear modulus, and b is the Burgers vector. When most precipitates are shearable, i.e. the alloy is underaged, Eq. (7.3) is written as follows:

$$\frac{d\rho}{d\varepsilon} = k_1 \sqrt{\rho} - k_2 \rho. \quad (7.7)$$

Integrating Eq. (7.7) and substituting into Eq. (7.6) yields the contribution of dislocations to the flow stress when most precipitates are shearable (i.e. underaged alloy) [10]:

$$\sigma_h = \frac{\alpha G b M k_1}{k_2} \left(1 - \exp\left(\frac{-k_2}{2} \varepsilon\right) \right), \quad (7.8)$$

On the other hand, when most precipitates are non-shearable (i.e. the alloy is overaged), k_D becomes more important than $k_1 \sqrt{\rho}$ for moderate values of ρ or deformation [10]. In this case it is reasonable to assume $k_I=0$. The integration of Eq. (7.3) and substitution into Eq. (7.6) yields [10]:

$$\sigma_h = \alpha G b M \left[\frac{k_D}{k_2} (1 - \exp(-k_2 \varepsilon)) \right]^{1/2}, \quad (7.9)$$

The transition from the shearable to the non-shearable regime is supposed to happen when mean radius is equal to r_{trans} .

- **Efficiency of dislocation storage around precipitates**

In the previous part, parameter k_D was introduced as dislocation storage term in overaged alloys. This parameter has been developed assuming that all (non-shearable) precipitates act as dislocation accumulation centers. However, a sharp transition from shearable precipitates regime to non-shearable precipitate regime when the average radius reaches r_{trans} is too rigid. During deformation, precipitates of radius larger than r_{trans} will be bypassed by moving dislocations. This process results in the formation of an Orowan loop around the precipitate. This Orowan loop experiences an increasing stress due to the pile up of other dislocations. Finally, depending on the precipitate size, this might result in shearing the precipitate and annihilation of the loop [12]. This has been schematically shown in Fig. 7.1.

7. Strain Hardening of Al-Mg-Si alloys

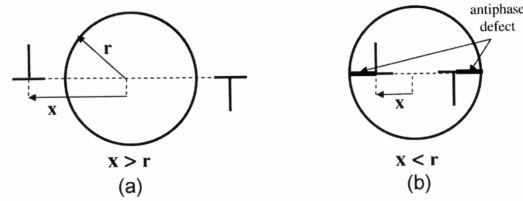


Figure 7.1: Precipitates of radius r a) having an Orowan loop and b) being sheared by the dislocation loop [12]

Based on the abovementioned argument, one can divide the size range of precipitate into three stages:

- $r < r_{trans}$, where precipitate shearing is taking place,
- $r_{trans} < r < r_{cl}$, where Orowan loops around precipitates are not stable.
- $r_{cl} < r$, in this regime precipitates having sizes bigger than critical radius r_{cl} are only bypassed and shearing is not possible. r_{cl} is the transition radius between unstable Orowan loop regime to the stable Orowan loop regime and corresponds to the transition between partially coherent to fully incoherent interfaces.

An efficiency factor φ has been introduced to take into account the effect of the stability of Orowan loops on the storage of dislocations around precipitates [12]. The efficiency factor should increase with increasing radius, since the difficulty of precipitate shearing increases with precipitate radius, which simply means that more dislocation pile-up (storage) is needed before the instability of Orowan loop occurs. A straightforward linear function for φ has been proposed as follows [12]:

$$\varphi = \frac{r - r_{trans}}{r_{cl} - r_{trans}} \quad (7.10)$$

For precipitates smaller than r_{trans} there is no dislocation storage around precipitates and for $r > r_{cl}$ efficiency factor, φ , is equal to unity. The factor k_D is then replaced by φk_D in equations (7.3), (7.4) and (7.9). The condition $k_1 \sqrt{\rho} \ll \varphi k_D$ used to derive equation (7.9)

7. Strain Hardening of Al-Mg-Si alloys

is not satisfied anymore for very small values of φ , i.e. for precipitate radius just above r_{trans} . The radius r_{trans}^* at which $k_1\sqrt{\rho} = \varphi k_D$ is given by

$$r_{trans}^* = \frac{r_{trans}}{1 - (r_{cl} - r_{trans})k_1\sqrt{\rho} \frac{b}{\alpha_D M} \sqrt{\frac{2\pi}{f}}}. \quad (7.11)$$

In most practical cases, this radius is very close to r_{trans} and the domain for which the condition $k_1\sqrt{\rho} \ll \varphi k_D$ is not fulfilled is very small. In this domain, equation (7.7) is used, neglecting φk_D . To summarize, the evolution of stress increment due to dislocation hardening with plastic strain, depending on the mean radius, can be obtained by below mentioned equations, the application of which depends on the average precipitates size:

$$\begin{cases} \sigma_p = \frac{\alpha G b M k_1}{k_2} \left(1 - \exp\left(\frac{-k_2}{2} \varepsilon\right) \right) & r \leq r_{trans}^* \\ \sigma_p = \alpha G b M \left[\frac{\varphi k_D}{k_2} (1 - \exp(-k_2 \varepsilon)) \right]^{1/2} & r_{trans}^* < r < r_{cl} \\ \sigma_p = \alpha G b M \left[\frac{k_D}{k_2} (1 - \exp(-k_2 \varepsilon)) \right]^{1/2} & r_{cl} \leq r \end{cases} \quad (7.12)$$

Other contributions to the flow stress, including pure aluminium yield strength, σ_0 , solid solution hardening, σ_{ss} , and precipitation strengthening, σ_{ppt} , are added to the strain hardening by the generalized form of addition law as follows:

$$\sigma = \sigma_0 + \sigma_{ss} + \left(\sigma_h^n + \sigma_{ppt}^n \right)^{1/n}, \quad (7.13)$$

The way how to calculate different contributions to yield strength has been explained in previous chapters. n in Eq. (7.13) is taken equal to 1.0 when most precipitates are shearable and equal to 2.0 in case most precipitates are non-shearable [10].

7.3. Experimental and modeling results

The alloy used in this study was 1-mm thick AA6061 (Al-0.95wt%Mg-0.62wt%Si-0.2wt%Cu) sheet, which were delivered in T4 condition (several months

7. Strain Hardening of Al-Mg-Si alloys

storage at room temperature). The material was first solutionized (for 20 min at 560°C), water quenched and then aged at 180, 220, and 250°C for various times. The time interval between water-quench and ageing was less than 2 min. Room temperature tensile test were carried out on a Gleeble machine with the deformation rate of 0.02 s⁻¹. Figure 7.2 shows the dimensions of the tensile specimen. Figure 7.3 shows the evolution of true stress-true strain curve with ageing time for the alloy AA6061, aged at 220 °C. The yield strength increases up to 270 Mpa, corresponding to peak-age, followed by a decrease during overageing.

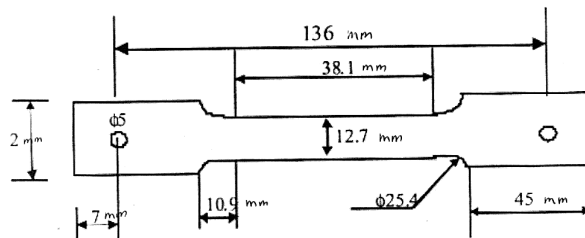


Figure 7.2: Drawing of the tensile specimen

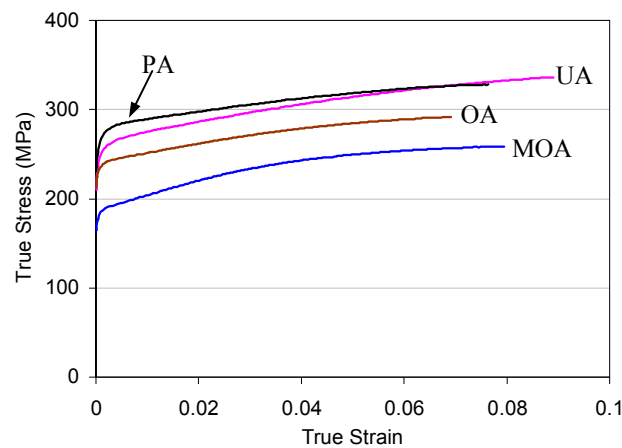


Figure 7.3: True stress-true strain curve for the alloy AA6061 aged at 220 °C for 5 min (UA: underaged sample), 2 h (PA: peak-aged sample), 7 h (OA: overaged sample) and 80 h (MOA: massively overaged sample)

7. Strain Hardening of Al-Mg-Si alloys

It is conventional to present the work-hardening behavior of Al-Mg-Si alloys by plotting the instantaneous work-hardening rate, $\theta = \frac{d\sigma}{d\varepsilon}$, vs. the flow stress increase (i.e., $\sigma - \sigma_y$, where σ_y is the yield strength of the alloy). Figure 7.4 shows two schematic diagrams of the work-hardening rate vs. the flow stress increase. As it is seen the value of θ initially rapidly decreases, which can be attributed to the elastic-plastic transition [7]. After the elastic/plastic transition, two distinctive types of behavior have been reported. For some conditions, there is an approximately linear decrease of work-hardening rate as the flow stress increases. For the other conditions, after the elastic/plastic transition, there is a plateau in the work-hardening followed by a decrease in hardening rate as the deformation continues. In order to characterize the work-hardening behavior of Al-Mg-Si alloys quantitatively, two parameters are important. The first parameter is θ_{max} , which is named the dislocation storage parameter and it is defined as the maximum work-hardening rate in the plastic regime. The second parameter $\beta = -\frac{d\theta}{d\sigma}$, the slope of the curve, is named the dynamic recovery rate. The way to obtain these two parameters is shown in Fig. 7.4.

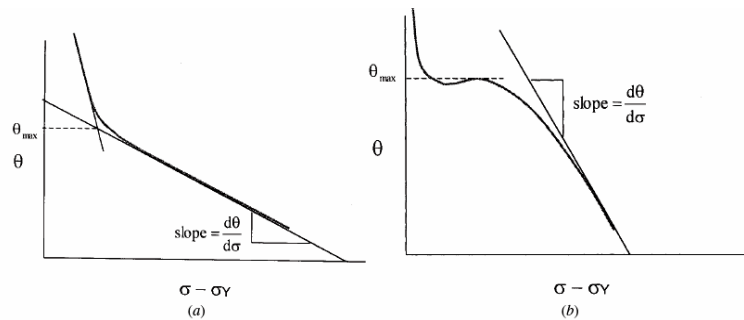


Figure 7.4: Schematic diagrams of the work-hardening rate vs. the flow stress increase [7]

Figures 7.5 and 7.6 show the evolution of θ vs. flow stress increase for the alloy AA6061 aged at 220 and 250 °C for various times. As it is seen for the underaged alloys (Figs. 7.5a, 7.5b, 7.6a, and 7.6b), there is an immediate linear decrease of θ after the initial

7. Strain Hardening of Al-Mg-Si alloys

elastic-plastic transition region. In contrast, in overaged alloys (Figs. 7.5c, 7.5d, 7.5e, 7.5f, 7.6c, 7.6d, 7.6e, 7.6f,) there is a plateau in between.

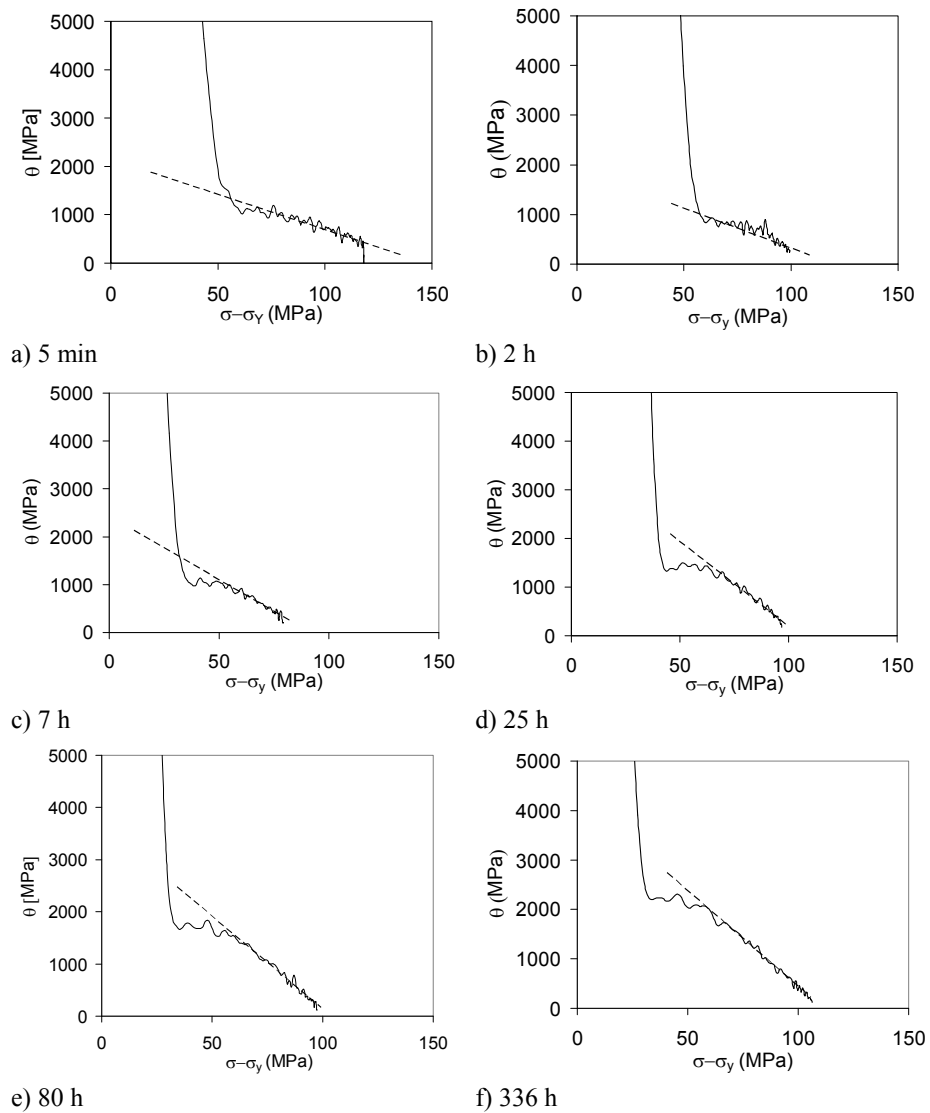


Figure 7.5: Evolution of θ vs. flow stress increase for the alloy AA6061 aged at 220 °C for different times.

7. Strain Hardening of Al-Mg-Si alloys

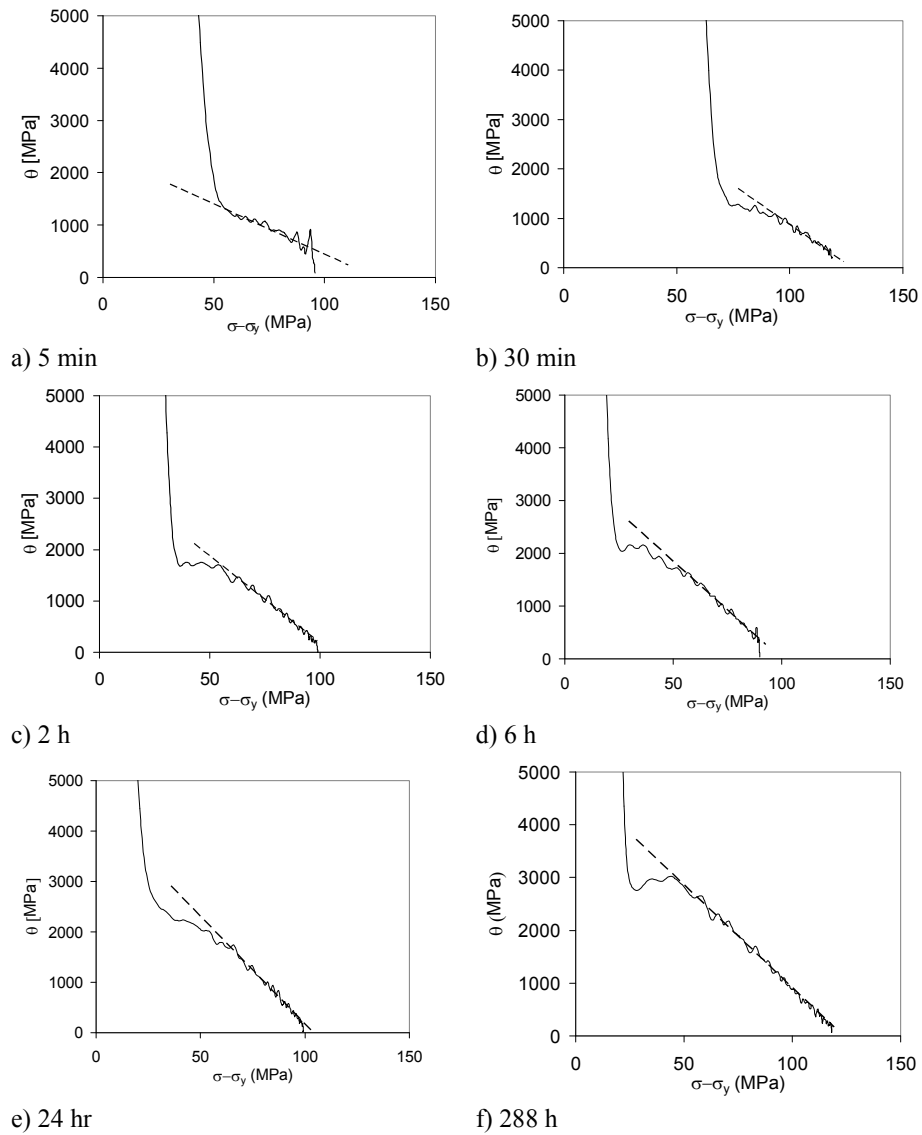


Figure 7.6: Evolution of θ vs. flow stress increase for the alloy AA6061 aged at 250 °C for different times.

7. Strain Hardening of Al-Mg-Si alloys

In order to have a better overview of the evolution of θ_{max} and β during ageing, these two parameters have been plotted vs. mean radius, as shown in Fig. 7.7. The mean radius is obtained from the KWN-based aging model presented in chapter 3. The modeling results in chapter 3 showed that the mean radius, corresponding to peak-age, is 5 nm. It can be observed that for all investigated temperatures θ_{max} decreases with increasing the mean radius to a minimum at around mean radius 7 nm, which corresponds to the mean radius in a slightly overaged sample. After this minimum, θ_{max} increases with increasing mean radius of precipitates. Dynamic recovery rate, β , does not show any minimum close to 5 nm. The plateau in the work-hardening curves, shown in Fig. 7.4b, is only seen in overaged alloys with mean radius larger than 5 nm. Simar [12] did the same analysis for the alloy AA6005A (Al-0.81wt%Mg-0.48wt%Si-0.09wt%Cu). Her results are presented in Fig. 7.8 for the sake of comparison with our experimental data. Obviously, the results for the alloy AA6005A are in a very close qualitative agreement with those of the alloy AA6061. In the case of the alloy AA6005A one can also see that there is a minimum for both θ_{max} and β close to peak-age, when the mean radius is around 3 nm. It is also noticeable that at the very overaged alloy (i.e. mean radius equal to 100 nm) both θ_{max} and β decrease to very low values. Such drop is not seen in our alloys, due to insufficient ageing time.

7. Strain Hardening of Al-Mg-Si alloys

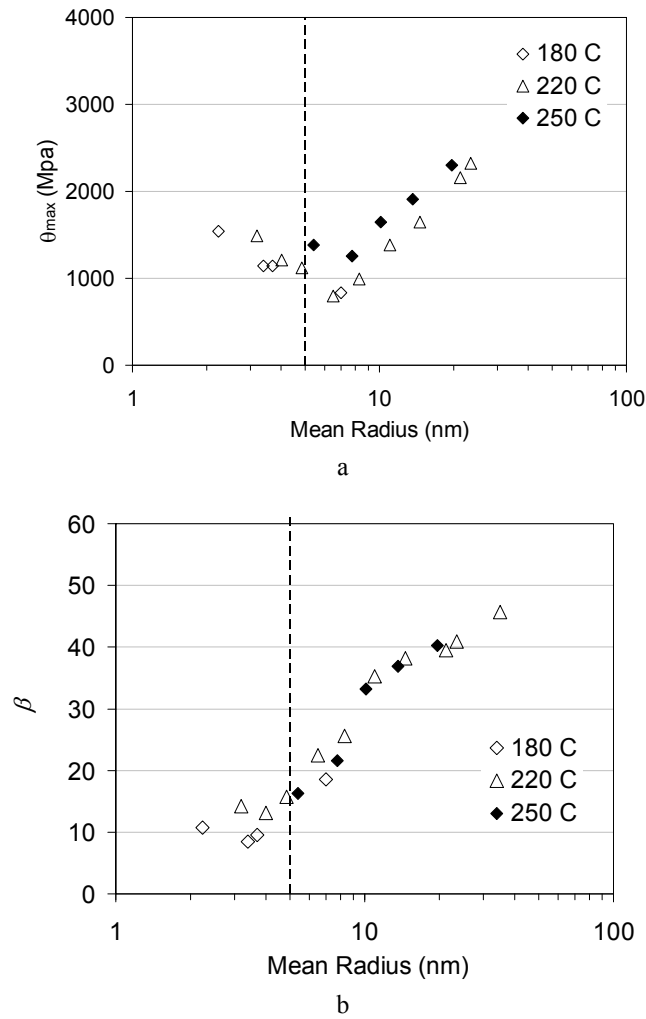


Figure 7.7: Evolution of the experimental strain hardening parameters a) θ_{max} and b) β for the alloy AA6061 with the mean radius (note that the mean radius is calculated by the KWN model (chapter 3)) (Error range for θ_{max} and β is ± 50 MPa and ± 3 respectively), (the dashed line shows the mean radius at peak-age, which is 5 nm)

7. Strain Hardening of Al-Mg-Si alloys

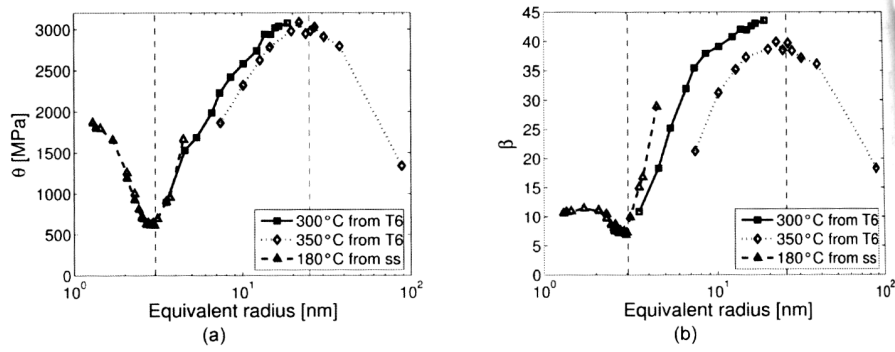


Figure 7.8: Evolution of the experimental strain hardening parameters a) θ_{max} and b) β for the alloy AA6005A [12]

Table 7.1 shows the parameter values used in the strain hardening model. r_{cl} , k_1 , and k_2 are obtained by fitting. The microstructural input, mean radius and volume fraction of precipitates, are calculated by the KWN-based ageing model, as is presented in chapter 3.

Table 7.1: Parameters used in the strain hardening model

Parameter	Value	Parameter	Value
α	0.3	k_1	$7.5 \times 10^8 \text{ m}^{-1}$
M	2.7	k_2	27
G	$2.7 \times 10^{10} \text{ N/m}^2$	α_D	0.3
b	$2.84 \times 10^{-10} \text{ m}$	r_{trans}	5.0 nm
r_{cl}	25.0 nm	r_{trans}^*	5.02 nm

Figure 7.9 shows the prediction of true stress-true strain curve compared with the experimental data. Obviously, the model results are in a good agreement with the experimental data. Figure 7.10 shows the values of θ_{max} and β for the alloy AA6061 obtained from the model, plotted with the experimental data. As it is seen the model shows an overestimation of θ_{max} . However, the dynamic recovery rate is predicted very well.

7. Strain Hardening of Al-Mg-Si alloys

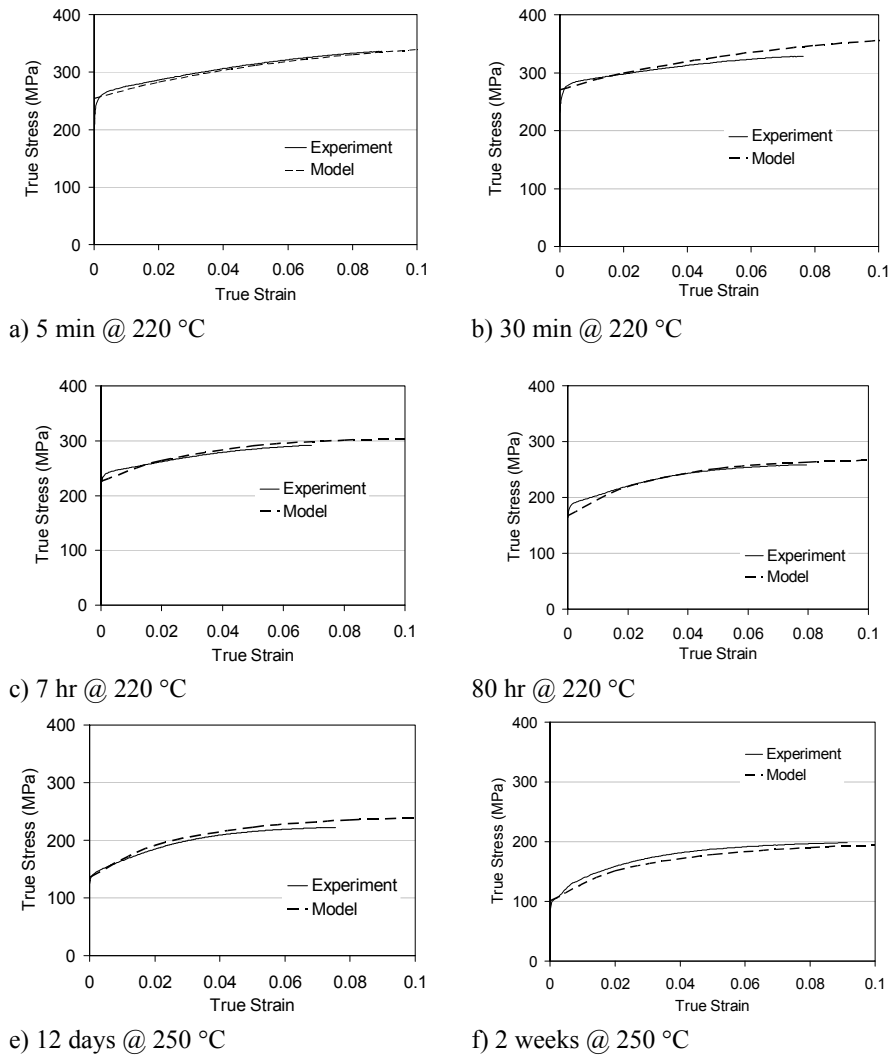
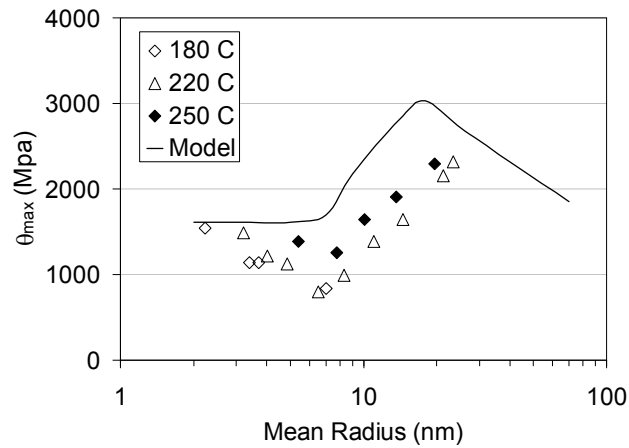
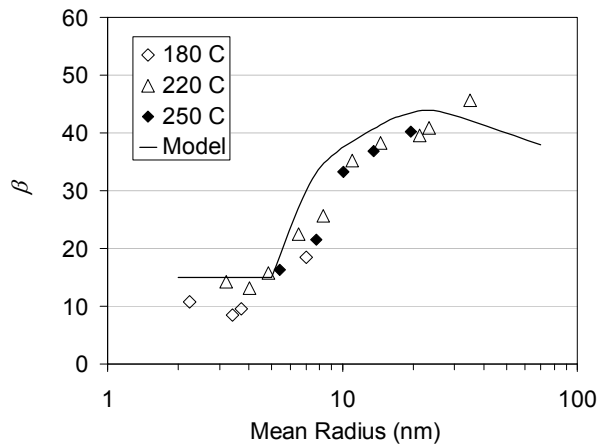


Figure 7.9: Comparison of experimental and model true stress vs. true strain of the alloy AA6061 aged at different conditions

7. Strain Hardening of Al-Mg-Si alloys



a



b

Figure 7.10: Prediction of the evolution of the strain hardening parameters a) θ_{max} and b) β for the alloy AA6061

7.4. Discussion

Effects of ageing treatment on the work-hardening behavior of Al-Mg-Si alloys have been studied. Al-Mg-Si alloys, depending on the mean precipitate radius, can be classified into two categories: i) alloys in which most precipitates are shearable

7. Strain Hardening of Al-Mg-Si alloys

(underaged alloys); and ii) those in which most precipitates are non-shearable (overaged alloys). Transition from underaging to overaging is associated with the maximum yield strength (peak-strength). The results of this study show that there are indeed differences between the work-hardening behaviors of these two groups of microstructures. First of all, when the alloy is overaged, there is an intermediate plateau between the initial elastic-plastic behavior and the linear decrease of θ . This plateau, however, is not seen for underaged alloys. It is also seen that the dislocation storage parameter, θ_{max} , decrease with ageing time until the mean radius becomes equal to 7 nm. By increasing the mean radius, θ_{max} increases. The dynamic recovery rate, β , shows a plateau in the underaging regime and increases in the overage regime.

In the underage regime, the growth of shearable precipitates depletes the matrix from alloying elements. This would have two contradictory influences on the dynamic recovery: i) increasing the dynamic recovery rate because of more depleted matrix and accordingly less solute drag and solute friction effects [8]; and ii) decreasing the dynamic recovery rate due to the formation of bigger precipitates, making the annihilation process (dynamic recovery) more difficult, since dislocations need to first pass through precipitates to annihilate each other. Experimental results from this study shows that these two effects are balancing each other, resulting in a plateau in the dynamic recovery rate with mean radius (ageing time) in the underage regime (see Figs. 7.7b). However, the experimental data from the literature shows a clear minimum of dynamic recovery rate at peak-age for the alloy AA6005 (see Fig. 7.8b). The same results also show that the average values of β in the underage regime for different 6xxx alloys are similar. Using a constant value for k_2 , which is proportional to β , is therefore a reasonable assumption. The decreasing trend of the maximum work-hardening, θ_{max} , in the underage regime (see Fig. 7.7a and 7.8a) has been attributed to the effect of solute depletion [13] or to the formation of shearable precipitates. When growing, the intrinsic strength of shearable precipitates on moving dislocations increases and becomes closer to one of forest dislocations. As a consequence the exponent, n , in the stress addition law should increase, which will result to a decrease of the maximum work-hardening, θ_{max} [7]. There are, however, no well established models to calculate k_1 and n as a function of the progress of ageing before peak-age. For this reason, constant values are used in the current model.

7. Strain Hardening of Al-Mg-Si alloys

When precipitates become non-shearable (i.e. the alloy is overaged), Orowan loops are formed during deformation. Orowan loops are geometrically necessary, because they are required to keep the precipitate compatible with the matrix [14]. There is a linear stress-strain relationship when the Orowan loop formation is dominant with a slope proportional to the volume fraction of non-shearable precipitates [15], meaning that the work-hardening rate is constant. This could be the reason for the observed plateau in θ vs. $(\sigma - \sigma_y)$ curves for overaged alloys (see Figs. 7.5 and 7.6). As deformation proceeds, the stress due to dislocation pile up increases. This can lead to some relaxation mechanisms like formation of prismatic loops or secondary dislocations [14]. In the prismatic loops relaxation mechanism, the Orowan loop is transformed to two prismatic loops by a cross-slip mechanism [12]. These prismatic loops glide away from precipitates, decreasing the stress around them. When this relaxation occurs, the material does not show the linear stress-strain relationship, and consequently, the work-hardening rate decreases [14]. Another relaxation mechanism is generation of secondary dislocations in other slip planes than the primary slip plane. This happens when the glide of prismatic loops becomes more difficult due to the stack of primary prismatic loops. This would make the slip distribution more homogeneous [12].

The increase in θ_{max} during overageing is attributable to the formation of bigger and stronger precipitates which can accommodate more Orowan loops. This effect has been taken into consideration in the modified KME model by introducing dislocation storage efficiency term. When the precipitates become fully incoherent ($r > r_{cl}$), they cannot be sheared by Orowan loops anymore and work-hardening is controlled by the mean free path between precipitates. The distance between precipitates increases during overageing and this can explain the observed decrease in θ_{max} for long ageing time. Regarding the evolution of dynamic recovery rate during overageing, it is not easy to make a conclusive statement about the reason behind the observed increase in dynamic recovery. This is due to the activation of different mechanisms and different contributions to the dynamic recovery [12, 13]. Regardless of the exact mechanism, the model will predict an increase of the dynamic recovery rate, β , as a consequence of introducing the k_D term in the microstructure evolution equation.

Based on the extended KME modelling approach, the stress-strain relations can be derived for different ageing conditions. Input parameters, needed to calculate stress-strain relationship, are only precipitates mean radius and precipitates volume fraction,

7. Strain Hardening of Al-Mg-Si alloys

which can be obtained from the KWN model (introduced in chapter 3). Several important assumptions, including constant θ_{max} and β in the underage regime, have been made to develop the work-hardening model. However, the developed model reproduces the most important features of the microstructure influence on work-hardening; the work-hardening and dynamic recovery rates are low for underaged material and increase for overaged material up to a maximum, followed by a subsequent decrease.

7.5. Summary

The work-hardening behavior of Al-Mg-Si has been studied, using a series of room-temperature tensile tests on the alloy AA6061 previously aged at different temperatures and times. In order to analyse the effects of ageing on work-hardening, the evolution of the work-hardening rate, θ , as a function of the stress increment, $(\sigma - \sigma_y)$, was also plotted. The following conclusions can be drawn based on the observed results:

- The value of θ initially rapidly decreases, which can be attributed to the elastic-plastic transition. After the elastic/plastic transition, there are two distinctive types of behavior. For underaged samples, there is an approximately linear decrease of work-hardening rate as the flow stress increases. For the other samples, after the elastic/plastic transition, there is a plateau in the work-hardening followed by a decrease in hardening rate as the deformation continues.
- The observed plateau in the overaged alloys can be attributed to the Orowan loops. When Orowan loops are stable, there is a linear stress-strain relationship, resulting in a constant θ .
- It can be observed that the maximum work-hardening rate, θ_{max} , decreases with increasing the mean radius to a minimum, followed by an increase with increasing mean radius of precipitates.
- Dynamic recovery rate, β , shows more or less a plateau in the underage regime. In the overage regime β increases with ageing time.
- During overageing, Orowan loops can shear through precipitates as a result of the stress increase due to dislocation pile-up. This mechanism explains the increase of θ_{max} with increasing the size of non-shearable precipitates.

7. Strain Hardening of Al-Mg-Si alloys

- Based on the extended KME modelling approach, the stress-strain relations were derived as a function of the ageing state of the material. Although several important assumptions have been made to obtain an analytical solution, the current model includes the most important features of the microstructure influence on work-hardening; the work-hardening and dynamic recovery rates are low for underaged material and increase for overaged material up to a maximum. Comparison of the experimental stress-strain curves with the simulation results show good agreement.

References:

- [1] Kocks UF, J. Eng Mater Tech, 98 (1976) 76.
- [2] Mecking H and Kocks UF, Acta Metall, 29 (1981) 1865.
- [3] Nes E: Prog Mater Sci, 1997, vol. 41 (3) 129.
- [4] Marthinsen K and Nes E: Mater Sci Eng A, vols. 234-236 (1997) 1095.
- [5] Kocks UF: Metall Trans A, vol. 16A (1985) 2109.
- [6] Holmedal B, Ryen Ø, Nes E, Myhr OR, Grong Ø, Furu T, Marthinsen K, Mater Sci Forum 519-521 (2006) 1901.
- [7] Cheng LM, Poole WJ, Embury JD, and Lloyd DJ, Metall Mater Trans 34A (2003) 2473.
- [8] Embury JD, Poole WJ, and Lloyd DJ, Mater Sci Forum 519-521 (2006) 71.
- [9] Kocks UF and Mecking H, Prog Mater Sci 48 (2003) 171.
- [10] Poole WJ and Lloyd DJ, Proceeding of the 9th Int. Conference on Al Alloys (2004) 939.
- [11] Simar A, Bréchet Y, de Meester B, Denquin A, Pardoën T, Mater Sci Eng A, Volume 486, Issues 1-2 (2008) 85.
- [12] Aude Simar, A multiscale multiphysics investigation of aluminum friction stir welds, PhD thesis, July 2006, pp. 153.
- [13] Lloyd, Mat Sci Forum, 519-521 (2006) 55
- [14] Martin JW, Micromechanics in particle-hardened alloys, Cambridge University Press, 1980, 73.
- [15] Hirsch PB and Humphreys FJ, Proc Roy Soc Lond A 318 (1970) 45.

7. Strain Hardening of Al-Mg-Si alloys

Summary

Al-Mg-Si alloys are heat treatable alloys in which strength is obtained by precipitation hardening. Precipitates, formed from a supersaturated solid solution during ageing heat treatment, are GP-zones, β'' , β' and β -Mg₂Si. Precipitation kinetics and strength vary with alloy composition and process parameters. There is still a need for property and process optimization and therefore to investigate precipitation in this system. Therefore, the general objective is to develop process models to study precipitation kinetics and precipitation sequence in Al-Mg-Si alloys.

Precipitates in Al-Mg-Si alloys usually nucleate with a spherical morphology but grow with an elongated shape. An age-hardening model is used to study the effects of morphology of precipitate on the strengthening of Al-Mg-Si alloys (Chapter 2). The results show that age-hardening models, assuming elongated precipitates of constant aspect ratio, do not give an overall better prediction of precipitation and strength evolution during ageing and the assumption of spherical precipitates remains, as a first approximation, an acceptable assumption. The Kampmann-Wagner numerical (KWN) framework, as a base ageing model, is introduced in chapter 3. The KWN model is a method for modelling coupled nucleation, growth, and coarsening. In this method, the precipitate size distribution is simulated using a finite difference method.

Current precipitation models, applied to aluminium alloys, usually assume that thermodynamic equilibrium is always fulfilled at the precipitate-matrix interface. This implies the assumption of an infinite interface mobility, which means very fast transformation of matrix to precipitate as soon as the local equilibrium is disturbed by diffusion. The validity of this assumption has been investigated in chapter 4. A modified version of KWN model is introduced in which a mixed-mode growth model has been implemented instead of the only diffusion-controlled growth equation. Using this model a comprehensive systematic study has been done on the effects of diffusivity, and type of precipitate, i.e. interface energy and mobility, on the kinetics and character of precipitation in Al-Mg-Si alloys. The results show that changes in the interfacial energy have almost no effect on the precipitation character. However, changes in diffusivity and interface mobility have significant influence on the character of precipitation. For example, it is shown that there is a certain radius below which precipitation character is always interface controlled.

Summary

In chapter 5, the complexity of the precipitation sequence and its effect on the precipitation kinetics during ageing has been investigated with a multi-component multi-precipitate model, based on the assumption of maximum Gibbs free energy dissipation. In this modelling framework it is possible to consider simultaneous formation of GP-zones, β'' , β' , β , and free-Si. The model predicts that a large fraction of nuclei of different precipitate species form during quenching from solutionizing temperature and during heating to ageing temperature. Nucleation is first followed by the growth of the less stable species, which dissolve at some point in favor of more stable precipitates. In the end, only thermodynamically stable precipitates like β and free-Si remain in the alloy. The model also confirms that maximum strength is reached when β'' is the dominant precipitate.

The effects of secondary precipitates, induced by interrupted ageing, on the age hardening of Al-Mg-Si alloys have been presented in chapter 6. In the interrupted ageing the alloy is first aged at an elevated temperature (e.g. 170 °C), quenched and then exposed to a lower temperature (e.g. 25-100 °C), and aged again at elevated temperatures. From the results it appears that the influence of secondary precipitates is highly dependent on the interruption temperature. Secondary precipitation stimulated by interruption at temperatures below 50 °C has almost no influence on the alloy strength, while when the interruption temperature is above 50 °C, it increases the hardness significantly. The proposed scenario to explain this behavior is based on the temperature-dependent competitive growth of GP-I and GP-II precipitates. According to this model, interruption temperature below 50 °C stimulates the formation of GP-I zones, which have a very slow kinetics of transformation and therefore they have almost no influence on the mechanical properties. On the other hand, when the alloy is interrupted at temperatures above 50 °C, the formation of GP-II zones is more likely to take place, consequently resulting in the higher density of β'' precipitates during re-ageing and better mechanical properties.

Previous precipitation models were linked to a strength model to predict the yield strength evolution during ageing. However, the whole work-hardening behavior is also important for many applications of Al-Mg-Si alloys. In the last chapter, the influence of ageing on work-hardening is investigated from tensile tests. A modified version of Kocks-Mecking-Estrin (KME) model is then employed to simulate the work-hardening response as a function of the precipitation state. Results reveal that underaged material shows a linear decrease of the work-hardening rate with flow stress, while overaged

Summary

material shows an initial constant work-hardening rate before decreasing linearly. This distinct behavior has been related to the stability of the Orowan loops.

In conclusion, the thesis addresses several important issues concerning precipitation and work-hardening behavior of Al-Mg-Si alloys, including precipitates morphology, precipitation sequence, precipitation character, and interrupted ageing. This allows for a better understanding of precipitation sequence, precipitation and hardening kinetics in these alloys. The results of this study can be used for optimization of both chemical composition and ageing parameters in order to achieve desirable microstructure and mechanical properties.

Summary

Samenvatting

Al-Mg-Si legeringen zijn legeringen waarin gedurende een warmtebehandeling verhoging van de sterkte wordt verkregen door precipitatieharden. De precipitaten die gedurende een verouderingswarmtebehandeling gevormd worden uit een oververzadigde oplossing in de aluminiummatrix, zijn GP-zones, β' , β'' , en β -Mg₂Si. De kinetiek van de precipitatie en het effect op de sterkte variëren met de legeringssamenstelling en procesparameters. Er is nog steeds behoefte aan eigenschaps- en procesoptimalisatie en daarmee het onderzoeken van precipitatie in deze legeringen. Daarom is de algemene doelstelling het ontwikkelen van procesmodellen voor de studie van precipitatiekinetiek en de precipitatievolgorde in Al-Mg-Si legeringen.

Precipitaten in Al-Mg-Si legeringen vormen meestal een nucleus met een bolvormige morfologie, maar ze groeien met een langgerekte vorm. In dit proefschrift wordt een verouderingsmodel gebruikt om de effecten van de morfologie van de precipitaten op de versterking van de Al-Mg-Si-legeringen (hoofdstuk 2) te bestuderen. De resultaten laten zien dat verouderingsmodellen uitgaande van langwerpige precipitaten met constante afmetingsverhouding in het algemeen geen betere voorspelling geven van de precipitatie en de sterkte-evolutie tijdens de veroudering en de veronderstelling van bolvormige precipitaten blijft, als eerste benadering, een aanvaardbare veronderstelling.

Het uitgangspunt voor de verouderingsmodellen in dit proefschrift wordt gevormd door het numerieke Kampmann-Wagner (KWN) model. Dit model wordt geïntroduceerd in het hoofdstuk 3. Huidige precipitatiemodellen, toegepast op aluminiumlegeringen, gaan er meestal vanuit dat altijd aan het thermodynamisch evenwicht wordt voldaan aan het precipitatie/matrix-grensvlak. Dit impliceert de aanname van een oneindig grote grensvlakmobiliteit, leidend tot een zeer snelle transformatie van de matrix tot precipitaat zodra het lokale evenwicht verstoord is door diffusie. De geldigheid van deze aanname is onderzocht in hoofdstuk 4. Een aangepaste versie van het KWN-model wordt geïntroduceerd, waarbij een *mixed-mode* groei-model is toegepast in plaats van de vergelijking voor alleen door diffusie bepaalde groei. Met dit model is een uitgebreide systematische studie uitgevoerd naar de effecten van diffusie, en het type precipitaat, gekenmerkt door de grensvlakenergie en -mobiliteit, op de kinetiek en het karakter van de precipitatie in Al-Mg-Si legeringen. De resultaten laten zien dat veranderingen in de grensvlakenergie bijna geen effect op de precipitatiekenmerken hebben. Echter,

Samenvatting

veranderingen in de diffusiecoëfficiënt en grensvlakmobiliteit hebben een grote invloed op het karakter van de precipitatie. Er wordt bij voorbeeld aangetoond dat er een bepaalde afmeting voor het precipitaat is waaronder het precipitatiekarakter altijd bepaald wordt door de grensvlakmobiliteit.

In hoofdstuk 5 wordt de complexiteit van de precipitatie-reeks en het effect op de precipitatiekinetiek gedurende het verouderen onderzocht met een multi-component multi-precipitatie model. Dit model is gebaseerd op de veronderstelling van de maximale dissipatie van Gibbs vrije energie. In dit raamwerk is het mogelijk de gelijktijdige vorming te modelleren van GP-zones, β' , β'' , en vrij-Si-precipitaten. Het model voorspelt dat een groot deel van de nucleï van de verschillende soorten precipitaten zich vormen tijdens het afschrikken vanaf de oplosttemperatuur en het opwarmen naar de verouderingstemperatuur. Nucleatie wordt aanvankelijk gevolgd door de groei van de minder stabiele precipitaten, die op een bepaald punt oplossen ten gunste van de meer stabiele precipitaten. Op het einde zijn alleen de thermodynamisch stabiele precipitaten zoals β en vrije-Si aanwezig in de legering. Het model bevestigt ook dat de maximale sterkte wordt bereikt wanneer β'' de dominante precipitatie is.

Secundaire precipitaten worden gevormd door de veroudering te onderbreken met een langdurige warmtebehandeling op een lagere temperatuur. Het effect van deze secundaire precipitaten op de sterkte van de Al-Mg-Si legeringen wordt gepresenteerd in hoofdstuk 6. Tijdens de onderbroken veroudering wordt de legering eerst verouderd op de verouderingstemperatuur (b.v. 170 °C), dan afgeschrikt en vervolgens blootgesteld aan een lagere temperatuur (b.v. 25-100 °C), waarna het opnieuw wordt gegloeid bij verhoogde temperatuur. Uit de resultaten blijkt dat de invloed van secundaire precipitaten sterk afhankelijk is van de onderbrekingstemperatuur. Secundaire precipitatie, gestimuleerd door onderbreking bij temperaturen onder 50 °C, heeft vrijwel geen invloed op de legeringsterkte, terwijl bij onderbrekingstemperaturen boven 50 °C de hardheid aanzienlijk wordt verhoogd. Het voorgestelde scenario om dit gedrag te verklaren is gebaseerd op de temperatuurafhankelijke concurrerende groei van de GP-I en GP-II precipitaten. Volgens dit model stimuleert een onderbrekingstemperatuur lager dan 50 °C de vorming van GP-I zones, die een zeer langzame kinetiek van transformatie hebben en daarom vrijwel geen invloed op de mechanische eigenschappen hebben. Wanneer de legering wordt onderbroken bij temperaturen boven 50 °C, zal de waarschijnlijkheid van de vorming van GP-II zones toenemen, het geen resulteert in een

Samenvatting

hogere dichtheid van β'' precipitaten tijdens het laatste deel van de warmtebehandeling en betere mechanische eigenschappen.

Voorgaande precipitatiemodellen werden gekoppeld aan een model om de evolutie van de vloeigrens te voorspellen tijdens het verouderingsproces. Echter, niet alleen de vloeigrens, maar het hele verstevigingsgedrag is van belang voor de vele toepassingen van Al-Mg-Si legeringen. In het laatste hoofdstuk, hoofdstuk 7, wordt de invloed van de veroudering op het verstevigingsgedrag onderzocht met behulp van trekproeven. Een aangepaste versie van het Kocks-Mecking-Estrin (KME) model wordt vervolgens gebruikt voor de simulatie van het verstevigingsgedrag als functie van de precipitatietoestand. Resultaten tonen aan dat onder-verouderd materiaal een lineaire daling vertoont van de verstevigingsnelheid met vloeispanning, terwijl het over-verouderde materiaal aanvankelijk een constante verstevigingsnelheid vertoont vóór een latere lineaire afname. Dit gedrag is gerelateerd aan de stabiliteit van de Orowan loops van dislocaties rond precipitaten.

In samenvatting, het proefschrift behandelt een aantal belangrijke kwesties met betrekking tot precipitatie en het verstevigingsgedrag van Al-Mg-Si-legeringen, met inbegrip van de precipitaatmorfologie, de precipitatievolgorde, het precipitatiekarakter, en onderbroken veroudering. Dit zorgt voor een beter begrip van de precipitatievolgorde en -kinetiek en de sterkte-toename van deze legeringen. De resultaten van deze studie kunnen worden gebruikt voor de optimalisatie van zowel de chemische samenstelling als de verouderingsparameters om hiermee de gewenste microstructuur en mechanische eigenschappen te bereiken.

Samenvatting

ACKNOWLEDGEMENTS

This research was carried out under Project No. MC4.05213 in the framework of the strategic research program of the Materials Innovation Institute M2i (www.m2i.nl). First of all, I would like to extend my sincere thanks to M2i for funding this project. My special thanks are dedicated to Monica Reulink from HR department of M2i for her supports during my PhD.

Many thanks to my supervisors Dr. Alexis Miroux and Professor Jilt Sietsma for their important, helpful and stimulating discussions and supports. This thesis would not have been made a reality without the support and help of these two.

Professor Leo Kestens and Professor Laurens Katgerman are also thanked for their useful comments and discussions.

Industrial partners of this project (Corus, Nedal Aluminum, Boal, and TNO) are warmly thanked for their collaborations.

I enjoyed collaborations with all members of “Microstructure Control of Materials” (MCM) group. Their friendship and many pleasant and useful discussions are warmly appreciated.

I would also like to thank my Iranian colleagues Ali, Mehdi, Vahid, Farid, Hossein, Masoud, Peyman and Sepideh for all they have done for me during this period.

I am always grateful to my previous supervisors during my Master and Bachelor courses, especially Professor M.A. Gologazr, Dr. M. Shamanian, Dr. Ali Shafyei, and Dr. M. Madaah Hosseini, who helped me to learn fundamentals of Materials Science.

I am also thankful to my friend Alert Adema, who helped me to translate the summary of my thesis to Dutch.

Finally, I would like to thank my wife and my parents for their love, support, and encouragement during my Ph.D. work. I would also like to dedicate this work to my wife, Maryam, for her support and understanding.

Curriculum Vitae

Abbas Bahrami

born on 14-11-1980 in Tehran, Iran

PhD. (2006- 2010)

Materials Science and Engineering, Technical university of Delft, the Netherlands.
Supervisors: Dr. Alexis Miroux and Prof. J. Sietsma

Thesis:

Microstructure control during ageing of Al-Mg-Si alloys for forming applications

MSc. (2003- 2005)

Materials Science and Engineering, Sharif University of Technology, Tehran, Iran
Supervisors: Dr. H.R. Madaah-Hosseini

Thesis:

Production and characterization of nanocrystalline soft magnetic Fe-Si-Ni powders using mechanical alloying

BSc. (1999- 2003)

Materials Science and Engineering, Esfahan University of Technology, Esfahan, Iran
Supervisors: Dr. M.A. Golozar, Dr. M. Shamanian

Thesis:

Wear and tribology behavior of hot-work tool steels